UNIVERSITY OF CALIFORNIA, SAN DIEGO

Cardiac Stretch-Induced Transcriptomic Changes are Axis-Dependent

A dissertation submitted in partial satisfaction of the requirements for the degree

Doctor of Philosophy

in

Bioengineering

by

Kyle Stephen Buchholz

Committee in Charge:

Professor Jeffrey Omens, Chair
Professor Andrew McCulloch, Co-Chair
Professor Ju Chen
Professor Karen Christman
Professor Robert Ross
Professor Alexander Zambon

2016

The Dissertation of Kyle Stephen Buchholz is approved and it is acceptable in quality and form for publication on microfilm and electronically:

Co-Chair

Chair

University of California, San Diego

2016

Dedication

To my beautiful wife, Rhia.

Table of Contents

List of Figures

List of Tables

List of Abbreviations

TF	Transcription factor
MLP	Muscle LIM protein
Tcap	Titin-cap
FHL1	Four-and-a-half LIM domains 1
MARP	Muscle ankyrin-repeat protein
BNP	Brain natriuretic peptide
NFAT	Nuclear factor of activated T-cells
KO	Knockout
ERK	Extracellular regulated kinase
TAC	Transverse aortic constriction
MAPK	Mitogen-activated protein kinase
CARP	Cardiac ankyrin repeat protein
Ankrd2	Ankyrin repeat domain protein 2
DARP	Diabetes-related ankyrin repeat protein
PKA	Protein kinase A
PKC	Protein kinase C
DCM	Dilated cardiomyopathy
ARVC	Arrhythmogenic right ventricular cardiomyopathy
ECM	Extracellular matrix
ILK	Integrin-linked kinase
SERCA	Sarco/endoplasmic reticulum calcium-ATPase

FAK	Focal adhesion kinase
PI3K	Phosphoinositide 3-kinase
Akt	Protein Kinase B
JAK	Janus-Associated Kinase
STAT	Signal Transducers and Activators of Transcription
RhoA	Small GTPase Ras homolog gene family member A
ROCK	Rho-associated coiled-coil containing kinase
MEK	Mitogen-activated protein kinase kinase
MEKK	Mitogen-activated protein kinase kinase kinase
JNK	c-Jun N-terminal kinase
PDK1	Phosphoinositide-dependent kinase-1
mTOR	Mammalian target of rapamycin
eIF4E	Eukaryotic translation initiation factor 4E
GSK3B	Glycogen synthase kinase-3 beta
GATA4	GATA-binding protein 4
SR	Sarcoplasmic reticulum
ROS	Reactive oxygen species
CaMK	Calcium-calmodulin-dependent protein kinase
DAG	Diacylglycerol
HDAC	Histone deacetylase
MEF2	Myocyte enhancer factor-2
Rcan1	Regulator of calcineurin 1
MRTF	Myocardin-related transcription factor

SRF	Serum response factor
NFkB	Nuclear factor kappa-light-chain-enhancer of activated B cells
CREB	Cyclic adenosine monophosphate response element-binding protein
FoxO	Forkhead box O
IkB	Inhibitor of kappa B
IKK	Inhibitor of kappa B kinase
AP-1	Activator protein 1
ANP	Atrial natriuretic peptide
RNA-Seq	RNA sequencing
DE	Differentially expressed
dNTP	Deoxynucleotide
SAM	Sequence alignment map
BAM	Binary alignment map
RPKM	Reads per kilobase of exon per million mapped reads
FDR	False discovery rate
GO	Gene Ontology
DAVID	Database for Annotation, Visualization and Integrated Discovery
KEGG	Kyoto Encyclopedia of Genes and Genomes
STRING	Search Tool for the Retrieval of Interacting Genes/Proteins
GeneMANIA	Gene Multiple Association Network Integration Algorithm
ChIP	Chromatin immunoprecipitation
EC_{50}	Half-maximal effective concentration
PDMS	Polydimethylsiloxane

PBS	Phosphate buffered saline
RT-PCR	Reverse transcription polymerase chain reaction
GAPDH	Glyceraldehyde 3-phosphate dehydrogenase
BSA	Bovine serum albumin
DAPI	4',6-diamidino-2-phenylindole
FFT	Fast Fourier transform
RIPA	Radioimmunoprecipitation assay
SDS	Sodium dodecyl sulfate
PAGE	Polyacrylamide gel electrophoresis
PVDF	Polyvinylidene fluoride
TBS	Tris buffered saline
I_{Ks}	Slow delayed rectifying potassium current potassium current
MSN	Mechanosignaling network
NHE	Sodium hydrogen exchanger
Trp	Transient receptor potential
EGFR	Epidermal growth factor receptor
TPR	True positive rate
TNR	True negative rate
I_{K1}	Inward rectifier current
I_{Kr}	Repolarizing potassium current
BIM-1	Bisindolylmaleimide I

Acknowledgements

I would first like to thank my mentors, Jeffrey Omens and Andrew McCulloch, who brought me into the Cardiac Mechanics Research Group (CMRG) and supported my undertaking of this exciting research project. They have been terrific at providing me guidance and feedback throughout my entire PhD. My PhD research has used a mix of experimental, bioinformatics, and computational approaches. I have had many lab members and collaborators aid me with their expertise in these disciplines.

Jennifer Stowe has been extremely helpful on the experimental side for my entire PhD. She was always available when I had a question about a molecular biology technique and would happily train me on different procedures. Emily Pfeiffer allowed me to shadow her at the beginning of my PhD and taught me the basics of cell culture and how to use our stretch devices.

There were many times where I did not have time to perform certain techniques myself and required the assistance of others. I would like to thank Kate Herum and Michelle Ma for performing neonatal mouse cardiac myocyte isolations, and Justin Tan, Jenny “Tik-Chee” Cheng, and Christopher Chen for producing mass quantities of micropatterned PDMS.

Over the past few years, I have had the opportunity to collaborate with other departments. Specifically, I would like to acknowledge Indroneal Banerjee and Stephan Lange from the school of medicine. I am grateful for the opportunity to work on genetically engineered mouse models with them.

With regard to bioinformatics analysis, I really appreciate the direction of Alex Zambon. At the start of my dissertation, I was not familiar with RNA-Seq and did not know what I was getting myself into. Alex helped me identify the tools and programs to perform this analysis. I also appreciate working with Zoe Gan. It was very nice to have another lab member analyzing RNA-Seq data, and it enabled us to bounce ideas off of each other.

I would like to thank Jeffrey Saucerman and Philip Tan for introducing me to computational modeling of signaling networks. It has been a great experience to collaborate with another lab across the country with expertise in this area.

Last but not least, I would like to thank my wife, Rhiannon Buchholz. Rhia has been a supportive and motivating influence over my six years of graduate school. She has always been there for me during my times of need and believed in me when I was questioning my own abilities and drive.

Chapters 2 and 4, in part, are currently being prepared for submission for publication of the material. Buchholz, Kyle S; Tan, Philip; Zambon, Alexander C; Saucerman, Jeffrey J; McCulloch, Andrew D; Omens, Jeffrey H. Reprinted with permission from all co-authors. The dissertation author was the primary researcher and author of this material.

Chapter 3, in part, is currently being prepared for submission for publication of the material. Tan, Philip; Buchholz, Kyle S; Omens, Jeffrey H; McCulloch, Andrew D; Saucerman, Jeffrey J. Reprinted with permission from all co-authors. The dissertation author was a primary investigator and author of this material.

Vita

Education:

2016 PhD in Bioengineering
University of California, San Diego

2013 MS in Bioengineering
University of California, San Diego

2010 BS in Chemical Engineering and Biomedical Engineering
Carnegie Mellon University

Publications:

Banerjee I, Zhang J, Moore-Morris T, Pfeiffer E, **Buchholz KS**, Liu A, Ouyang K, Stroud MJ, Gerace L, Evans SM, McCulloch A, Chen J. (2014). "Targeted ablation of nesprin 1 and nesprin 2 from murine myocardium results in cardiomyopathy, altered nuclear morphology and inhibition of the biomechanical gene response." PLoS Genet 10(2): e1004114.

Sun LT, **Buchholz KS**, Lotze MT, Washburn NR. (2010). "Cytokine binding by polysaccharide-antibody conjugates." Mol Pharm 7(5): 1769-77.

Abstract of the Dissertation

Cardiac Stretch-Induced Transcriptomic Changes are Axis-Dependent

by

Kyle Stephen Buchholz

Doctor of Philosophy in Bioengineering

University of California, San Diego, 2016

Professor Jeffrey Omens, Chair

Professor Andrew McCulloch, Co-Chair

Cardiac myocytes are striated muscle cells with myofilaments running along their length and Z-discs in a transverse direction. These cells contain structures that are sensitive to mechanical stretch and transduce this signal into a biochemical response. By altering the major axis of biaxial, mechanical stretch, I hypothesized that different

signaling pathways and transcription regulators would be activated and lead to divergent gene expression profiles in cardiac myocytes.

To investigate the effect of stretch axis, cardiac myocytes were cultured on a micropatterned substrate, and the primary stretch axis was applied either parallel or transverse to the myofibril direction. RNA sequencing (RNA-Seq) was conducted to study whole genomic expression changes after acute cardiac myocyte stretch. After 30 minutes of stretch, 53 and 168 genes were considered differentially expressed (DE) from transverse and longitudinal stretch, respectively. After 4 hours, the number of DE genes increased to 795 in longitudinal stretch while it decreased to 35 in transverse stretch. Gene ontology (GO) term analysis indicated enrichment of transcription factor (TF) activity and protein kinase activity by both stretch axes; whereas longitudinal but not transverse stretch induced expression of genes involved in sarcomere organization and cytoskeletal protein binding.

Although researchers have identified sensors, pathways, and TFs involved in cardiac mechanotransduction, I, for the first time, integrated this information into a logic-based network model of cardiac myocyte stretch signaling. This model was validated against independent data and correctly predicted the effect of stretch or effect of inhibitors on stretch response in 54 of 61 experiments.

This network model was used in conjunction with the RNA-Seq data to identify the mechanisms regulating gene expression changes due to longitudinal and transverse stretch. Analysis of this network identified serum response factor (SRF) and myocyte enhancer factor-2 (MEF2) as critical TFs in regulating longitudinal stretch-induced gene changes whose activity is modulated by protein kinase C (PKC). In addition, cyclic

adenosine monophosphate response element-binding protein (CREB) was found to be activated by both longitudinal and transverse stretch. The network model provides evidence that cardiac myocytes engage different transcriptional regulators in response to different principal orientations of biaxial stretch.

Chapter 1: Introduction

1.1. Mechanotransduction

Mechanotransduction is the process by which cells convert mechanical forces into a biochemical response [1-3]. Several intracellular pathways and mechanisms have been implicated in the response to mechanical loading [2,4]. In general, a membrane or cytoskeletal structural protein may be sensitive to changes in mechanical loading and trigger the activation of signaling pathways within the cytoplasm. These pathways propagate the signal to the nucleus and alter the activity of transcription factors (TFs), which regulate the expression of their target genes, dictating the cellular response to the mechanical stimulus [2]. A prominent phenotypic response to mechanical stretch is hypertrophy or the enlargement of cells.

In vivo cardiac hypertrophy is a compensatory response to elevated stresses, which may be caused by hypertension or mitral valve regurgitation. Eventually, the heart is unable to maintain its function of pumping oxygen through systemic circulation in its enlarged state and undergoes decompensated heart failure. Cardiovascular disease is the leading cause of death in the United States with a death rate of 223 per 100,000 Americans in 2013 [5]. Therefore, it is of the utmost importance to uncover the mechanisms leading to heart failure. By better understanding these mechanisms, more precise therapeutic targets can be identified for cardiac disease prevention.

1.1.1. Mechanosensors

Mechanical stretch must first be sensed near the cell periphery in order to trigger downstream signaling events. Various mechanosensors have been proposed to sense

mechanical loading in cardiac myocytes. This section will focus on three locations of mechanosensors: sarcomere, intercalated disc, and sarcolemma.

1.1.1.1. Sarcomere

The sarcomere is the contractile unit within cardiac myocytes and is composed of myofilaments (actin and myosin) [6]. Myosin heads can attach to binding sites on actin filaments, which allows for force generation during muscle contraction [7]. This process drives the heart to pump blood to the systemic circulation. The Z-disc of the sarcomere is also directly connected to the cytoskeleton, which provides evidence that sarcomeric proteins may be involved in force transmission [8].

Titin is a giant protein that connects the Z-disc to the M-line and is responsible for the passive stiffness of cardiac muscle [9]. Titin has been proposed to be a key mechanosensor and interacts with many proteins that have been implicated in mechanosensitive signaling pathways [10]. These cytoskeletal proteins that can bind to titin include muscle LIM protein (MLP), titin-cap (Tcap), four-and-a-half LIM domains 1 (FHL1), and muscle ankyrin-repeat protein (MARP) family members [11].

MLP and Tcap form a complex with titin that may function as a stretch sensor [12]. MLP-deficient neonatal mouse cardiac myocytes do not experience upregulation of the fetal gene, brain natriuretic peptide (BNP), in response to mechanical stretch [12]. This indicates that MLP may be involved in mechanotransduction. Binding of MLP to Tcap is abolished by a polymorphism in MLP (W4R-MLP). Loss of this MLP-Tcap interaction may affect the elastic properties of titin, and thereby the ability of this complex to sense mechanical stress [12]. MLP also has a role in anchoring calcineurin to

the Z-disc [13]. Calcineurin is a calcium-activated phosphatase that dephosphorylates nuclear factor of activated T-cells (NFAT), which allows NFAT to translocate to the nucleus and transcribe hypertrophic genes [14]. Reduced MLP levels in heterozygous knockout (KO) mice lead to calcineurin mislocalization and diminished NFAT signaling [13]. This interaction between MLP and calcineurin-NFAT signaling provides a mechanism for MLP to transduce mechanical stresses to the nucleus.

FHL1 binds to the N2B region of titin and can serve as a scaffold for extracellular regulated kinase-2 (ERK2). When FHL1 KO mouse hearts were exposed to pressure overload by transverse aortic constriction (TAC), they experienced a blunted hypertrophic response and a lack of ERK2 phosphorylation. These mice also had a decrease in cardiac muscle stiffness, which may be due to the lack of binding between FHL1 and titin [15]. Studies indicate that FHL1 promotes hypertrophy through mitogen-activated protein kinase (MAPK) signaling and that FHL1 increases cardiac muscle stiffness by inhibiting titin N2B phosphorylation [16].

Similar to FHL1, all 3 MARP members including cardiac ankyrin repeat protein (CARP), ankyrin repeat domain protein 2 (Ankrd2), and diabetes-related ankyrin repeat protein (DARP) bind to titin. However, MARP members bind to the N2A region instead of the N2B region. In response to stretch of neonatal rat cardiac myocytes, CARP and DARP translocate to the nucleus [17]. Additionally, eccentric contractions of skeletal muscle cause upregulation of CARP and Ankrd2 gene expression [18]. MARP members have been linked to protein kinase A (PKA) and protein kinase C (PKC) [19].

1.1.1.2. Intercalated Disc

The intercalated disc is the cell-cell junction, which longitudinally connects neighboring cardiac myocytes. In response to volume overload of rabbit hearts, the intercalated disc undergoes ultrastructural changes that may be associated with sarcomere assembly and hypertrophic growth [20]. The three types of cell junctions that make up an intercalated disc are fascia adherens, desmosomes, and gap junctions. Fascia adherens are anchoring sites for cytoskeletal actin and connect to the closest sarcomere. Intermediate filaments bind to desmosomes [21]. Gap junctions allow for ions to pass through them, which allows for action potentials to propagate down muscle fibers.

The fascia adherens junctional complex is composed of proteins, such as cadherins, catenins, and catenin-binding proteins [22]. N-cadherin can form attachment sites with neighboring cardiac myocytes and transmit forces between cells [23]. It has also been shown that N-cadherin is upregulated in response to mechanical stretch [24]. N-cadherin KO hearts have altered cell-cell mechanosensing that affects their sarcomere structure and causes dilated cardiomyopathy (DCM). These KO cardiac myocytes do not have identifiable fascia adherens junctions, and their sarcomeres are shorter in length. Beta-1 integrin levels are increased in N-cadherin KO hearts, which indicates a compensatory response where other mechanotransductive proteins increase in expression due to the deficit of N-cadherin [25]. Alpha-catenin recruits vinculin to the fascia adherens junction. Similar to KO of N-cadherin, KO of alpha-catenin alters the structure of the intercalated disc and leads to DCM. Vinculin localization is lost at the fascia

adherens junction; however, vinculin also localizes to the costamere and still remains there after alpha-catenin KO [26].

Desmosomes contain cadherins, desmocollin-2, and desmoglein-2 and link the intermediate filament networks between cardiac myocytes. Mutations in these proteins are associated with arrhythmogenic right ventricular cardiomyopathy (ARVC) [21]. Desmoplakin connects desmosomes to the intermediate filaments [21]. Desmoplakin KO causes sarcomeric defects and loss of desmosomal but not N-cadherin-based proteins, and has only been associated with ARVC [27].

Gap junctions are cell-cell connections that permit ions to pass between neighboring cells. Connexin-43 is gap junctional protein that is upregulated in response to mechanical stretch [28]. Upregulation of Connexin-43 is accompanied by an increased number and size of gap junctions as well as an accelerated conduction velocity [29].

1.1.1.3. Sarcolemma

The cell membrane of cardiac myocytes is referred to as the sarcolemma. The sarcolemma contains transmembrane proteins, such as integrins and dystroglycans, which can bind to components of the extracellular matrix (ECM) [30]. Similar to the intercalated disc proteins allowing for force transmission at the longitudinal ends of the cell, these transmembrane proteins can transduce mechanical loads on the lateral surfaces of the cell [31].

Integrins are receptors that form dimers with alpha and beta subunits, which can bind ECM proteins including fibronectin, laminin, and collagen [32]. In response to pressure overload hypertrophy, the subunits alpha1, alpha5, alpha7, and beta1D increase

in expression [33]. Additionally, it was shown that beta1 integrin KO hearts have a blunted hypertrophic response to TAC [34]. Integrins are connected to signaling proteins, such as integrin-linked kinase (ILK). ILK is a key regulator of sarco/endoplasmic reticulum calcium-ATPase (SERCA) and phospholamban, which are both involved in myocyte contractility [35].

The costamere is composed of proteins, such as vinculin and talin, and links integrins to the actin cytoskeleton [36]. Vinculin is present at both the costamere and at the intercalated disc, which has made it difficult to determine its specific function in mechanotransduction [37]. Mice with a heterozygous KO of vinculin have decreased cardiac function after 6 weeks of TAC [38]. Talin is a cytoskeletal protein increases in protein expression in response to TAC. In addition, talin-1 KO mice have a blunted hypertrophic response to TAC [39]. Talin can recruit focal adhesion kinase (FAK) to the costamere [40]. FAK is a key regulator of cytoskeletal organization and hypertrophic gene expression [41].

The dystroglycan complex also connects to the ECM protein, laminin [42]. Dystroglycan is attached to the actin cytoskeleton via dystrophin [43]. Dystrophin mutations lead to Duchene muscular dystrophy, which is an X-linked muscle-wasting disease [44,45]. Normalized force production and power output are significantly reduced in skeletal muscle of dystrophin KO mice [46].

1.1.2. Stretch Signaling Pathways

Mechanical stretch activates multiple signaling pathways in cardiac myocytes. Some of these pathways include MAPK, Phosphoinositide 3-kinase and Protein Kinase B

(PI3K-Akt), calcium, PKC, calcineurin, Janus-Associated Kinase and Signal Transducers and Activators of Transcription (JAK-STAT), and Small GTPase Ras homolog gene family member A and Rho-associated coiled-coil containing kinase (RhoA-ROCK) signaling pathways.

1.1.2.1. MAPK Signaling

MAPKs are serine/threonine kinases that phosphorylate and activate TFs and other kinases [47]. These MAPKs are downstream of mitogen-activated protein kinase kinases (MEKs) and mitogen-activated protein kinase kinase kinases (MEKKs). The three major MAPKs include ERK, p38 MAPK, and c-Jun N-terminal kinase (JNK). All three MAPKs are activated by mechanical stretch in a matter of 15 minutes [48,49].

These three MAPKs are also involved in hypertrophic signaling. Specific activation of ERK by MEK1 overexpression induces concentric hypertrophy [50]. Similarly, activators of p38 MAPK, MEK3 and MEK6, are sufficient to stimulate cardiac hypertrophy *in vitro* [51]. Thirdly, overexpression of MEK7 activates JNK and causes hypertrophy of cultured cardiac myocytes [52].

1.1.2.2. PI3K-Akt Signaling

PI3K-alpha is a heterodimer that consists of a p110 catalytic subunit and a p85 regulatory subunit [53]. Activated PI3K recruits Akt and phosphoinositide-dependent kinase-1 (PDK1) to the sarcolemma, which allows PDK1 to phosphorylate and activate Akt [54]. Akt1 KO mice do not undergo exercise-induced cardiac hypertrophy, which indicates that PI3K-Akt signaling is critical for physiological hypertrophy [55]. However, chronic overexpression of Akt can lead to cardiac dysfunction. A transgenic mouse with

Akt overexpression was generated and tracked for up to 6 weeks. After 2 weeks, the hearts experience compensated hypertrophy. However, by 6 weeks of Akt overexpression, the phenotype becomes pathological with cardiac dilation [56].

Akt enhances protein synthesis by activation of mammalian target of rapamycin (mTOR). mTOR regulates ribosomal biosynthesis and protein translation by activation of S6 kinases and eukaryotic translation initiation factor 4E (eIF4E) [54,57]. Glycogen synthase kinase-3 beta (GSK3B) is a negative regulator of cardiac TFs and is normally active, but GSK3B is inhibited by Akt-mediated phosphorylation. Targets of GSK3B include NFAT and GATA-binding protein 4 (GATA4) [54,57]. Overexpression of GSK3B blunts cardiac hypertrophy in response to TAC [58].

1.1.2.3. Calcium Signaling

Mechanical stretch induces an increase in intracellular calcium [59,60]. Multiple mechanisms have been proposed to cause this stretch-sensitive increase in calcium. This increase could be caused by an influx of calcium through non-selective stretch-activated cation channels and the L-type calcium channel, which triggers calcium release from the sarcoplasmic reticulum (SR) by ryanodine receptors [59]. Another mechanism is due to an increase in reactive oxygen species (ROS) concentration by stretch. ROS increases the calcium sensitivity of ryanodine receptors, which includes the frequency of calcium sparks [61]. Myofilaments could also supply the increase in intracellular calcium [62]. This could be caused by stretch-induced changes in myofilament calcium sensitivity [63] or by cross-bridge detachment leading to calcium dissociation from troponin C [64]. Elevated calcium levels can enhance PKC, calcineurin, and calcium-calmodulin-

dependent protein kinase (CaMK) signaling and thereby lead to downstream gene expression changes.

1.1.2.4. PKC Signaling

PKC is a serine/threonine kinase that can be activated by secondary messengers, such as calcium or diacylglycerol (DAG) [65]. Mechanical stretch of neonatal cardiac myocytes has been shown to activate PKC [66,67]. PKC can phosphorylate Raf to activate the ERK pathway. PKC activation also leads to phosphorylation of histone deacetylase 5 (HDAC5), which causes nuclear export of HDAC5 [68]. When localized to the nucleus, HDACs promote chromatin condensation. HDAC5 physically interacts with myocyte enhancer factor-2 (MEF2) and inhibits transcription of its target genes by condensation of the promoter region [69]. Therefore, translocation of HDAC5 from the nucleus to the cytoplasm promotes hypertrophic gene expression.

1.1.2.5. Calcineurin Signaling

Calcineurin is a serine/threonine phosphatase that is specifically activated by calcium and calmodulin. NFAT is directly downstream of calcineurin and translocates to the nucleus in response to dephosphorylation [14]. NFAT has a target gene, regulator of calcineurin 1 (Rcan1), which functions as an inhibitor of calcineurin signaling. Rcan1 increases in expression in response to mechanical stretch, which indicates that stretch initiates this negative feedback loop for calcineurin signaling [70]. Additionally, it was found that TAC-induced hypertrophy is blunted by inhibition of calcineurin [71].

1.1.2.6. JAK-STAT Signaling

JAKs are protein tyrosine kinases that become activated by the transmembrane glycoprotein, gp130 [72]. JAKs phosphorylate STATs, which cause STATs to dimerize and translocate to the nucleus. In the nucleus, STATs bind to promoter regions of their target genes and activate gene transcription [49]. The JAK-STAT pathway is activated in stretch of cardiac myocytes [73]. Additionally, overexpression of a dominant negative mutant of gp130 is able to blunt TAC-induced cardiac hypertrophy [74].

1.1.2.7. RhoA-ROCK Signaling

Mechanical stretch can lead to activation of RhoA through integrins [75]. RhoA then binds to ROCK whose signaling prevents actin depolymerization [76]. ROCK can also enhance myosin light chain phosphorylation and increase stress generation by actin and myosin [77]. A consequence of these effects is an increase in the number of focal adhesions [78]. RhoA mediates nuclear translocation of myocardin-related transcription factor (MRTF), which is a co-activator of serum response factor (SRF), and thereby regulates RhoA-dependent gene expression [79].

1.1.3. Stretch-induced Transcription Factors

The various mechanosensitive signaling pathways converge at the nucleus to mediate activation of TFs. Some of these TFs include GATA4, nuclear factor kappa-light-chain-enhancer of activated B cells (NFkB), MEF2, SRF, NFAT, STAT, cyclic adenosine monophosphate response element-binding protein (CREB), forkhead box O (FoxO), cFos, cJun, and cMyc.

1.1.3.1. GATA4

GATA4 is a zinc-finger-containing TF that has been implicated as a mechanical load-responsive mediator of transcription. GATA4 regulates the expression of genes that contribute to cardiac remodeling and ventricular hypertrophy, such as BNP [80]. Overexpression of GATA4 produces cardiac hypertrophy [81]. In contrast, GATA4 KO mice do not hypertrophy in response to TAC [82].

1.1.3.2. NFkB

NFkB transcriptional activity is regulated by inhibitor of kappa B (IkB) and inhibitor of kappa B kinase (IKK). In its inactive state, NFkB is bound to the inhibitor protein IkB and is localized in the cytosol. However, activated IKK phosphorylates IkB causing IkB to dissociate from NFkB. This allows NFkB to translocate to the nucleus and bind to its DNA response element [83,84]. NFkB and IKK activity levels are increased for up to 6 weeks in response to TAC. Transfection of IkB into rat hearts attenuates cardiac hypertrophy and blunts NFkB activity after TAC [85].

1.1.3.3. MEF2

MEF2 is a MADS-box-containing TF that binds to the promoters of muscle-specific differentiation genes and has also been implicated in regulating hypertrophic gene expression [86]. MEF2 transcriptional activity can be enhanced by multiple mechanisms. MEF2 can be directly phosphorylated by p38 MAPK and ERK5 [87,88]. Additionally, nuclear export of HDAC by CaMK and PKC relieves its inhibitory effect of MEF2-dependent transcription [68,69]. Mechanical stretch of cardiac myocytes increases the DNA binding activity of MEF2 [89]. In response to 2 weeks of TAC, mice with

overexpression of MEF2 exhibit DCM as presented with an increase in heart size, a decrease in the ratio of wall thickness to chamber diameter, and a decrease in fractional shortening [90].

1.1.3.4. SRF

SRF regulates transcription by binding to its consensus DNA sequence, $CC(A/T)_6GG$, which is referred to as the CArG box or the serum response element [91,92]. Elevated calcium levels activate CaMK signaling, which causes dissociation of HDAC4 from SRF. This leads to nuclear export of HDAC4 and thereby enhances SRF-dependent transcription [93]. Mechanical stretch causes MRTF to translocate to the nucleus and activate SRF. In addition, mutation of an SRF binding site within the BNP promoter reduces the response of BNP to mechanical stretch [94]. Overexpression of SRF leads to hypertrophy *in vivo* whereas SRF KO leads to DCM [95,96].

1.1.3.5. NFAT

NFAT is a family of TFs that includes NFATc1, NFATc2, NFATc3, NFATc4, and NFAT5, which localizes to the cytoplasm when phosphorylated. The calcium-dependent phosphatase, calcineurin, can dephosphorylate NFAT, which uncovers its nuclear localization signal leading to nuclear import. Conversely, it has been shown that GSK3B can phosphorylate NFAT to mask these signals and induce nuclear export [14]. This is consistent with findings that GSK3B is a negative regulator of hypertrophy [58]. NFAT activity increases in response to cyclic, mechanical stretch of neonatal cardiac myocytes [97]. In addition to directly binding target genes, NFAT is able to physically

interact with other cardiac TFs, such as GATA4 and MEF2, in order to enhance their transcriptional activity [98,99].

1.1.3.6. STAT

STAT is a TF that is phosphorylated by JAK and translocates to nucleus to activate its target genes [49]. Activation of JAK by gp130 mediates this process [72]. Mechanical stretch of cardiac myocytes increases the phosphorylation [73] and DNA binding activity of STAT [100]. Overexpression of STAT3 is sufficient to induce hypertrophy in cardiac myocytes [101].

1.1.3.7. CREB

Cyclic mechanical stretch of cardiac myocytes increases the ratio of nuclear to cytosolic CREB [28]. A binding site for CREB is located in the promoter region of Connexin-43 [102]. These findings indicate that CREB can translocate to the nucleus in response to stretch and activate mechanosensitive genes.

1.1.3.8. FoxO

FoxO TFs are phosphorylated by Akt, which leads to their nuclear export and thereby inactivates FoxO-dependent transcription [103,104]. FoxO signaling regulates atrophy-related genes including atrogin-1. Transfection of FoxO3 into cardiac myocytes prevents stretch-induced increases cell size [105]. These results indicate that FoxO is a negatively regulator of hypertrophy, and it is inhibited by Akt under biomechanical stimulation.

1.1.3.9. cFos and cJun

cFos and cJun are TFs that complex together to form a heterodimer, activator protein 1 (AP-1), which binds to DNA in the promoter region of target genes. An example target gene is a classical marker of cardiac hypertrophy, atrial natriuretic peptide (ANP). The binding site of AP-1 is located at -496 to -489 of the ANP promoter [106]. Mechanically activated ERK1/2 and JNK are transmitted to the nucleus to activate AP-1 [107]. Multiple studies have shown that cFos and cJun are upregulated in cardiac myocytes after mechanical stretch [108,109].

1.1.3.10. cMyc

cMyc is a member of the basic region/helix-loop-helix/leucine zipper family of transcriptional regulators and has a consensus binding sequence of CA(C/T)GTG called the E box [110]. Overexpression of cMyc in mouse hearts induces cardiac hypertrophy as measured by increases in heart size and wall thickness [111]. cMyc also increases in protein expression after cyclic stretch of cardiac myocytes [112].

1.1.4. Anisotropic Stretch

Cardiac myocytes have a rod-like structure with myofilaments spanning the length of the cells and Z-discs oriented in a perpendicular direction. Myocytes also have mechanosensors located both on the longitudinal and the transverse edges of the cell. Therefore, we hypothesized that by stretching cardiac myocytes along orthogonal axes, different signaling pathways and transcription regulators would be activated, which would lead to divergent gene expression profiles. There have been some but not many studies that have explored the effect of stretch axis on the myocyte response.

In micropatterned neonatal rat cardiac myocytes, 24 hours of transverse stretch caused larger increases in the protein expression of Actin, N-cadherin, Connexin-43, and ANP than longitudinal stretch [113]. Another group found that 24 hours of transverse stretch produced a greater increase in the protein expression of phosphorylated and total PKC-delta than longitudinal stretch [67]. Additionally, protein turnover in cardiac myocytes is regulated by stretch axis. After 24 hours, transverse stretch suppressed turnover of contractile proteins, actin, and myosin heavy chain, and therefore promoted protein accumulation. In contrast, longitudinal stretch had no effect on protein turnover [114].

Differences in myocyte response to acute mechanical loading have been observed as well. After 20 minutes of static stretch, ERK1/2 phosphorylation was shown to increase in cardiac myocytes due to longitudinal and transverse stretch. In contrast, FAK phosphorylation only increased with transverse stretch but not with longitudinal stretch [115]. *Ex vivo* mechanical loading of mouse diaphragm muscle for 20 minutes showed that phosphorylation of ERK1/2 and DNA binding activity of AP-1 are induced by both longitudinal and transverse stretch. However, the pathways upstream of this response varied based on stretch axis. Inhibiting the activity of PI3K, Akt, PKC, calcium, or NFkB blunted the response only to longitudinal stretch, whereas inhibition of PKA activity specifically affected the response to transverse stretch [116,117]. These studies support the idea that different signaling pathways are activated in response to mechanical stretch being applied in orthogonal axes.

1.2. RNA Sequencing

RNA sequencing (RNA-Seq) is surpassing microarrays and is becoming the new standard for probing expression changes in the whole genome in response to an experimental stimulus. Some limitations of microarrays include the requirement to decide *a priori* which probe sets will be placed on the microarray and also higher background signal, which makes detection of lowly expressed genes more difficult to identify [118]. The samples are sequenced and then mapped to a reference genome. This approach allows for calculation of gene abundance of known transcripts as well as identification of novel genes.

An RNA-Seq experiment can be broken into three distinct processes once RNA has been obtained from the samples of interest. The first process is preparing the RNA samples and running them on a sequencer to generate RNA-Seq reads. The second step is analysis of these reads in order to determine genes that are differentially expressed (DE) between experimental conditions. The final phase is to perform bioinformatics on these DE genes to identify functions, processes, regulators, and pathways that are involved.

In this dissertation, RNA-Seq was utilized to detect gene expression changes within cardiac myocytes in response to mechanical loading. This section outlines the procedures to perform RNA-Seq and conduct analysis of the data obtained from sequencing.

1.2.1. Preparation of RNA-Seq Samples

RNA is converted to a library of cDNA fragments with adapters ligated to the ends. These adapters prime the fragments to be sequenced and can include a unique

barcode of 5-7 base pairs in length in order to uniquely label fragments that were generated from the same sample. By multiplexing the fragments with these barcodes, fragments may be pooled together and run on the same lane of a flow cell, which eliminates batch and lane effects that could cause variance between samples [119]. RNA-Seq reads can vary from 30 to 400 base pairs in length with longer read lengths being preferable to shorter ones. Additionally, fragments can either be sequenced from one end (single-end) or from both ends (paired-end). The additional information in paired-end reads allows them to be more accurately mapped to their reference genome [120]. However, the tradeoff with longer, paired-end reads is increased cost, which could prevent the user from including sufficient biological replicates for each condition. There are multiple platforms that can be used to sequence RNA. The most common platforms include Illumina HiSeq, Thermo Fisher Ion Torrent, and Roche 454. Each of these platforms has its own mechanism for performing sequencing.

1.2.1.1. Illumina HiSeq

The Illumina HiSeq conducts sequencing by synthesis. The adapters attach the fragments to the flow cell as single stranded DNA. Modified deoxynucleotides (dNTPs) containing a terminator with a fluorescent label are added. The terminator ensures that only one base is added per reaction, and the fluorescent label is unique to one of the 4 dNTPs (dATP, dCTP, dGTP, dTTP). After each reaction, an image is recorded, so that the sequencer can determine the base that was just added. The terminator is then cleaved, and the reaction is repeated to determine the next base in the sequence [121].

1.2.1.2. Thermo Fisher Ion Torrent

The Ion Torrent utilizes semiconductor sequencing technology and relies on changes in pH to sequence the fragments. The system is flooded with a specific dNTP. If that dNTP is complementary to the next base on the template fragment, then the dNTP will be incorporated and a hydrogen ion will be released. If the fragment has multiple, identical bases in a row, then multiple dNTPs will be incorporated multiple hydrogen ions will be released. A change in pH will indicate that specific dNTP was incorporated, and the magnitude of pH change will indicate how many consecutive dNTPs were incorporated. The system is then washed free of that specific dNTP and then one of the other three dNTPs is introduced into the system [121].

1.2.1.3. Roche 454

The Roche 454 system was the first successful next generation system; however, they have recently decided to shut down their sequencer department since they were not able keep up with the other technologies. The Roche 454 system used pyrosequencing technology, which is quite similar to sequencing by synthesis where the dNTP that is incorporated is detected. Instead, pyrosequencing detects the pyrophosphate released during dNTP incorporation [121]. Similar to the other technologies, one of the four dNTPs are added at a time, and the process is repeated to sequence the fragment.

1.2.2. Analysis of RNA-Seq Reads

1.2.2.1. FASTQ Files

The output files from an RNA-Seq experiment are very large in size and are in FASTQ format. Figure 1.1 shows an example of one RNA-Seq read. The first line is the

sequence identifier. This specifies information, such as the sequencer name, the location of the cluster on the flow cell, and the sequence of the index for multiplexing. The second line is the base pair sequence of the RNA-Seq read with the possible letters being A, C, G, and T. The third line is often blank. The fourth line represents the quality score for each base pair in the read. This score indicates the probability that base called by the sequencer was correctly identified. The quality scores in Figure 1.1 are in Sanger format and range from 0 to 40. Each character represents a unique value. For example, "I" represents a score of 40, "D" signifies a score of 35, and "@" corresponds to a score of 31. The equation below shows the conversion from quality score to error probability:

$$Q = -10 \log_{10} P$$

where Q = Quality Score and P = Base-calling Error Probability

Therefore, a quality score of 40 would denote an error probability of 0.01% whereas a score of 30 would be equivalent to an error probability of 0.1%. These FASTQ files often take up a lot of hard disk space since each file contains millions of RNA-Seq reads. As an example, one sample that contains 40 million reads of 51 base pairs in length can occupy about 6.5 gigabytes of disk space. It is important to ensure that there is sufficient storage space on the computer prior to commencing RNA-Seq analysis.

@HWI-ST1001:176:C0GYKACXX:2:1101:1202:2133 1:N:0:NGATGT
GGTGAACCCCCAGACGAAGCGCTCCCGCTGCTTCGGCTTCGTGACCCCCCC
+
@@@DDDDFHHHHGEHIGIIBHIEHIIEGBHEIIBGGGIIEEA=ABBEFDDD

Figure 1.1| Example RNA-Seq Read. An example RNA-Seq read from an RNA-Seq experiment. The first line is the sequence identifier, which indicates information, such as the sequencer name, the location of the cluster on the flow cell, and the sequence of the index for multiplexing. The second line is the 51 base pair sequence of the RNA-Seq read. The fourth line indicates the quality score for each base pair in the read.

1.2.2.2. Quality Control

The first step in an RNA-Seq Analysis pipeline is to perform quality control on the reads. Various tools can be used to determine the read quality of each sample. One such tool is FastQC [122], which provides a comprehensive report with multiple graphs to assess read quality. Two graphs of particular interest display the quality score as a function of the read position and the distribution of quality scores over all sequences. A common feature of reads generated on the Illumina platform is that they tend to decrease in quality as move towards the 3'-end. Too many mismatches between the read and the reference genome can prevent the read from mapping to the genome. One option is to trim off these low quality bases using a tool like FASTX-Toolkit [123] in order to reduce the number of mismatches between the read and the reference genome. This can allow reads to map to the reference genome, which otherwise would not map without trimming.

1.2.2.3. Read Alignment

After quality control is performed, the next step is to align the RNA-Seq reads with the reference genome of interest. Again, there are multiple tools that can be used for

read alignment. The Tuxedo protocol is a common method for RNA-Seq analysis and utilizes the tools, Bowtie [124] and TopHat [125]. Bowtie is a short read aligner that maps large sets of short DNA sequences to large genomes. Bowtie tolerates a specified number of mismatches between the read and the reference genome when performing the alignment. This is why trimming can sometimes allow reads to be mapped by Bowtie that otherwise would not. TopHat is a splice junction mapper for RNA-Seq reads.

Read alignment proceeds in two phases. First, Bowtie tries to directly map reads to the reference genome. Next, TopHat analyzes the mapping results from Bowtie to identify splice junctions that span exons. This second step is necessary because mRNA was used for library preparation, and therefore, intronic regions are not present in the RNA-Seq reads. Therefore, if a read spans multiple exons, then Bowtie will not be able to map the read, but TopHat may be able to. The output files of read mapping are either in sequence alignment map (SAM) or binary alignment map (BAM) format. SAMtools [126] can be used to convert between these two formats, which is important for downstream processing.

1.2.2.4. Estimation of Transcript Abundance

Following read alignment, the next step in the RNA-Seq analysis pipeline is to estimate the abundance of each transcript. Generally speaking, this process utilizes a reference transcriptome and counts the number of reads that uniquely map to each transcript. One interesting point of discussion is how to handle reads that map to multiple locations on the reference transcriptome. If a read maps to two locations, it would be inaccurate to count the read as mapped to both locations since this would be double

counting. Two common tools for calculating transcript abundance, HTSeq [127] and Cufflinks [128], have different approaches to manage multi-mapped reads.

HTSeq has a Python script, htseq-count, which counts the number of aligned RNA-Seq reads (supplied in a SAM or BAM file) that overlaps with the reference transcriptome. This script discards any reads that map to multiple locations. On other hand, Cufflinks, which is a tool in the Tuxedo protocol along with Bowtie and TopHat, does not discard multi-mapped reads. Under the default settings, Cufflinks will uniformly divide each multi-mapped read by the number of locations that it maps to. For example, a read that maps to five locations would count as 0.20 reads at each location. Cufflinks has a couple optional parameters to more accurately estimate transcript abundance. The first option is to provide the fasta file for the reference genome that the reads were mapped to. This instructs Cufflinks to run a bias detection and correction algorithm, which can significantly improve accuracy [129]. Cufflinks also has a multi-mapped read correction option. Cufflinks will perform an initial estimate of transcript abundance based on uniformly distributed multi-mapped reads. Estimates will then be re-calculated by the probability that a read maps to each of its possible genomic locations.

1.2.2.5. Read Normalization and Differential Expression Testing

The next phase is to normalize the read counts and perform differential expression testing. The three most utilized tools used to identify DE genes are edgeR [130], DESeq [131], and Cuffdiff [128]. edgeR and DESeq are both Bioconductor packages that are implemented in R. The first factor that needs to be accounted for in read normalization is the difference in sequencing coverage between samples. For example, if two samples are

sequenced at 20 million reads and 40 million reads, one would expect the read counts to be twice as high in the sample with 40 million reads. A simple strategy to account for this difference in coverage between samples is to divide each read count in a given sample by the total number of mapped reads for sample [132]. This normalization can be biased by extremely abundant genes [133]. Therefore, an alternative method was developed that normalizes by the trimmed mean of M-values [134]. This method is utilized by edgeR, and it functions by calculating the total number of mapped reads only from moderately expressed genes. DESeq calculates scaling factors from the median of the geometric means of fragment reads across all samples [131]. Cuffdiff is a tool within Cufflinks. In addition to normalizing by coverage, Cuffdiff also normalizes by gene length. This normalization is called reads per kilobase of exon per million mapped reads (RPKM). RPKM normalization allows for comparison of gene abundance within a given sample. Read counts are biased by gene length since, by probability, reads are more likely to map to longer genes. It is important to note that normalizing by gene length is unnecessary when perform differential expression testing since the comparisons are made between samples for a given gene. In the classic RPKM normalization, reads counts are normalized by the total number of mapped reads. However, Cuffdiff has an option to instead normalize in the same fashion as DESeq.

Another factor to consider before differential expression testing is the variance of transcript abundance estimates. A Poisson probability distribution assumes that mean abundance is equal to the variance of the abundance. However, in RNA-Seq data, the variance is considerably high than the mean due to differences in biological replicates,

and therefore a Poisson distribution is not valid [131]. Instead, a negative binomial distribution provides a better fit since it includes an additional parameter to account for overdispersion. edgeR, DESeq, and Cuffdiff all utilize a negative binomial distribution, but they have various ways in calculating the dispersion parameter to determine variance. In edgeR, overdispersion is calculated by borrowing information between genes using an empirical Bayes procedure and averages the variability across all genes. DESeq calculates overdispersion in a similar manner to edgeR. However, DESeq fits a global trend to the relationship between mean and variance to calculate the dispersion in a more data-driven manner. Like edgeR and DESeq, Cuffdiff also models overdispersion using a negative binomial distribution. One advantage that Cuffdiff has over the other two tools is that it models uncertainty in read mapping. Alternative splicing and regions with repetitive bases can introduce uncertainty in abundance estimates. Cuffdiff models this uncertainty using a beta distribution [135]. Because edgeR and DESeq do not incorporate uncertainty into their variance estimates, they often define many more genes as DE than Cuffdiff [136]. This could lead to false positives in the genes defined as DE by edgeR and DESeq.

After read counts are normalized and variance has been calculated, a statistical test may be conducted to determine if gene has a statistically significant change in expression between experimental conditions and therefore considered DE. edgeR utilizes an exact test that is analogous to a Fisher's exact test to assess differential expression for each gene [130]. DESeq utilizes a Wald test. Cuffdiff calculates differential expression using the standard score of the logarithm of the ratio of RPKM values between

experimental conditions since this logarithm is approximately normally distributed [128]. The ratio of RPKM values or the ratio of gene abundances is often referred to as the fold change. The equation below depicts this calculation:

$$Z = \frac{\log(A) - \log(B)}{\sqrt{\sigma_{\log(A)} + \sigma_{\log(B)}}}$$

where Z = Standard Score, A = RPKM of sample A, and B = RPKM of sample B

In this equation, the logarithm of the fold change is divided by the standard deviation of the logarithm of the fold change. A standard score of ±1.96 corresponds to a p-value of 0.05. In all three tools, the Benjamini-Hochberg procedure is used to adjust the p-value and control the false discovery rate (FDR). This procedure corrects for multiple comparisons, which is important in RNA-Seq data analysis since thousands of genes are tested for differential expression. DE genes should be determined based on an FDR cutoff as opposed to a p-value cutoff. In addition, some researchers choose to enforce a minimum fold change below which changes in gene expression are considered biologically insignificant even if the changes are determined to be statistically significant.

1.2.3. Bioinformatics Analysis

RNA-Seq analysis identifies hundreds and sometimes thousands of DE genes. It can be very time-inefficient to individually examine all DE genes. Instead, it can often be useful to utilize bioinformatics tools to identify genes or groups of genes that are of interest. There are various methods to cluster genes into different groups, and multiple tools can be used perform these methods. Some different ways to group genes include

hierarchical clustering, molecular function, biological process, cellular component, pathway, upstream regulator, and interaction networks.

1.2.3.1. Hierarchical Clustering

Hierarchical clustering is a method to cluster genes that have similar gene expression profiles based on their fold change values. This method is most useful when there are multiple conditions or at least multiple samples. Each gene is considered an element with n dimensions where each condition and/or sample is a different dimension. Hierarchical clustering groups elements based on their distance from each other. Different metrics can be used to measure the distance between elements. Euclidean distance is a common metric and is referred to as the straight-line distance.

For example with two-dimensional elements, there could be three points or genes with the values: A = (2, 4), B = (5, 5), and C = (6, 6). These values could represent the logarithm of fold change at two different time points where the first coordinate corresponds to the first time point and the second coordinate corresponds to the second time point. Hierarchical clustering would group genes B and C together since they have high fold change values at both time points. In contrast, gene A would be grouped separately since its fold change values are lower, and it has a change in expression between the first and second time point.

Hierarchical clustering can be particularly useful for a time series experiment. In an experimental with two experimental time points, behaviors can be observed, such as genes that are slowly activated, genes that are quickly activated and remain activated, and genes that are quickly activated and return to baseline by the second time point.

Hierarchical clustering will also differentiate between genes that are upregulated and those that are downregulated. The possible expression patterns increase in complexity as additional time points are added, which necessitates using an automated clustering program. Multiple programs, such as MATLAB (The MathWorks, Inc., Natick, MA, USA) and AltAnalyze [137], include scripts to conduct hierarchical clustering.

1.2.3.2. Gene Ontology Analysis

The Gene Ontology (GO) consortium has defined terms that represent the molecular functions, biological processes, and cellular components that genes belong to. This can be useful to identify genes that are involved in a similar function or genes whose protein products are localized together. Enrichment analysis can be performed on a set of DE genes to identify the enriched GO terms. This analysis typically uses a Fisher's exact test to determine the GO terms have a statistically significantly higher number of DE genes than would be expected by random chance. Tools that can be used to perform enrichment analysis include Database for Annotation, Visualization, and Integrated Discovery (DAVID) [138], ToppGene [139], and GO-Elite [140].

1.2.3.3. Pathway Analysis

Multiple databases including Kyoto Encyclopedia of Genes and Genomes (KEGG), WikiPathways, and Reactome contain cellular signaling pathways. These databases can help detect the specific pathways involved in regulating the gene expression changes seen in the RNA-Seq data. Enrichment analysis can also be performed using the same tools and tests in order to identify enriched pathways.

1.2.3.4. Upstream Regulator Analysis

Genes can also be grouped together by having a transcriptional regulator in common. Within QIAGEN's Ingenuity Pathway Analysis (QIAGEN Silicon Valley, Redwood City, CA, USA), there is an upstream regulator analysis tool that can be used to identify the enriched transcriptional regulators mediating the gene expression changes observed in RNA-Seq data. Interactions between transcriptional regulators and target genes are curated in Ingenuity's database. This analysis also produces a consistency to indicate the agreement of the direction of gene expression change between Ingenuity's database and the user's RNA-Seq data.

1.2.3.5. Interaction Networks

Another way to classify genes is by their interaction network. Many of these interactions are derived from yeast two-hybrid systems, which are used to find protein-protein interactions. Tools, such as Search Tool for the Retrieval of Interacting Genes/Proteins (STRING) [141] and Gene Multiple Association Network Integration Algorithm (GeneMANIA) [142], have curated databases of interactions and can be used to identify the interaction networks of DE genes from RNA-Seq data.

1.3. Computational Signaling Network Models

Computational models can be utilized to analyze the function of cell signaling networks [143]. In these signaling networks, nodes are representative of a biochemical species, such as a protein or gene, and edges signify interactions between nodes. These interactions can represent many biological processes, such as protein phosphorylation,

translocation, degradation, or production. In this dissertation, a logic-based network model of cardiac stretch signaling was constructed in order to uncover the mechanisms causing gene expression changes in response to mechanical loading of cardiac myocytes.

1.3.1. Transcriptional Regulatory Networks

Transcriptional regulatory networks can be used to describe gene expression as a function of interactions between regulatory proteins and DNA. Several approaches have been used to construct these networks. Chromatin immunoprecipitation (ChIP) is an experimental technique that can be used to determine if a specific protein, such as a TF, can bind to the promoter region of a gene. Furthermore, ChIP can be combined with a DNA microarray or sequencing in order to probe all genomic regions for potential binding by the TF. These techniques identify direct interactions between TFs and target genes and are critical for constructing transcriptional regulatory networks.

Even though ChIP is able to identify a binding event, it does not necessarily implicate a functional interaction between the TF and target gene. The TF of interest can be perturbed by genetic ablation, suppression through RNA interference, or overexpression [144]. These studies are complemented with genome-wide expression profiling to observe genes that are DE when the TF activity is altered. The direction of change in target gene expression can be used to deduce whether the TF functions as an activator or repressor on the given target gene. A drawback of this technique is that direct and secondary effects cannot be discerned. However, this weakness is circumvented by performing ChIP sequencing in conjunction. These two types of experiments allow for the accurate development of transcriptional regulatory networks.

Typically, these networks are constructed from prior knowledge using the types of experiments described above. However, sometimes this data is not available for the TF of interest. Computational approaches can be used to predict binding interactions between TFs and target genes. Binding motif analysis tools, such as iRegulon [145], utilize position weight matrices to identify the TFs that can bind to a set of genes. These approaches have been used to construct transcriptional regulatory networks in a variety experimental conditions and cell types, such as myogenic differentiation [146], cardiac differentiation [147], and control of cell cycle progression by E2F TFs [144].

Computational models have been generated for some transcriptional regulatory networks. However, many of these models were constructed for lower-level organisms, such as *Saccharomyces cerevisiae* (yeast) [148] and *Escherichia coli* (bacteria) [149]. A network model was constructed for the cold shock response in *Saccharomyces cerevisiae*. A parameter estimation technique using a penalized nonlinear least squares approach was utilized to determine rate constants for the model based on time course microarray data. After estimating appropriate parameters, the model accurately predicted gene expression dynamics and identified the most important TFs in the acute response to cold shock. In another example, a computational model was used to study the transcriptional regulatory network mediating the nutritional stress response in *Escherichia coli* [149]. In regulatory networks with a low number of molecules, it is possible to model the stochastic behavior of their change in concentrations. Gillespie's stochastic stimulation algorithm was used to model the fluctuations in the time delay between biochemical reactions in *Escherichia coli* [150].

1.3.2. Underlying Equations in Network Models

A common feature of signaling network models is that a set of equations will govern how these interactions transmit a signal between nodes. The equation below represents the general form of the change in species concentration in these models [151].

$$\frac{dx_i}{dt} = g_i(x) - d_i(x)$$

where x_i = concentration of species i, g(x) = growth, and d(x) = decay

The specific equations used vary based on the type of model. Hill equations are known to fit well to synthesis and activity rates [151]. Below is an example of a Hill function.

$$g(A) = \frac{[A]^n}{(EC_{50})^n + [A]^n}$$

where [A] = Concentration of species A, EC_{50} = Half-maximal effective concentration, and n = Hill coefficient

The hill coefficient (n) corresponds to the cooperativity of the reaction. A value of one represents no cooperativity, greater than one represents positive cooperativity, and less than one represents negative cooperativity. By this design, g(A) ranges from 0 to 1 as the concentration of A varies from 0 to infinity.

The degradation term in this equation can be expressed by exponential decay.

$$d(A) = \gamma[A]$$

where [A] = Concentration of species A and γ= Decay rate

Hill equations have been used in heart-specific signaling network models, such as a model of cardiac myocyte hypertrophic signaling [152] a model of cardiac beta-adrenergic signaling [153], and a model of cardiac fibroblast signaling [154].

Another example of how to model signaling networks is to use biochemical reactions, which require the initial concentration of reactants and rate constants of each interaction to be specified [155]. Biochemical models have also been used to investigate cardiac beta-adrenergic signaling but required many more parameters to do so [156,157]. The reaction below represents an interaction where species A and B would bind together to form AB.

$$A + B \overset{k_f, k_r}{\Longleftrightarrow} = AB$$

where A, B, and AB are species, k_f = forward rate constant, and k_r = reverse rate constant

The change in concentration of species AB can be modeled by mass action kinetics as follows.

$$\frac{d[AB]}{dt} = k_f[A][B] - k_r[AB]$$

where [A], [B], and [AB] are species concentrations,

k_f = forward rate constant, and k_r = reverse rate constant

A third example is to use flux-based analysis as in the equation below [158]. Metabolic networks using flux-based analysis have been incorporated with transcriptional regulatory network models to predict gene expression changes in *Escherichia coli* [159].

$$\frac{dX}{dt} = S \cdot v$$

where S = stoichiometric matrix, v = reaction fluxes, and X = metabolite concentration

1.3.3. Logic-based Models

Logic-based models are a simple, intuitive way to represent signaling networks. An advantage of logic-based models is that they do not require detailed knowledge of the biochemistry for each interaction. The building blocks of logic-based network models are the logical operators: NOT, OR, and AND. Each of these operators can represent a different biological interaction. A reaction with no logical operators could symbolize transcriptional activation of a target gene. A NOT relationship is representative of an inhibitory reaction. An example of this could be dephosphorylation by a phosphatase. An OR relationship denotes a reaction where the output can be activated by multiple inputs. A biological example would be a protein that has multiple phosphorylation sites for different kinases and binding to either site leads to activation of the target protein. Lastly, an AND gate requires the simulation activation of multiple inputs. This could be symbolic of a reaction where multiple transcription factors must bind to the promoter region in order to activate gene transcription. These operators are shown graphically in Figure 1.2. Nodes, edges, and these logic gates are combined together in order to form a logic-based network model.

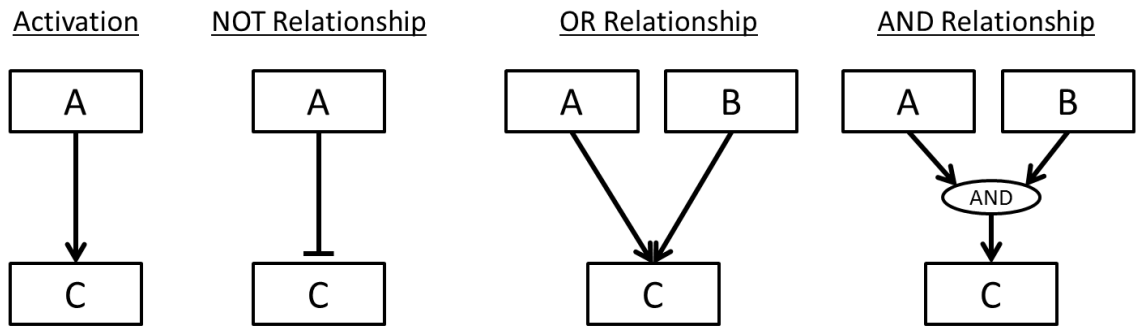

Figure 1.2| Logical Operators. The figure above depicts the various operators used in logic-based models. Nodes A and B represent input nodes, and Node C represents an output node.

In a Boolean network, the possible values of each node are either 1, which indicates the node is on or activated, or 0, which indicates the node is off or inhibited. For a given reaction, truth tables list output values for all possible combinations of input values (Table 1.1). This makes it rather simple to calculate the values of each node in the network.

Table 1.1| Truth Tables The truth tables specify the value of output node C given the values of input nodes A and B. An example is given for each logic gate.

Activation	
A	**C**
0	0
1	1

NOT	
A	**C**
0	1
1	0

OR		
A	**B**	**C**
0	0	0
1	0	1
0	1	1
1	1	1

AND		
A	**B**	**C**
0	0	0
1	0	0
0	1	0
1	1	1

1.3.4. Fuzzy Logic

The assumption in Boolean logic that all nodes are either on or off often does not accurately depict the activity state of a protein. To overcome this, approaches have been developed to model intermediate states of activity in logic-based models. One method is to use a multi-state discrete model to include additional states. A second method is to use fuzzy logic, which transfers logic operators into functions that relate input and output values on a continuous scale [143]. A common transfer function to represent a NOT relationship is:

$$C = 1 - A$$

This formulation allows for input node A to be any value between 0 and 1, inclusive, and the value of output node C will also be on this scale. Different transfer functions have been utilized to represent OR and AND relationships. A common way is to use Zadeh operators where a maximum function represents an OR relationship and a minimum function represents an AND relationship [160]. These representations are pretty intuitive. For example, the input node values could be A = 0.7 and B = 0.4. In an OR reaction, the larger input will determine the output, and therefore the output would be 0.7. In an AND reaction, node B would be the limiting reagent and only allow the output to reach a value of 0.4.

Algebraic relationships can also be used as transfer functions. The equation below is commonly used to represent an OR relationship:

$$C = A + B - A * B$$

This equation leads to different output values than a maximum function. Using the same input node values, the value of output node C would equal 0.82, which is greater than 0.70 obtained by a maximum function. This formulation implies synergy between nodes A and B in the activation of node C.

Similarly, the equation below can represent an AND relationship:

$$C = A * B$$

Again, the outputs from this formulation differ than those from a minimum function. The value of node C would be 0.28 in this example.

1.3.5. Normalized-Hill Differential Equation Modeling Approach

Fuzzy logic overcomes some of the limitations of Boolean networks by allowing nodes to reach intermediate values between 0 and 1. However, there are a couple limitations of fuzzy logic network models. In fuzzy logic, activation is modeled by setting the output node value to the input node value. However, many biological networks exhibit smoothly saturating activation profiles, which are well-approximated by Hill functions [153]. Another drawback of fuzzy logic models is that they do not capture the time course of activation and are limited to the steady-state values. A normalized-Hill differential equation modeling approach surmounts these problems by including both normalized Hill functions and ordinary differential equations. This does increase the number of parameters in the model as compared with fuzzy logic models. However, these models require drastically less data to parameterize than biochemical, kinetic models.

The first part of this modeling approach is to use normalized Hill functions to represent each interaction. In a typical Hill equation, the output value will range from 0 to

1 as the concentration of A varies from 0 to infinity. However, node activity ranges from 0 to 1 for all nodes in logic-based models. In order to constrain the output activity to be 1 when the input node value is 1, a parameter, β, is introduced. Using a normalized Hill function, the steady-state activation of output node C by input node A would be represented as follows:

$$C = f(A) = \frac{\beta * A^n}{K^n + A^n}$$

where A = Activity of node A, C = Steady-State Activity of node C, n = Hill coefficient, β = Normalization parameter #1, and K = Normalization parameter #2

In a typical Hill function, the parameter, K, would represent the half-maximal effective concentration (EC_{50}). However, by normalizing the Hill function by β, this is no longer the case. K can be related to EC_{50} in the following manner:

$$K = \frac{EC_{50}}{\sqrt[n]{1 - 2 * (EC_{50})^n}}$$

In addition, β can be related to EC_{50} using the relationship:

$$\beta = \frac{(EC_{50})^n - 1}{2 * (EC_{50})^n - 1}$$

Therefore, only two parameters, EC_{50} and n, need to be set in order to define the Hill function relating input node A to output node C. By assigning default values to these parameters, reasonable qualitative results may be obtained from these normalized Hill models. Additionally, these parameters can be measured in cellular experiments to quantitatively refine model predictions [153].

The second part of this modeling approach adds ordinary differential equations to the model formulation, which allows for predictions of kinetic behavior. The following equation describes this in the example where input node A activates output node C:

$$\frac{dC}{dt} = \frac{1}{\tau}\left(\frac{\beta * A^n}{K^n + A^n} - C\right)$$

where A = Activity of node A, C = Activity of node C, n = Hill coefficient, τ = Time constant, β = Normalization parameter #1, and K = Normalization parameter #2

By defining the relationship using an ordinary differential equation, only one additional parameter, τ, is added. This parameter may also be set with kinetic data of each reaction. Alternatively, it is possible to assign identical τ values based on the reaction type. For example, phosphorylation events may be assigned one value, translocation events could be assigned a different value, and transcriptional events could be given a third value.

1.4. Aims of the Dissertation

The objective of this dissertation was to investigate differences in the response of cardiac myocytes to different axes of mechanical loading. Experimental and modeling approaches were utilized to identify the signaling pathways, TFs, genes, and gene functions that altered by longitudinal and by transverse stretch. These results grant a better understanding of the regulatory mechanisms downstream of anisotropic stretch in cardiac myocytes.

The first aim of this dissertation was to determine the genes, gene functions, and pathways that are altered in response to longitudinal and transverse stretch. An RNA-Seq experiment was conducted to probe the entire mouse genome for gene expression changes, and bioinformatics analysis was performed to determine the GO terms and pathways enriched with these DE genes. The results showed a more robust gene response to longitudinal than to transverse stretch as evidenced by a greater number of DE genes after 30 minutes and 4 hours of stretch. GO term analysis indicated enrichment of TF activity and protein kinase activity by both axes of stretch; whereas longitudinal but not transverse stretch induced expression of genes involved in sarcomere organization, cytoskeletal protein binding, and potassium channel activity. KEGG pathway analysis indicated that the MAPK signaling pathway was enriched in both transverse and longitudinal stretch. However, the PI3K-Akt signaling pathway and regulation of actin cytoskeleton were specifically enriched in longitudinal response. Overall, this RNA-Seq experiment identified certain genes, pathways, and GO terms that were DE or enriched by both stretch axes as well as additional ones that were specific to longitudinal stretch.

The second aim was to construct a computational model of the mechanical stretch signaling network in cardiac myocytes based on prior knowledge from the literature. This model was validated against independent data from *in vitro* stretch of cardiac myocytes. The model accurately predicted changes in activity/expression of proteins/genes in response to stretch as well as the effect of inhibitors on the stretch response in 54 of 61 data sets. This validated model was then extended to incorporate transcriptional regulation of 645 target genes previously shown to be regulated by the 11 TFs in the

signaling model. This network model includes the signaling pathways and TFs involved in cardiac stretch and can predict the direction and timing of gene expression changes.

The third aim of the dissertation was to utilize the extended signaling network model to identify the mechanisms regulating the gene expression changes seen in the RNA-Seq data. The model correctly predicted the direction of gene expression changes in 95 of the 116 target genes observed to be DE in the RNA-Seq data. GO term analysis on the DE target genes identified SRF and MEF2 as critical regulators of longitudinal stretch-specific upregulated genes that encode for sarcomeric and cytoskeletal proteins. Sensitivity analysis of this expanded network model found that the responses of SRF and MEF2 are regulated by calcium and PKC. Additionally, the model identified CREB as an important regulator of transient activation of its target genes that are sensitive to both transverse and longitudinal stretch and then rapidly deactivated by GSK3B. By analyzing the RNA-Seq data with this model, calcium, PKC, SRF, and MEF2 were implicated as regulators of longitudinal stretch signaling while CREB and GSK3B were identified as mediators of both longitudinal and transverse stretch signaling.

Chapter 2: RNA-Seq Experiment

2.1. Introduction

In the heart, strain induces an increase in size of individual cardiac myocytes [1,3,161], leading to different modes of ventricular hypertrophy [162]. Several intracellular pathways and mechanisms have been implicated in the myocyte response to mechanical loading [2]. The organization of the sarcomere and cytoskeleton suggest that myocytes may respond differentially to mechanical loading applied along different axes. In micropatterned neonatal rat cardiac myocytes, responses to 24 hours of transverse stretch differed significantly from those to longitudinal stretch [67,113]. *Ex vivo* mechanical loading of mouse diaphragm muscle showed that phosphorylation of ERK1/2 and DNA binding activity of AP-1 are induced by both longitudinal and transverse stretch. However, the pathways upstream of this response varied based on stretch axis. Inhibiting the activity of PI3K, Akt, PKC, calcium, or NFkB blunted the response only to longitudinal stretch, whereas inhibition of PKA activity specifically affected the response to transverse stretch [116,117]. Since studies have shown that enough sarcomeres add in neonatal myocytes subjected to longitudinal stretch within six hours that the rest sarcomere length is restored [163], the initial responses to a step change in length are likely to occur much sooner than 24 hours. Moreover, many studies have shown evidence of paracrine and autocrine responses to stretch that may confound stretch axis-dependent responses seen after 24 hours [164]. Therefore, we examined the gene expression profile induced by 30 minutes and 4 hours of anisotropic myocyte stretch using RNA-Seq in

micropatterned neonatal mouse cardiac myocytes stretched primarily longitudinally or transversely to their myofilament axes.

Results of this RNA-Seq analysis displayed a more robust gene response to longitudinal than to transverse stretch as evidenced by a greater number of DE genes after 30 minutes and 4 hours of stretch. GO terms, such TF activity and protein kinase activity, were enriched with genes DE by both stretch axes. On the other hand, longitudinal but not transverse stretch induced expression of genes involved in sarcomere organization, cytoskeletal protein binding, and potassium channel activity. KEGG pathway analysis indicated that the MAPK signaling pathway was enriched in both transverse and longitudinal stretch. However, the PI3K-Akt signaling pathway and regulation of actin cytoskeleton were specifically enriched in longitudinal response. This RNA-Seq experiment identified certain genes, pathways, and GO terms that were DE or enriched by both stretch axes as well as additional ones that were specific to longitudinal stretch.

2.2. Methods

2.2.1. Micropatterning

Cardiac myocytes were cultured on a flexible, microgrooved substrate and subjected to a static mechanical load according to methods derived from previous studies [113,165,166]. The microgrooved substrates were fabricated using soft photolithography and polydimethylsiloxane (PDMS) molding to provide mechanical and extracellular matrix cues to cells on three sides, and permit cell coupling across groove walls. Silicon wafer master molds were micropatterned with SU-8 2005 negative photoresist

(MicroChem Corp., Newton, MA) using a custom photomask (Advance Reproductions Corp., North Andover, MA). Sylgard 186 PDMS, prepared at 10 parts base to 1 part curing agent, was spin-coated on the molds, degassed, and cured at 70 °C for 30 minutes and at room temperature overnight. The resulting 10 μm wide microgrooves were 5 μm in depth and spaced 10 μm apart. The microgrooved PDMS was mounted in custom cell stretchers, and murine laminin (Sigma-Aldrich, St. Louis, MO) was adsorbed under 350 nm wavelength radiation at 10 μg/ml in phosphate buffered saline (PBS) (MediaTech, Manassas, VA). Excess protein was removed by rinsing twice in PBS prior to plating cells.

2.2.2. Isolation and Culture

Cardiac myocytes were isolated from 1–2 day old C57Bl/6J mouse hearts as described previously [166]. Cells were plated in the stretchers at a density of 2 million cardiac myocytes in an area of 1 square inch per stretcher. The cell media consisted of Dulbecco's modified Eagle medium and Medium 199 supplemented with 10% horse serum, 5% fetal bovine serum, 100 units/mL penicillin, and 100 μg/mL streptomycin, and incubated at 37 °C with 10% CO_2. At 72 hours after plating, media was changed to a serum-free media, and cells were cultured for another 24 hours prior to stretch.

2.2.3. Stretch and RNA Extraction

Elliptical stretchers applied an anisotropic, biaxial load on the PDMS with a Lagrangian strain of 14% along the minor axis and 3.6% along the major axis [113]. The PDMS orientation was adjusted during stretcher assembly, such that the cell alignment would be parallel to either the minor (longitudinal stretch) or the major axis (transverse

stretch). Two stretch durations, 30 minutes and 4 hours, and both axes of stretch were studied for a total of 4 different stretch conditions. A fifth condition of non-stretched cells was used as a control. Three stretchers for each condition served as biological replicates. Total RNA was extracted using RNeasy mini kit (Qiagen, Hilden, Germany) and eluted into a volume of 30 µl.

2.2.4. RNA-Seq and Reverse Transcription Polymerase Chain Reaction

TruSeq RNA Sample Prep Kit v2 was used to prepare the cDNA library. The first step was to purify the poly-A–containing mRNA molecules using poly-T oligo-attached magnetic beads. The mRNA was then fragmented into 120–210 base pair pieces by incubating at 94 °C for 8 minutes. The cleaved RNA fragments were copied into first strand cDNA using reverse transcriptase and random hexamers. Second strand cDNA synthesis utilized DNA polymerase I and RNase H. These fragments then went through an end repair process to blunt the ends. A single “A” base was added to the 3' end of the fragment, and then indexed adapters were ligated to the ends. Each adapter had a 7 base pair sequence that was unique to one of the fifteen samples. The products were purified and amplified with PCR. This cDNA was quantified using an Agilent Technologies 2100 Bioanalyzer and then subjected to high-throughput sequencing by Illumina HiSeq 2000. Reverse Transcription Polymerase Chain Reaction (RT-PCR) was performed in an Eppendorf Mastercycler Realplex^2 machine (Eppendorf, Hauppauge, NY, USA) with KAPA SYBR Fast Universal qPCR Kit (Kapa Biosystems, Woburn, MA, USA). Glyceraldehyde 3-phosphate dehydrogenase (GAPDH) was used as the reference gene

for fold change normalization. Primers for RT-PCR (ValueGene, San Diego, CA, USA) are listed in Table 2.1.

Table 2.1| List of RT-PCR Primers

Gene	Forward Sequence	Reverse Sequence
Fos	AGCCCCTGTGTACTCCCGTG	GCCTTGCCTTCTCTGACTGC
Jun	TTCCTCCAGTCCGAGAGCG	TGAGAAGGTCCGAGTTCTTGG
Abra	GCAACCCTGGTTATCAATTTGGC	TTTAGGAGCGTTAGGTAGGTCA
Bach2	GAGGAAACAATGGACTCAGAGAC	GTACTGGGTCAATGCACCCTT
Nppb	TGTTTCTGCTTTTCCTTTATCTGTC	CTCCGACTTTTCTCTTATCAGCTC
Otud1	CAGAGAAACAAGTACCGATTCCA	TCTGGTCCCCGTACACAGTC
Gapdh	AGGTCGGTGTGAACGGATTTG	TGTAGACCATGTAGTTGAGGTCA

2.2.5. RNA-Seq Analysis

A total of 642 million single-end reads with a read length of 51 base pairs were generated in FASTQ format. Quality analysis was performed using FastQC [122]. Based on quality control plots, the last six bases were trimmed from the 3' end of all reads using the FASTQ trimmer in the FASTX-Toolkit (Figure 2.1) [123]. The trimmed RNA-Seq reads were analyzed with the Tuxedo software suite. The reads were mapped to the *mus musculus* genome (UCSC genome mm9) using TopHat v1.4.1 [125]. Cufflinks v2.0.2 was used to assemble aligned reads into transcripts, estimate the abundance of each transcript, and perform differential expression testing [128,129,135]. Abundance of assembled transcripts was reported as RPKM values. Differential expression testing compared abundance in each stretch condition to the control condition, and adjustments for multiple comparisons were performed using the method described by Benjamini and

Hochberg. Genes with an FDR < 0.05 with respect to control were defined as DE. The RNA-Seq data was deposited at the GEO website, accession number GSE83655.

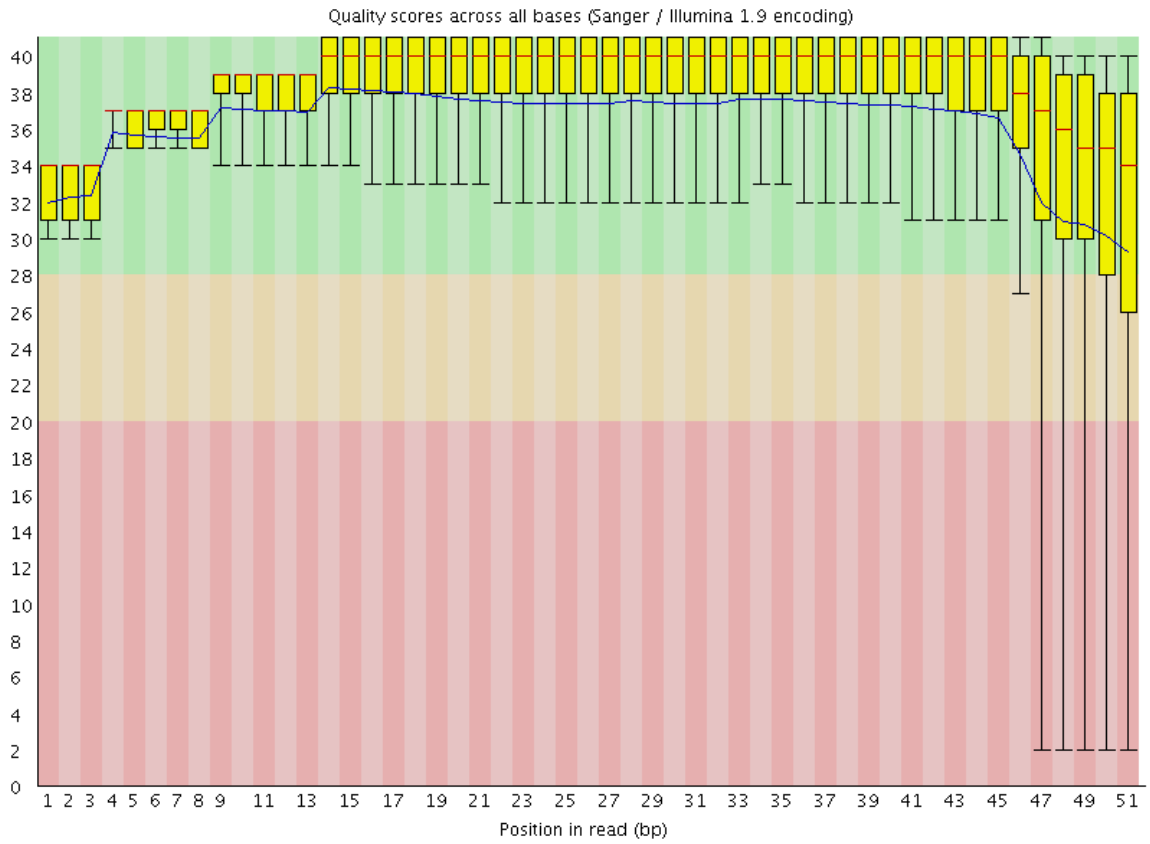

Figure 2.1| Quality Plot of RNA-Seq Reads at Each Position. The graph above is a box and whisker plot indicating quality score of all reads in the sample as a function of position in the read. The yellow box spans from 25% to 75% whereas the whiskers range from 10% to 90%. The mean quality score is displayed with the blue line and the median score is the red line. The background of the graph indicates quality scores that are good (green), reasonable (yellow), or poor (red).

2.2.6. Gene Ontology and Pathway Analysis

Functional and pathway enrichment analysis was performed by comparing DE genes with the GO term and KEGG pathway databases. DE genes were categorized into lists of upregulated or downregulated genes for each stretch condition. These lists were analyzed by ToppGene, which identified enrichment of genes in pathways and gene ontologies [139]. The criteria for classifying a term as enriched were: FDR < 0.05 and number of DE genes > 2.

2.2.7. Immunofluorescence

After stretch for up to 6 hours, cells were fixed in 100% methanol at -20 °C for 10 minutes. Myocytes were then blocked with 3% goat serum in PBS at room temperature for 1 hour. Cells were incubated overnight at 4 °C with mouse alpha-actinin antibody (Sigma-Aldrich #A7811, St. Louis, MO) diluted 1:50 in 1% bovine serum albumin (BSA) in PBS. Second antibody staining was conducted for 2 hour at room temperature with goat anti-mouse Alex Flour 488 (Thermo Fisher Scientific #A11029, Waltham, MA) diluted 1:100 in 1% BSA in PBS. SlowFade Gold Antifade Mountant with 4',6-diamidino-2-phenylindole (DAPI) (Thermo Fisher Scientific #S36938, Waltham, MA) was added to stain nuclei.

Cardiac myocytes were imaged on an Olympus FV1000 confocal microscope. An adapter was required for the stage in order to place the entire stretcher on the microscope. A long working, water-dipping distance 40X objective (Olympus UMPLFL 40XW) was used to image the cells through the PDMS. Figure 2.2 is a representative image of micropatterned cardiac myocytes imaged on the confocal microscope.

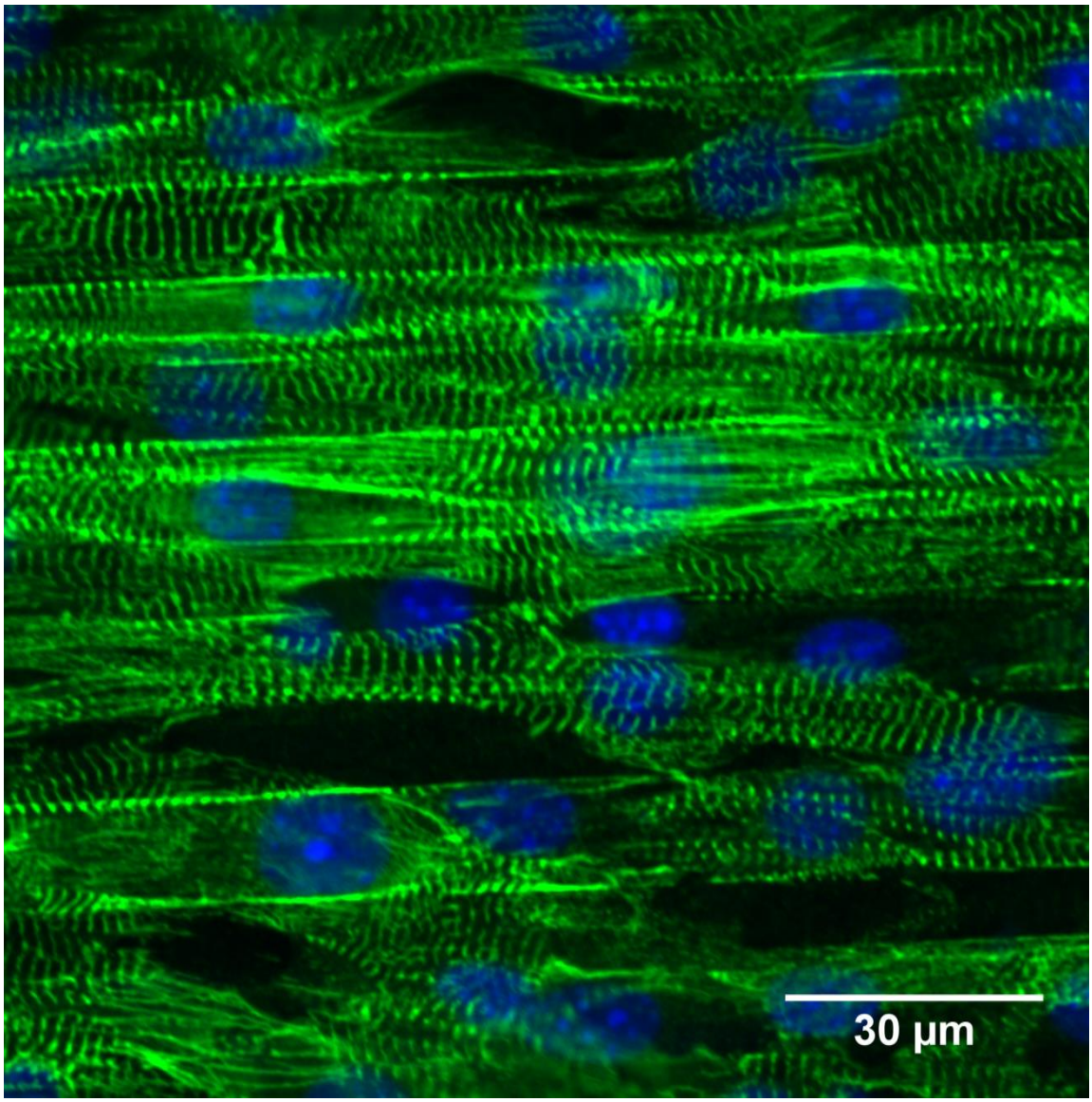

Figure 2.2| Aligned Cardiac Myocytes. The image above was taken at 40X magnification on an Olympus FV1000 confocal microscope. Alpha-actinin is a Z-disc protein and is stained in green. The nuclei are stained with DAPI in blue.

2.2.8. Sarcomere Length Measurement

Multiple images were taken from different fields of on each stretcher and uploaded to ImageJ [167]. To calculate sarcomere length, the intensity profile of the Alexa Fluor 488 channel was measured for regions of repeating sarcomeres (Figure 2.3). Each peak in the intensity profile represents high staining for alpha-actinin and therefore the location of a Z-disc. Sarcomere lengths were measured in approximately 80 cells per stretcher.

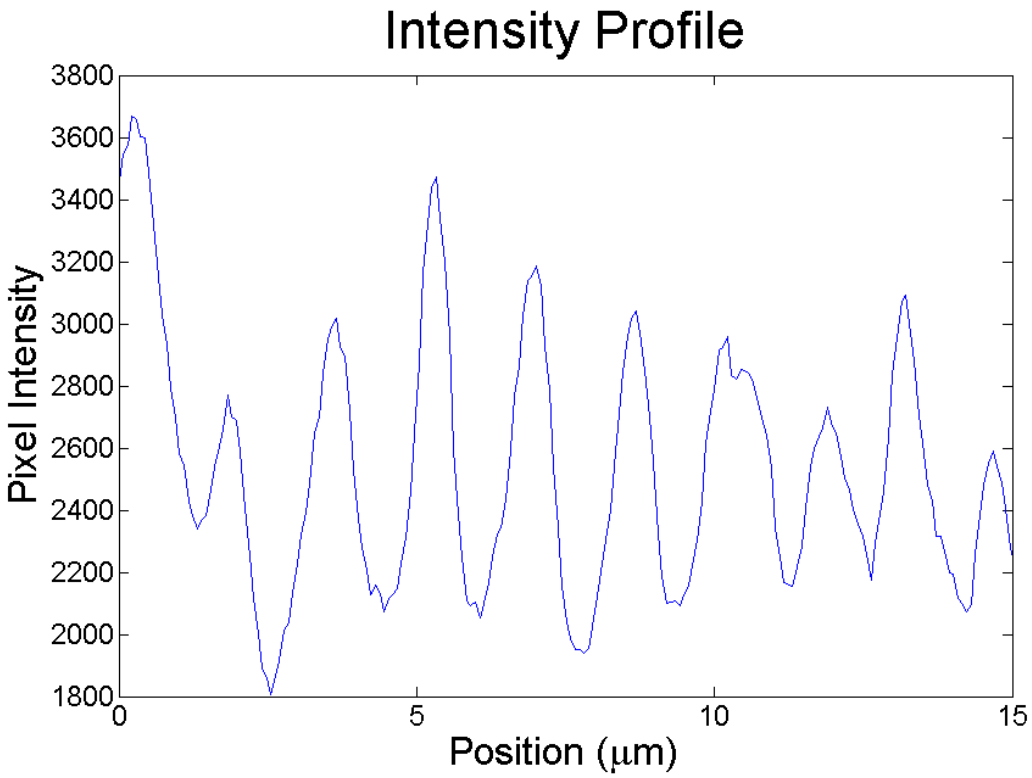

Figure 2.3| Intensity Profile of Alpha-Actinin. The line graph depicts the pixel intensity as a function of position for the Alexa Flour 488 channel, which was bound to alpha-actinin.

To calculate the average sarcomere length for a given intensity profile, a fast Fourier transform (FFT) was applied in MATLAB (The MathWorks, Inc., Natick, MA, USA).. The signal was first processed by detrending the profile to remove the mean value and linear trends from the intensity profile. A Hamming window was applied to account for windowing effects. Figure 2.4 is an FFT of the intensity profile from Figure 2.3. The average sarcomere length is calculated by taking the reciprocal of the frequency with the maximum power.

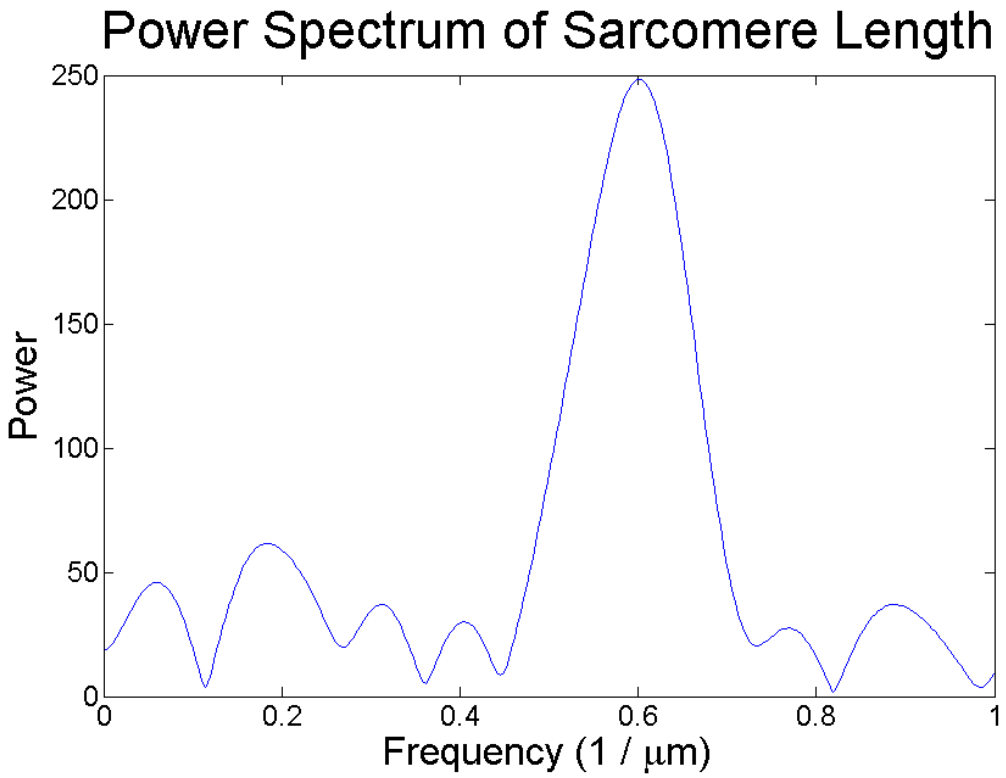

Figure 2.4| Power Spectrum of Sarcomere Length. The line graph is an FFT of the intensity profile of alpha actinin.

2.2.9. Western Blotting

After cardiac myocytes were stretched for 5 minutes, cell lysates were extracted in radioimmunoprecipitation assay (RIPA) buffer (50 mM Tris, 150 mM NaCl, 1.0% Triton X-100, 0.1% sodium dodecyl sulfate (SDS), 0.5% sodium deoxycholate) containing protease and phosphatase inhibitors. Protein concentration was quantified with a BCA Assay. Equal amounts of protein (30 μg) from cell lysates were separated by SDS-polyacrylamide gel electrophoresis (PAGE) and blotted onto polyvinylidene fluoride (PVDF) transfer membranes.

The membranes were blocked for 30 minutes with 5% BSA in Tris buffered saline (TBS)-Tween buffer (10 mM Tris, 0.1 M NaCl, 0.1% Tween 20, pH 7.4). Blots were incubated with rabbit phospho-ERK1/2 antibody (Cell Signaling Technology #9101, Danvers, MA) diluted 1:1000 in 5% BSA in TBS-Tween buffer overnight at 4°C with light agitation. This antibody detects ERK1 phosphorylation at threonine 202 and tyrosine 204 and ERK2 phosphorylation at threonine 185 and tyrosine 187.

Following incubation with primary antibody, blots were washed three times for 5 minutes each with TBS-Tween buffer and incubated with appropriate horseradish peroxidase-labeled anti-rabbit secondary antibody in 5% BSA in TBS-Tween buffer for 1 hour at room temperature. Following three washes of 5 minutes each with TBS-Tween buffer, proteins were detected using enhanced chemiluminescence. Signal from phosphorylated ERK1/2 was normalized to the total ERK1/2 protein, which was obtained by stripping the blot and re-probing with ERK1/2 antibody (Cell Signaling Technology #9102, Danvers, MA). Blots were again striped and probed with beta-tubulin antibody (Cell Signaling Technology #2146, Danvers, MA) to confirm equal loading. Quantification of bands was performed using AlphaView software (ProteinSimple, San Jose, CA).

2.3. Results

2.3.1. DE Genes from RNA-Seq Data

The primary stretch axis was applied either parallel to the cardiac myocyte orientation (longitudinal stretch) or transverse to the myocyte orientation (transverse

stretch). Significant changes in expression (FDR < 0.05), as measured by RNA-Seq, were identified in a total of 843 genes from all stretch conditions (Appendix A). Of these 843 DE genes, 53 are DE at 30 minutes of transverse stretch, 168 are DE at 30 minutes of longitudinal stretch, 35 are DE at 4 hours of transverse stretch, and 795 are DE at 4 hours of longitudinal stretch. The overlap of genes DE in multiple stretch conditions can be visualized in a Venn diagram (Figure 2.5) [168]. By far, the largest gene set contains genes that are only DE in 4 hour longitudinal stretch, which encompasses 652 (77%) of all 843 DE genes. The largest overlapping set contains genes that are DE in longitudinal but not transverse stretch. A high percentage of the genes that are DE with transverse stretch are also DE with longitudinal stretch at the same time point (52/53 = 98% at 30 m; 22/35 = 63% at 4 h). In contrast, only small portion of the DE genes with longitudinal stretch are also DE with transverse stretch at the same time point (52/168 = 31% at 30 m; 22/795 = 3% at 4 h). This finding may indicate that the response to transverse stretch is predominantly a subset of the longitudinal stretch response.

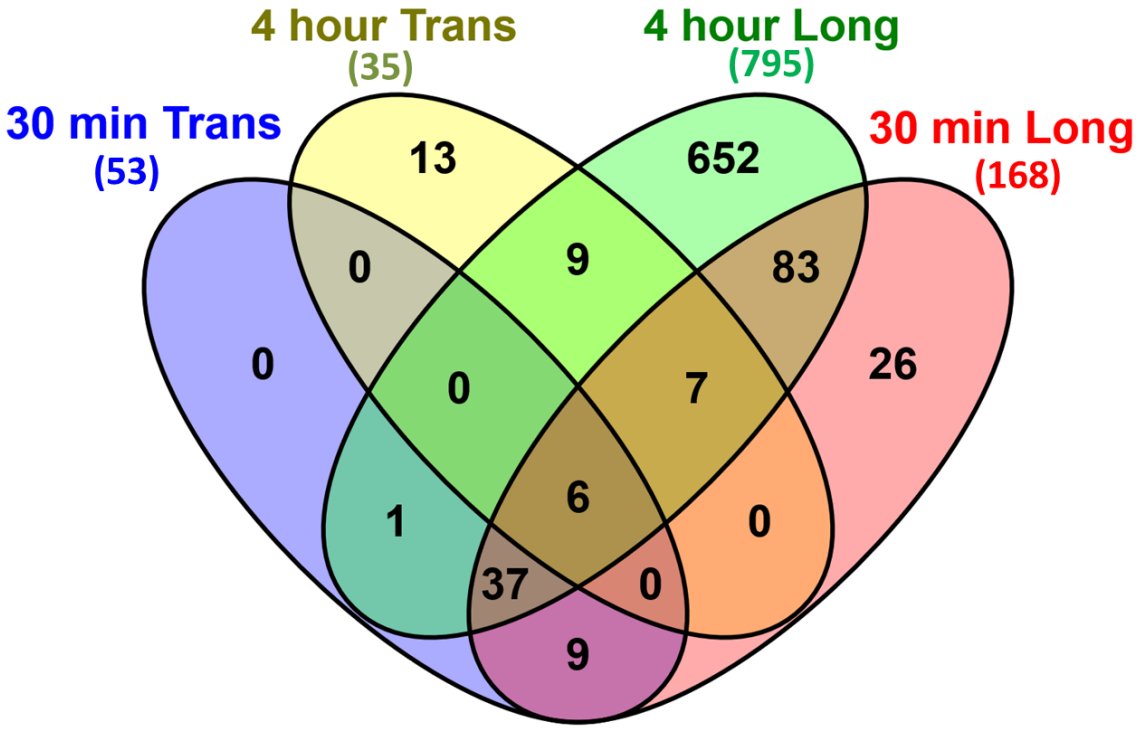

Figure 2.5| Venn Diagram of Stretch-induced DE Genes. Venn diagram displaying the number of DE genes in each stretch condition and their overlap with the other conditions.

Furthermore, the 843 DE genes can be subdivided into 525 upregulated and 318 downregulated genes (Appendix A). At 30 minutes, a large fraction of the DE genes are upregulated with stretch (53/53 = 100% at 30 m transverse; 144/168 = 86% at 30 m longitudinal). In contrast, these fractions are not quite so high at 4 hours (20/35 = 57% at 4 h transverse; 495/795 = 62% at 4 h longitudinal). Figure 2.6 displays the fold change of 30 DE genes that represent each of the 10 gene sets from Figure 2.5. Several genes including Fos, Jun, and Egr1 are highly activated by both longitudinal and transverse

stretch after 30 minutes of stretch but are returning to control expression levels by 4 hours. Other genes like Abra and Nppb remain highly expressed at 4 hours. Lastly, certain genes, such as Ucp3 and Xirp1, specifically change their expression levels due to longitudinal but not due to transverse stretch.

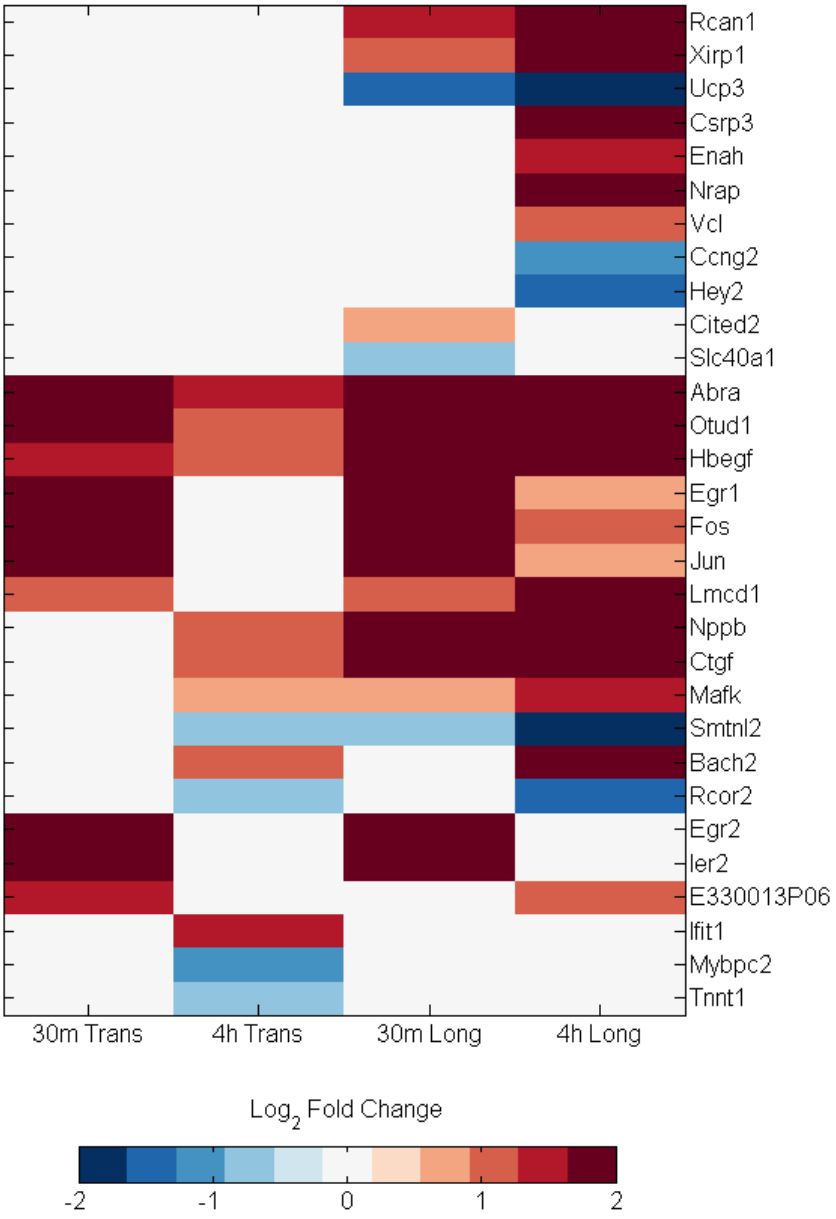

Figure 2.6| Heat Map of 30 Stretch-induced DE Genes. Heat map showing the expression of 30 DE genes, which encompass all 10 clusters from the Venn diagram. Log_2 fold change values are only displayed for genes with a statistically significant change in expression (FDR < 0.05) between stretch and control.

The fold change values for 6 of these genes were validated at 30 minutes or 4 hours using RT-PCR (Figure 2.7). Gene expression changes are very closely matched between RNA-Seq and RT-PCR for the 6 genes tested as seen by a Pearson Correlation Coefficient of 0.97.

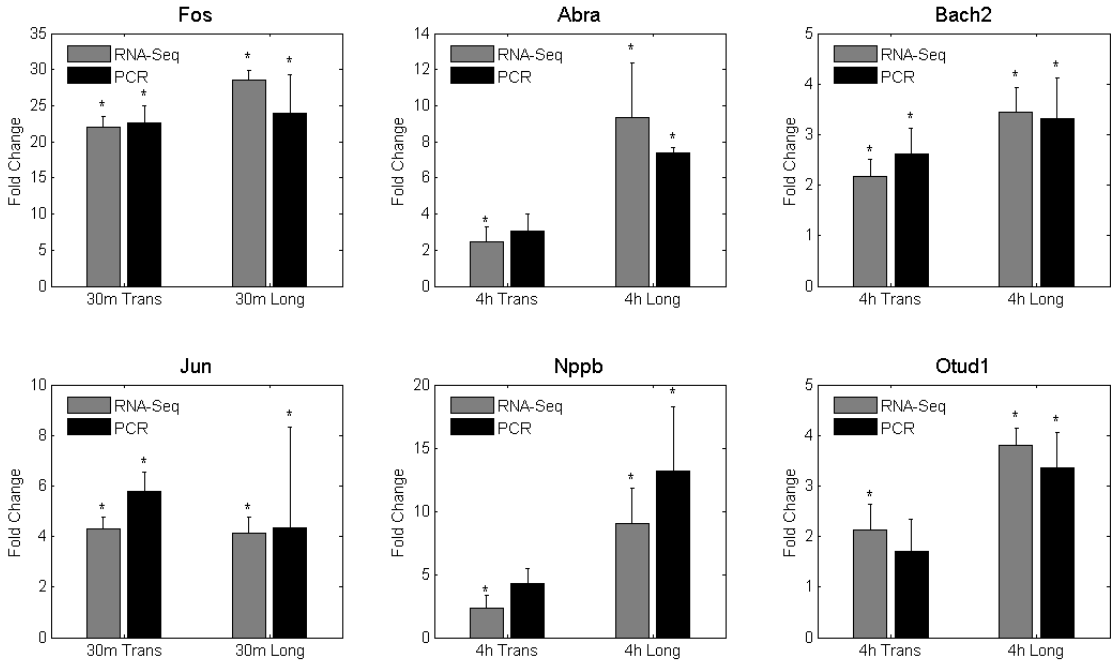

Figure 2.7| RT-PCR Validation of 6 Stretch-induced DE Genes. Fold change values in response to transverse and longitudinal stretch were validated with RT-PCR at 30m (Fos, Jun) and 4h (Abra, Bach2, Nppb, Otud1). Results were considered statistically significant at * $P < 0.05$. Bars represent mean +/- SEM.

2.3.2. Gene Ontology and Pathway Enrichment Analysis

Enrichment analysis of GO terms can help determine the processes, functions, and localization that involve the DE genes. Hundreds of GO terms are enriched with DE genes. Figure 2.8 displays a subset of the enriched biological processes, molecular

functions, and cellular components. Partitioning the DE genes into upregulated and downregulated genes allows us to determine whether enrichment of each GO term is due to increases or decreases in gene expression. Many of the biological processes including cell growth, proliferation, development, cell death, and cell cycle are enriched with upregulated genes in at least 3 of the stretch conditions. It is interesting that there is considerable overlap in GO terms enriched in both transverse and longitudinal stretch despite significantly more genes being DE with longitudinal stretch. This indicates that many of the longitudinal stretch-specific DE genes belong to the biological processes as genes DE by both stretch axes. On the other hand, a few biological processes are specific to longitudinal stretch. Muscle contraction, biological adhesion, and actin cytoskeleton organization are enriched with upregulated genes. Potassium ion transport and cardiac muscle cell action potential are enriched with downregulated genes.

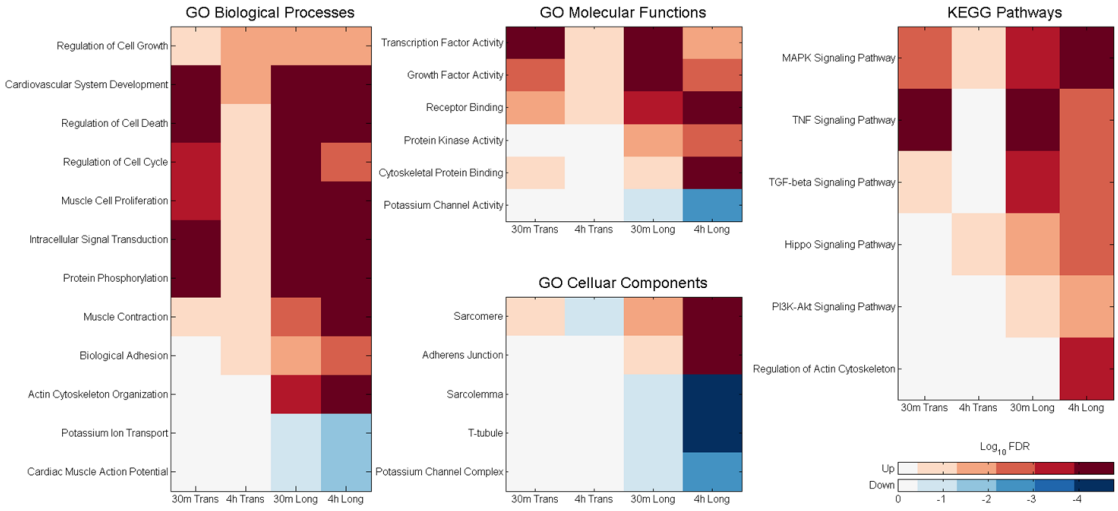

Figure 2.8| Enrichment of GO Terms and KEGG Pathways of RNA-Seq Data. Heat maps showing select terms that were enriched in at least 1 of the 4 stretch conditions. DE genes were categorized as upregulated or downregulated for each stretch condition. The shade of each element represents the $\log_{10}$ FDR of either the upregulated or downregulated genes of that stretch condition. The color indicates whether the upregulated (red) or downregulated (blue) genes had a lower FDR.

Enrichment of GO molecular functions displays a similar trend to the biological processes. There are molecular functions that are enriched in 3 of the stretch conditions, such as TF activity, receptor binding, and growth factor activity. Longitudinal-specific molecular functions include protein kinase activity, cytoskeletal protein binding, and potassium channel activity. Enrichment of GO cellular components is consistent with the other longitudinal-specific GO terms. For upregulated genes, sarcomere and adherens junction appear as enriched, whereas T-tubule and potassium channel complex are enriched with downregulated genes in longitudinal stretch.

Overall, this enrichment analysis identified two groups of associated GO terms that were specific to longitudinal stretch. The first group indicates that cytoskeletal-related functions and processes are specifically activated in longitudinal stretch. The second group of GO terms suggests that potassium ion channels are specifically downregulated with longitudinal stretch.

KEGG pathway enrichment analysis can aid in the identification of the pathways that are involved in regulating the DE genes. We identified 28 pathways enriched with the 525 upregulated genes (Table 2.2).

Table 2.2| KEGG Pathway Enrichment of Upregulated Genes This table lists the KEGG pathways that were enriched with the 525 upregulated genes. The pathway name, FDR, number of genes in a given pathway, and the number of those genes that were DE are displayed.

Name	FDR	DE Genes in Term	Genes in Term
MAPK signaling pathway	5.12E-08	29	259
Focal adhesion	9.56E-06	22	206
Proteoglycans in cancer	1.18E-04	21	225
TNF signaling pathway	1.38E-04	14	110
Hippo signaling pathway	3.20E-04	16	154
TGF-beta signaling pathway	5.19E-04	11	80
Pathogenic Escherichia coli infection	6.44E-04	9	55
Regulation of actin cytoskeleton	1.08E-03	18	215
Endocytosis	1.56E-03	17	203
Chagas disease (American trypanosomiasis)	3.48E-03	11	104
HTLV-I infection	3.48E-03	19	263
Osteoclast differentiation	6.46E-03	12	132
Estrogen signaling pathway	8.57E-03	10	100
Toxoplasmosis	1.00E-02	11	122
Salmonella infection	1.00E-02	9	86
Gap junction	1.21E-02	9	89
Amoebiasis	1.29E-02	10	109
Rap1 signaling pathway	1.29E-02	15	213
Rheumatoid arthritis	1.39E-02	9	93
Bacterial invasion of epithelial cells	1.42E-02	8	76
Cytokine-cytokine receptor interaction	1.43E-02	17	265
Tight junction	1.43E-02	11	134
Colorectal cancer	1.62E-02	7	62
PI3K-Akt signaling pathway	1.82E-02	20	346
Hepatitis B	2.47E-02	11	146
HIF-1 signaling pathway	2.52E-02	9	106
Influenza A	3.90E-02	12	179
Leukocyte transendothelial migration	4.75E-02	9	118

Only 2 pathways were enriched with the 318 downregulated genes (Table 2.3). Enriched pathways of interest include MAPK signaling pathway, PI3K-Akt signaling pathway, and regulation of actin cytoskeleton. We can also divide the genes up by stretch

condition to gain further insights (Figure 2.8). MAPK signaling is enriched in all stretch conditions except 4 hour transverse stretch. PI3K-Akt signaling pathway and regulation of actin cytoskeleton are only enriched at 4 hour longitudinal stretch. Implications of this pathway enrichment analysis are that PI3K-Akt signaling and cytoskeletal-related signaling may be specifically modulated by longitudinal stretch. On the other hand, MAPK signaling pathway appears to be insensitive to stretch axis since it was enriched with genes DE at 30 minutes of both transverse and longitudinal stretch.

Table 2.3| KEGG Pathway Enrichment of Downregulated Genes This table lists the KEGG pathways that were enriched with the 318 downregulated genes. The pathway name, FDR, number of genes in a given pathway, and the number of those genes that were DE are displayed.

Name	FDR	DE Genes in Term	Genes in Term
Circadian entrainment	2.23E-02	8	97
Axon guidance	2.23E-02	9	127

Calcium signaling is another pathway of interest. Although this pathway is not significantly enriched with DE genes, 8 of its 181 genes are DE with stretch. All 8 of these genes are DE with longitudinal stretch, and none are DE with transverse stretch. Seven are DE at 4 hours of longitudinal stretch, and two are DE at 30 minutes of longitudinal stretch. This finding indicates that calcium signaling appears to be specific to longitudinal and not transverse stretch.

2.3.3. Sarcomere Length Results

GO term analysis showed that cytoskeletal protein binding, actin cytoskeleton organization, and sarcomere were enriched with genes upregulated in longitudinal stretch. These genes may be markers of sarcomere remodeling. Therefore, sarcomere length was measured after the application of longitudinal stretch (Figure 2.9). Longitudinal stretch induced an acute increase in sarcomere length from 1.71 μm to 1.79 μm after 5 minutes of stretch. Sarcomere length then began to return to resting length. Sarcomere length decreased to 1.76 μm at 4 hours and then to 1.72 μm at 6 hours. This result supports the idea that cardiac myocytes have a preferred sarcomere length and that longitudinal stretch induces the addition of sarcomeres in series to maintain this length.

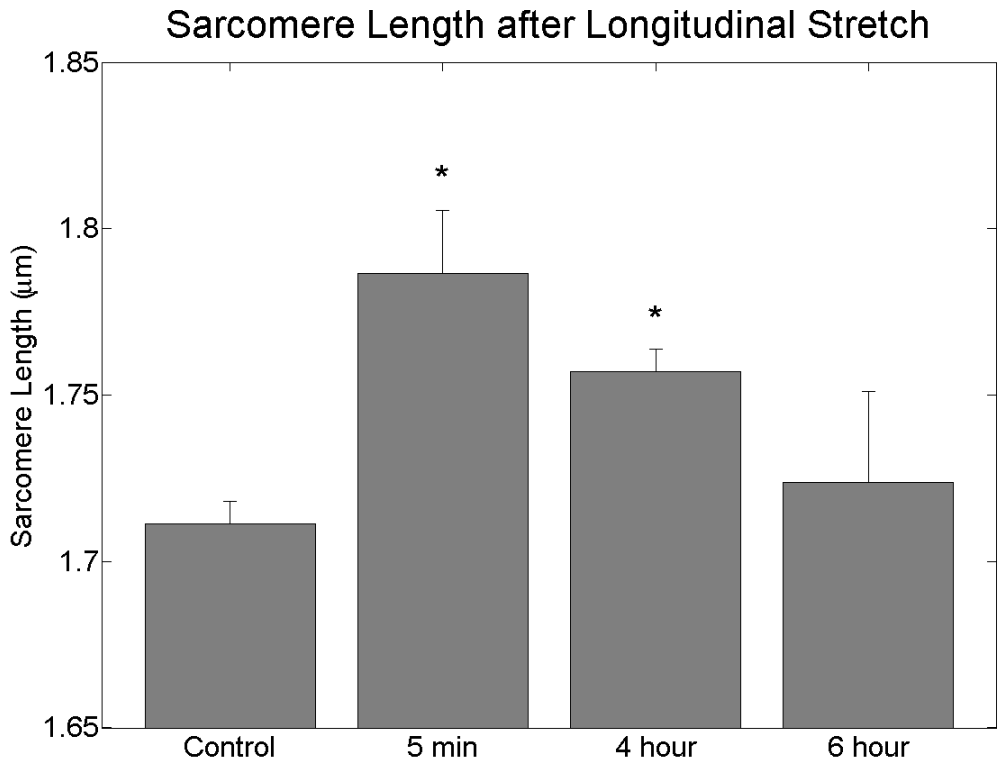

Figure 2.9| Sarcomere Length after Longitudinal Stretch. The bar plot shows the average sarcomere length of longitudinally stretched and non-stretched cardiac myocytes. Each bar is the average of 3stretchers except 5 minute stretch, which is the average of 4 stretchers. Sarcomere lengths were measured in approximately 80 cells per stretcher. Results were considered statistically significant at * $P < 0.05$. Bars represent mean +/- SEM.

2.3.4. MAPK Signaling is Induced by Both Stretch Axes

KEGG pathway analysis indicated that MAPK signaling was enriched with both longitudinal and transverse stretch. ERK1/2 is a kinase in the MAPK signaling pathway that can be rapidly by stretch [169]. Figure 2.10 shows the protein expression levels of phosphorylated and total ERK1/2.

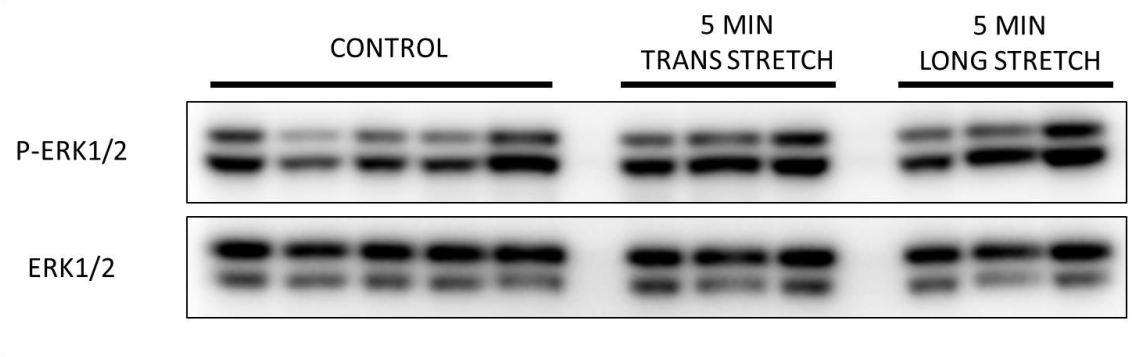

Figure 2.10| Western Blot of ERK Phosphorylation. The figure above is a representative Western Blot of phosphorylated ERK1/2 and total ERK 1/2. Cardiac myocytes were stretched for 5 minutes transversely or longitudinally to stimulate ERK phosphorylation.

In response to five minutes of either longitudinal or transverse stretch, there was an increase in ERK1/2 phosphorylation (Figure 2.11). This indicates that ERK1/2 is a rapidly activated kinase that is not sensitive to the axis of applied stretch.

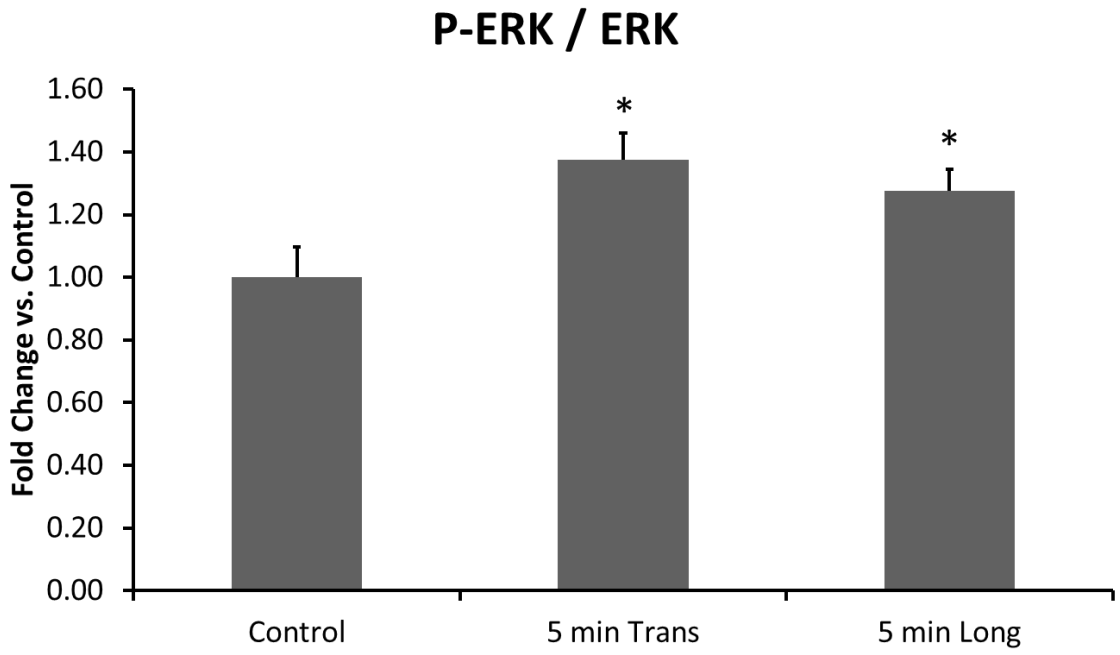

Figure 2.11| Bar Graph of ERK Phosphorylation. The figure above is a bar graph showing the average protein expression of phosphorylated ERK1/2 normalized to the total amount of ERK1/2 in stretched and non-stretched cardiac myocytes. The number of samples for each sample was 9 control stretchers, 6 transverse stretchers, and 7 longitudinal stretchers. Results were considered statistically significant at * $P < 0.05$. Bars represent mean +/- SEM.

2.4. Discussion

Mechanical stretch induces gene expression changes in cardiac myocytes, and many of these previously identified mechanosensitive genes were DE in this RNA-Seq experiment. By applying stretch along different axes, it was determined that longitudinal stretch induces a more robust response in gene expression than transverse stretch. Furthermore, few genes were specifically DE due to transverse stretch, and the majority of genes DE in transverse stretch were also DE in longitudinal stretch. This was especially true at 30 minutes of stretch where 52 of the 53 genes upregulated with

transverse stretch were also upregulated with longitudinal stretch. These results seem to indicate that there are two main groups of DE genes: stretch axis-insensitive genes and longitudinal stretch-specific genes.

Bioinformatics analysis can be used to gain a better understanding of these gene expression changes. Despite such a disparity in the number of DE genes, there was a strikingly similarity in the GO terms that were enriched by either stretch axis. Some of these GO terms in common include TF activity, regulation of cell growth, and cardiovascular system development. Both stretch axes activated immediate early genes, such as Fos, Jun, Egr2, and Ier2. Additionally, genes involved in cardiac hypertrophy, such as Nppb and Hbegf, were activated by longitudinal and transverse stretch.

There were also GO term terms that were specific to longitudinal stretch. Potassium channel activity is a GO molecular function that is enriched with downregulated genes in longitudinal stretch but not in transverse stretch, which may indicate that longitudinal stretch specifically regulates electrical remodeling in cardiac myocytes. Consistent with this RNA-Seq data, cyclic stretch of neonatal rat atrial myocytes for 24 hours has shown to decrease gene expression of the potassium ion channel genes, Kcnq1 and Kcnj2 [170]. Downregulation of the slow delayed rectifying potassium current potassium current (I_{Ks}), which is mediated by the channel encoded by Kcnq1, causes prolonged action potential duration and can promote early afterdepolarizations, which are common features in patients with cardiac dysfunction [171].

In addition, genes involved in cytoskeletal-related functions and processes are specifically activated in longitudinal stretch. We validated this finding by measuring sarcomere length changes after longitudinal stretch. Sarcomere length acutely increased and then by six hours of stretch, sarcomeres returned to their resting length. This mechanism has previously been identified as the addition of sarcomeres in series in order to maintain a preferred sarcomere length [163]. Furthermore, this finding has *in vivo* implications in that longitudinal strain seems to be a stimulus for eccentric hypertrophy, which is characterized by an increase in the length to width aspect ratio of cardiac myocytes due to the addition of sarcomeres in series [172].

Finally, KEGG pathway enrichment analysis was performed to identify the pathways regulating gene expression changes induced by longitudinal and by transverse stretch. MAPK signaling was enriched with genes induced by both stretch axes. Activation of the MAPK signaling pathway was confirmed by measuring changes in protein phosphorylation of ERK1/2. This finding is consistent with previous findings in mouse skeletal muscle that both transverse and longitudinal stretch activates ERK1/2 [116,117]. These results indicate that MAPK signaling is not sensitive to axis of stretch and that this pathway may just be a general growth response.

2.5. Acknowledgements

Chapter 2, in part, is currently being prepared for submission for publication of the material. Buchholz, Kyle S; Tan, Philip; Zambon, Alexander C; Saucerman, Jeffrey J;

McCulloch, Andrew D; Omens, Jeffrey H. Reprinted with permission from all co-authors. The dissertation author was the primary researcher and author of this material.

Chapter 3: Mechanosignaling Network Model

3.1. Introduction

A new network model was adapted from an earlier model of myocyte hypertrophic signaling that utilizes normalized Hill differential equations with logical operators in order to describe the interactions involved in stretch signaling in cardiac myocytes [152]. In this network, receptors are located at the top level and sense mechanical stretch at the cell membrane. Signaling pathways are activated by the receptors and propagate the signal to the nucleus to alter the activity of TFs. This model was validated against independent data from *in vitro* stretch of cardiac myocytes and accurately predicted changes in 54 of 61 data sets. The model was expanded to incorporate transcriptional control of 645 genes shown to be regulated by the 11 TFs in the signaling network model. This network model can be utilized to better understand the signaling pathways and transcriptional regulation that induce gene expression changes seen in response to mechanical stretch in cardiac myocytes.

3.2. Methods

3.2.1. Construction of Mechanosignaling Network

A mechanosignaling network (MSN) was constructed to investigate the mechanisms leading to the gene expression changes after stretch of cardiac myocytes. The interactions of nodes within this network are modeled by logic-based differential equations using normalized Hill functions as described previously [152]. This initial logic-based network contains 85 species (Appendix B) and 113 reactions (Appendix C),

which include receptors, MAPK signaling components, PI3K signaling components, calcium signaling components, cytoskeletal components, and 11 TFs (Figure 3.1).

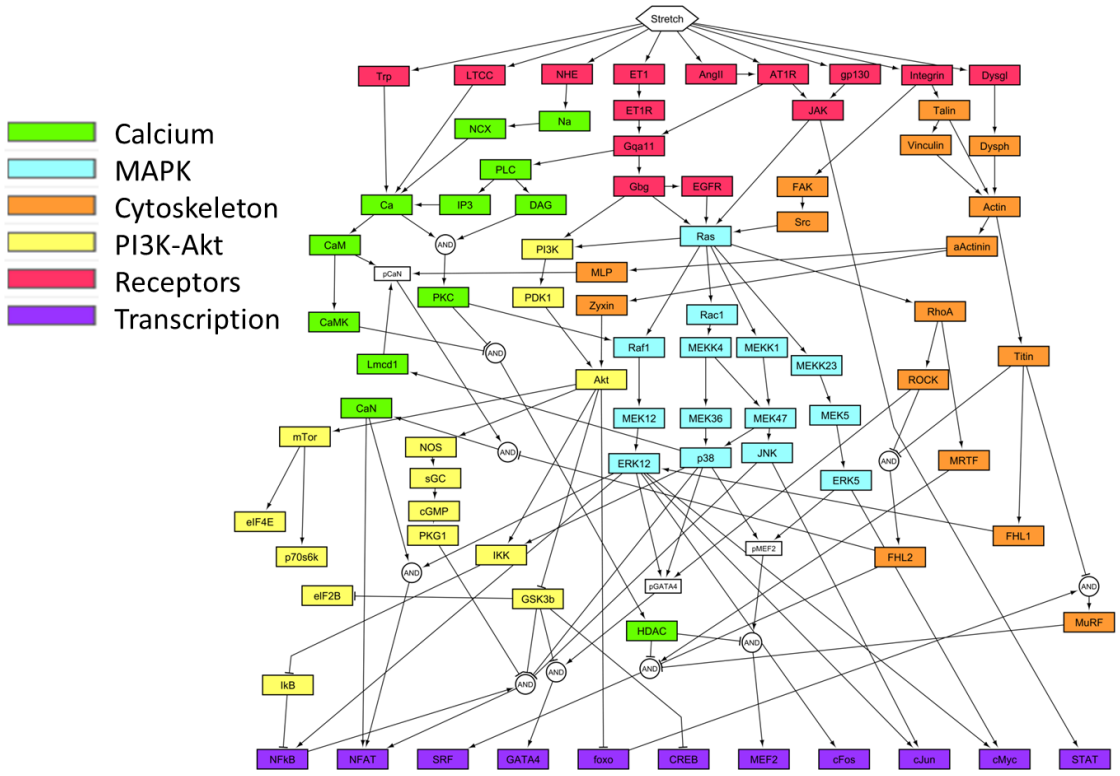

Figure 3.1| Signaling Modules of MSN. The diagram above contains the 85 species and 113 reactions in the MSN. This MSN contains 6 signaling modules, and nodes are colored based on signaling module.

3.2.2. Addition of Target Genes to MSN

Target genes of each TF were identified in the following manner. For each TF, a list of target genes was compiled and the TF's effect on expression direction. Each reaction was substantiated with both co-expression evidence and DNA binding evidence as suggested previously [173]. Co-expression evidence was identified using studies,

preferably in myocytes, where a TF was perturbed, and whole genomic changes were measured by microarray or RNA-Seq. Table 3.1 lists the references of evidence of co-expression between the TFs and their candidate target genes.

Table 3.1| References for Co-expression Evidence This table lists the references of evidence of co-expression between the TFs and their candidate target genes. For each TF, the article(s), the species, and cell type are listed.

TF Name	Author and Year	PubMed ID	Species and cell type
cFos	Durchdewald 2008	18757399 [174]	Mouse keratinocytes
cJun	Arthur-Farraj 2012	22920255 [175]	Mouse Schwann cells
cMyc	Bild 2006	16273092 [176]	Human epithelial cells
cMyc	Frye 2003	12736221 [177]	Mouse whole skin
CREB	Benito 2011	22171029 [178]	Mouse hippocampal neurons
FoxO	Tejera 2013	23733882 [179]	Mouse CD8 T cells
FoxO	Greer 2007	17711846 [180]	Mouse embryonic fibroblasts
GATA4	Chen 2015	26473289 [181]	Mouse Sertoli cells
MEF2	Wales 2014	25217591 [182]	Rat cardiac myocytes
MEF2	Sebastian 2013	23723416 [183]	Mouse myoblast cell line
NFAT	Suehiro 2014	25157100 [184]	Human endothelial cells
NFkB	Chien 2011	21979375 [185]	Human fibroblasts
SRF	Balza 2006	16368687 [186]	Mouse neonatal cardiac myocytes
STAT	Dauer 2005	15735721 [187]	Human epithelial cells

Candidate genes were validated for having a binding site for the TF using iRegulon [145]. iRegulon is a binding motif analysis tool that utilizes position weight matrices from TRANSFAC [188], JASPAR [189], and UNIPROBE [190] to identify the TFs that can bind to a set of genes. Once the target gene list was finalized (Appendix D), reactions were added to the model to simulate their gene transcription by TFs. Target genes regulated by multiple TFs were combined into one reaction with AND operators. Furthermore, the target gene list was cross-referenced against upstream nodes in the

MSN in order to implement feedback loops. Reactions were added to the model in order to simulate protein translation from gene product to the upstream protein node.

This expanded MSN has a total of 730 species, 774 reactions, and 7 distinct signaling modules. Receptors are located at the top level, which sense the mechanical stretch at the cell membrane. Four different signaling pathways, which include calcium signaling, MAPK signaling, PI3K-Akt signaling, and cytoskeletal-related signaling, are activated by the mechanoreceptors. These 4 signaling pathways converge at the nucleus to alter the activity of the 11 TFs, which regulate the expression of their 645 target genes. Of these 645 target genes, 16 encode for an upstream protein in the MSN and therefore feedback loops were included to represent protein translation for each of these. To conserve space, only these 16 target genes are displayed in Figure 3.2.

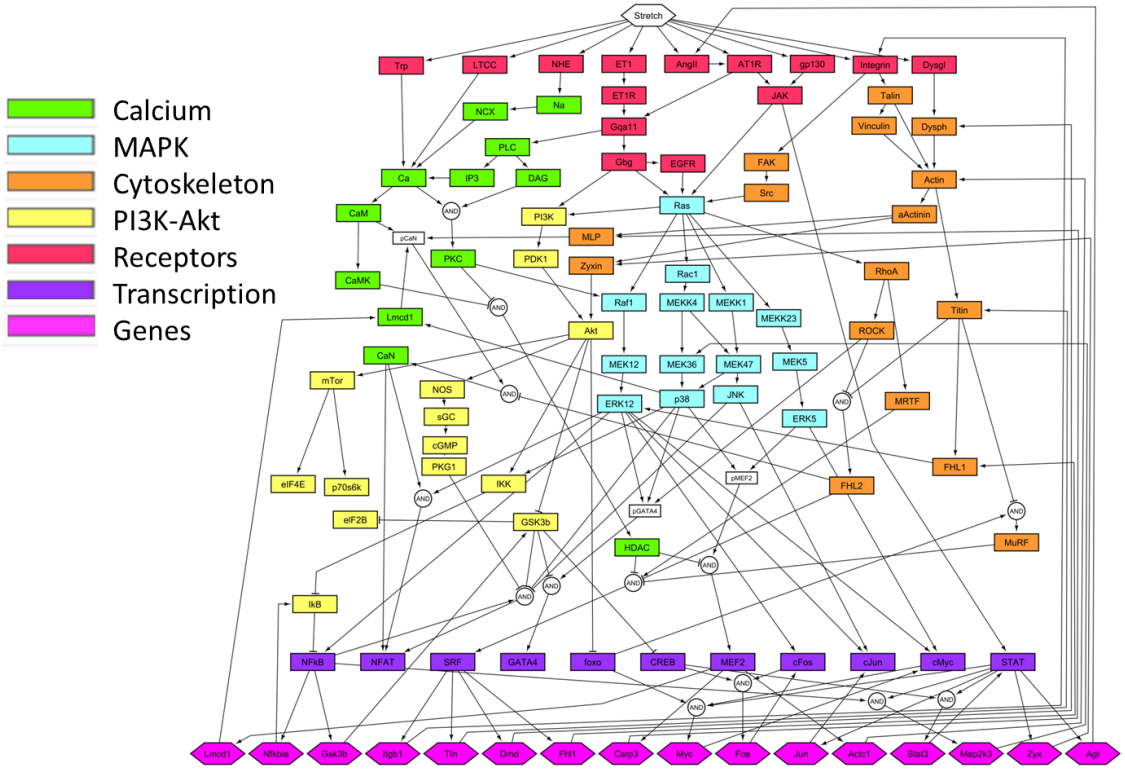

Figure 3.2| Signaling Modules of Expanded MSN. The diagram above contains 101 species, 145 reactions, and 7 signaling modules. Nodes are colored based on signaling module. Of the 645 target genes, the 16 that encode for an upstream protein in the MSN are displayed.

3.2.3. Network Model Parameters

A normalized-Hill differential equation approach, as described previously [153], utilized logical operators, normalized Hill functions, and differential equations to model the interactions between species within the MSN. The activity of each species is normalized and varies between 0 and 1. Default parameters values (weight = 1, n = 1.4, and EC_{50} = 0.5) except τ were used for all reactions. Kinetic parameters for target genes

were determined using an mRNA half-life database [191]. Half-life was converted to the time constant τ using the formula:

$$\tau = \frac{HL}{\ln 2}$$

where τ = Time constant and HL = Half-life

For all other nodes, τ = 30 seconds was used. This time constant allows ERK1/2 and p38 MAPK to reach peak activation by 10 minutes of stretch (Figure 3.3), which matches previous data that maximal phosphorylation of ERK1/2 and p38 MAPK is induced by 10 minutes of stretch [169]. Initial values for each species were determined by setting the input weight for the stretch node to 0 and running the simulation to steady-state.

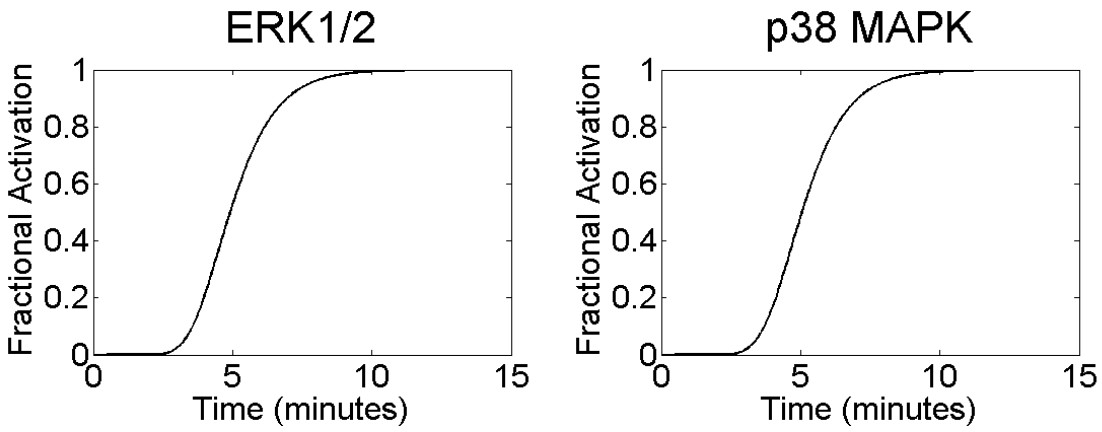

Figure 3.3| Activation of MAPKs by Stretch in MSN. These plots show the change in node activity of ERK1/2 and p38 MAPK after stretch is applied in the model.

3.2.4. Analysis of Network Topology

Network Analyzer [192] is a Cytoscape [193] plug-in that was used to perform topological analysis of the upstream MSN. Topological properties of the network include the mean number of neighbors and the characteristic path length from input to output.

3.2.5. Validation Literature

The upstream portion of MSN was validated against an independent set of stretch experiments. A total of 61 experiments were used for validation (Table 3.2). The names of each node can be found in Appendix B. Thirty-six of these experiments measured the change in a protein's activity or expression in response to stretch of neonatal cardiac myocytes. The remaining 25 experiments measured if a protein had a blunted response to stretch in the presence of an inhibitor. To compare these results with the model, a stretch stimulus of 0.23 was applied and run until steady-state. A minimum change of 10^{-5} was specified as the threshold activity change.

Table 3.2| MSN Validation Literature This table lists the references for the stretch experiments used to validate the MSN. For each experiment, the article, the output node and its measured change in expression or activity, and the node that was knocked out (if applicable) are listed.

Output Node	KO Node	Measurement	Author and Year	PubMed ID
Akt	None	Increase	Baba 2003	12909322 [194]
Ca	None	Increase	Katanosaka 2014	24874017 [195]
CaN	None	Increase	Zobel 2007	17264507 [196]
cFos	None	Increase	Komuro 1990	2105950 [108]
cJun	None	Increase	Sadoshima 1992	1534087 [197]
cMyc	None	Increase	Torsoni 2003	12805241 [112]
CREB	None	Increase	Salameh 2010	20378856 [198]
DAG	None	Increase	Sadoshima 1993	8385610 [66]
EGFR	None	Increase	Kudoh 1998	9727021 [199]
ERK12	None	Increase	Yamazaki 1995	7615816 [200]
FAK	None	Increase	Torsoni 2003	12805241 [112]
GATA4	None	Increase	Pikkarainen 2003	12704188 [201]
GSK3b	None	Decrease	Baba 2003	12909322 [194]
IP3	None	Increase	Sadoshima 1993	8385610 [66]
JAK	None	Increase	Pan 1999	10347087 [73]
JNK	None	Increase	Duquesnes 2009	19015044 [202]
Lmcd1	None	Increase	Luosujarvi 2010	20175653 [203]
MEKK23	None	Increase	Yamazaki 1995	7615816 [200]
MEF2	None	Increase	Nadruz 2005	15961069 [89]
MEK12	None	Increase	Yamazaki 1995	7615816 [200]
MLP	None	Increase	Boateng 2007	16963613 [204]
MRTF	None	Increase	Kuwahara 2010	20606005 [94]
NFAT	None	Increase	Finsen 2011	22164265 [97]
NFkB	None	Increase	Leychenko 2011	22174951 [205]
p38	None	Increase	Lal 2008	18926830 [143]
PI3K	None	Increase	Del Re 2008	18854312 [206]
PKC	None	Increase	Sadoshima 1993	8385610 [66]
PLC	None	Increase	Ruwhof 2001	11162845 [59]
Rac1	None	Increase	Yamane 2007	17207463 [207]
Raf1	None	Increase	Yamazaki 1995	7615816 [200]
Ras	None	Increase	Duquesnes 2009	19015044 [202]

Table 3.2| MSN Validation Literature (Continued) This table lists the references for the stretch experiments used to validate the MSN. For each experiment, the article, the output node and its measured change in expression or activity, and the node that was knocked out (if applicable) are listed.

Output Node	KO Node	Measurement	Author and Year	PubMed ID
RhoA	None	Increase	Kuwahara 2010	20606005 [94]
Src	None	Increase	Aikawa 2002	11847190 [208]
STAT	None	Increase	Wang 2004	15350851 [100]
NOS	None	Increase	Cheng 2009	19673940 [209]
p70s6k	None	Increase	Baba 2003	12909322 [194]
ERK12	Akt	Decrease	Duquesnes 2009	19015044 [202]
ERK12	AT1R	Decrease	Yamazaki 1995	7615816 [200]
Raf1	AT1R	Decrease	Yamazaki 1995	7615816 [200]
STAT	AT1R	Decrease	Wang 2004	15350851 [100]
cFos	Ca	Decrease	Sadoshima 1993	8385610 [66]
JNK	EGFR	No Change	Duquesnes 2009	19015044 [202]
MEK12	EGFR	Decrease	Duquesnes 2009	19015044 [202]
Ras	EGFR	Decrease	Duquesnes 2009	19015044 [202]
STAT	ET1R	No Change	Pan 1999	10347087 [73]
cMyc	FAK	Decrease	Torsoni 2003	12805241 [112]
STAT	gp130	Decrease	Pan 1999	10347087 [73]
STAT	JAK	Decrease	Wang 2004	15350851 [100]
NFAT	MLP	Decrease	Heineke 2005	15665106 [13]
STAT	NHE	Decrease	Pan 1999	10347087 [73]
ERK12	PI3K	Decrease	Duquesnes 2009	19015044 [202]
JNK	PI3K	No Change	Duquesnes 2009	19015044 [202]
Ras	PI3K	Decrease	Duquesnes 2009	19015044 [202]
Raf1	PKC	Decrease	Yamazaki 1995	7615816 [200]
cFos	PLC	Decrease	Sadoshima 1993	8385610 [66]
IP3	PLC	Decrease	Sadoshima 1993	8385610 [66]
ERK12	Ras	No Change	Duquesnes 2009	19015044 [202]
JNK	Ras	No Change	Duquesnes 2009	19015044 [202]
MEK12	Ras	Decrease	Duquesnes 2009	19015044 [202]
MRTF	RhoA	Decrease	Kuwahara 2010	20606005 [94]
Ca	Trp	Decrease	Katanosaka 2014	24874017 [195]

3.3. Results

3.3.1. Network Topology

Network topological properties describe the size and connectivity of the MSN (Table 3.3). The upstream MSN contains 85 species, which are connected by 113 reactions. Each node has an average of 2.884 neighbors, which indicates that there is a decent amount of crosstalk in the network. In a direct network without crosstalk, intermediate nodes would have 1 input node and 1 output, which would lead to an average number of nodes around 2 nodes. The characteristic path length is the average number of nodes between 2 species in the network, which is 4.597 for the upstream MSN.

The network contains 9 receptors of stretch, which include angiotensin II, angiotensin II type 1 receptor, endothelin-1, the L-type calcium channel, the sodium hydrogen exchanger (NHE), transient receptor potential (Trp) channels, gp130, dystroglycan, and integrins. The 11 TFs of the network are cFos, cJun, cMyc, CREB, FoxO, GATA4, MEF2, NFAT, NFkB, SRF, and STAT. There are 64 nodes located in between the receptors and the TFs. Five of these nodes, Ras, calcium, Akt, ERK1/2, and p38 MAPK, are considered hubs because they have at least 6 neighboring nodes. Hubs are influential of downstream signaling because they participate in so many reactions.

Table 3.3| Topological Properties of the Upstream MSN

Number of Species	85
Number of Reactions	113
Average Number of Neighbors	2.884
Characteristic Path Length	4.597
Number of Receptors	9
Number of TFs	11
Number of Hubs	5

The transcriptional regulatory network adds 645 species and 661 reactions to the MSN. The average number of neighbors decreases to 2.328 in the expanded network. This is not surprising since most target genes are only regulated by 1 TF and therefore just have 1 neighbor. The characteristic path length increases to 8.258. There are two reasons why the path length dramatically increases in the expanded MSN. The first reason is that the target genes add an additional level to the MSN, and therefore, one would expect the path length to increase by a little over 1. However, the primary reason is the addition of feedback loops for the 16 target genes that have a corresponding protein in the upstream portion of the MSN.

3.3.2. Validation of Upstream MSN

The upstream portion of the MSN from the receptors to the TF level was validated against stretch experiments, which were independent of the literature used to construct the network. The model correctly predicted the change in expression direction in 54 of the 61 (89%) experiments (Figure 3.4). All 36 input-output predictions changed in the correct direction. In the inhibitor, the investigators observed whether or not there was a

blunted response in the protein of interest when an upstream node was inhibited. Eighteen of the 25 inhibitor predictions were changed in the correct direction. These results validate that the upstream portion of the MSN accurately depicts the signaling pathways that regulate activation of TFs in cardiac myocytes.

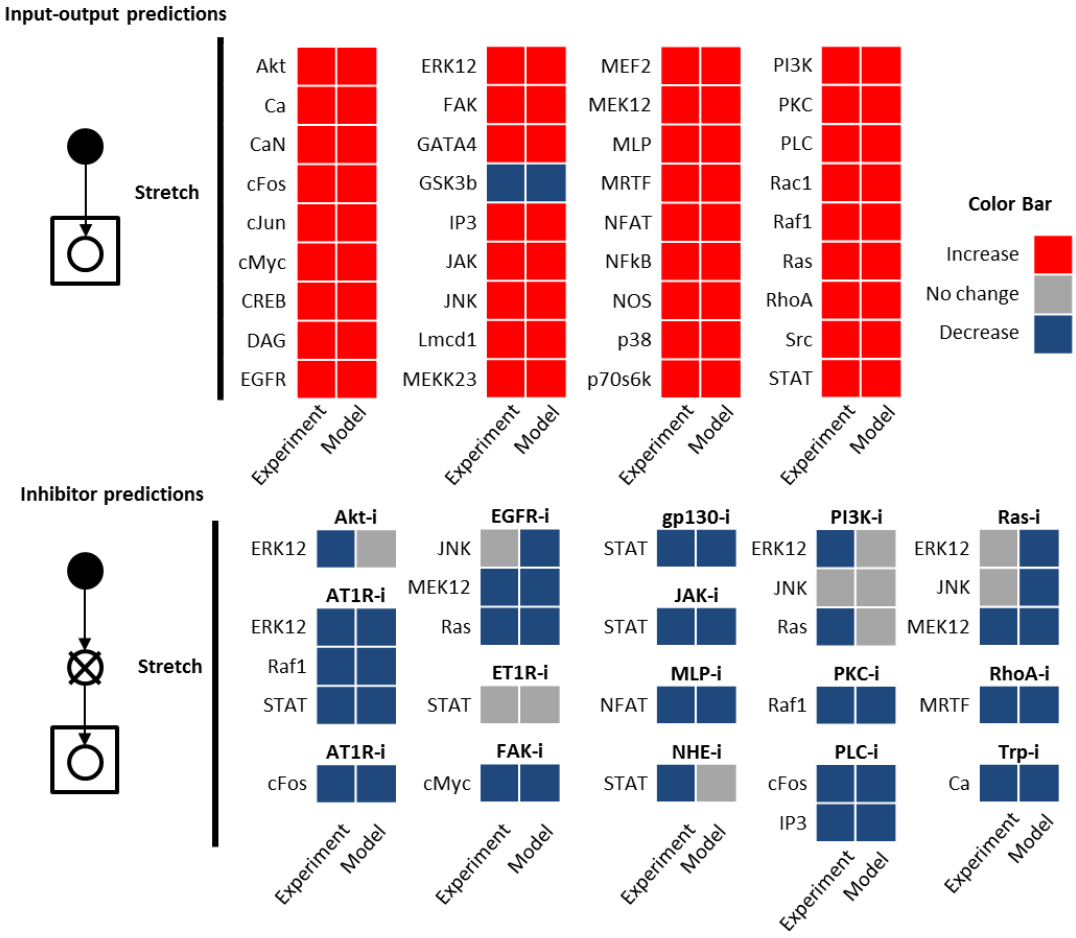

Figure 3.4| Comparison Between Model Predictions and Experiments. The figure above assesses the accuracy of model predictions against 61 independent experiments. For input-output experiments and predictions, red indicates an increase in activity, and blue indicates a decrease in activity after stretch. For inhibitor experiments and predictions, blue indicates a blunted stretch response in the presence of the inhibitor, and gray indicates that the inhibitor had no effect on the stretch response of the protein.

3.3.3. Activity Change of Nodes in MSN

In response to simulated mechanical stretch, nodes in the MSN change in their activity. After 2 minutes of stretch, all of the receptors are activated, but only the upstream nodes of the signaling pathways are activated (Figure 3.5).

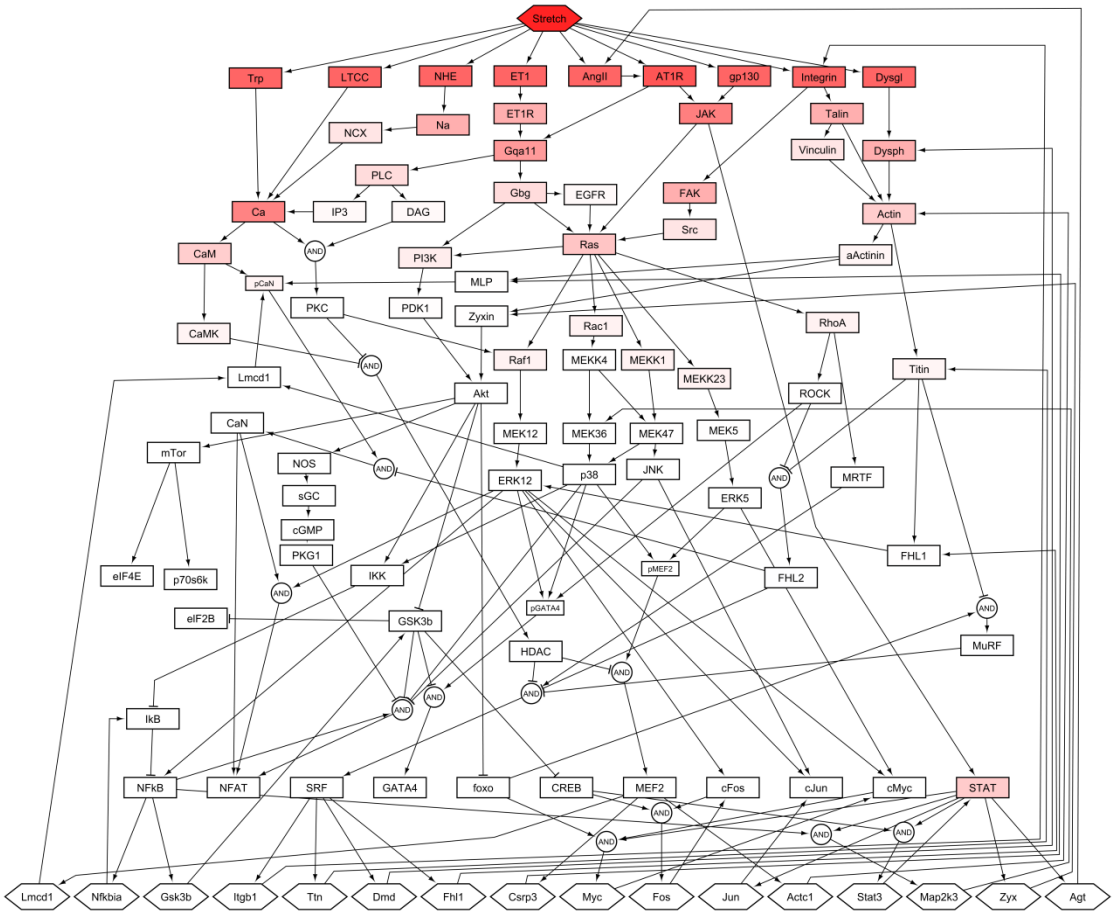

Figure 3.5| Node Activity Change After 2 Minutes of Stretch. The diagram above shows the change in activity of nodes in the MSN after 2 minutes of stretch. A stretch magnitude of 1 was applied. Red indicates an increase in activity, and blue indicates a decrease in activity.

As time progresses, the signal propagates to the nucleus. By 30 minutes of stretch, all nodes upstream of the target genes have reached saturating activity levels. Only 6 of

these 85 nodes decrease in expression with stretch. Some of the target genes have noticeably changed with stretch by 30 minutes, but many of the genes have slower kinetics (Figure 3.6).

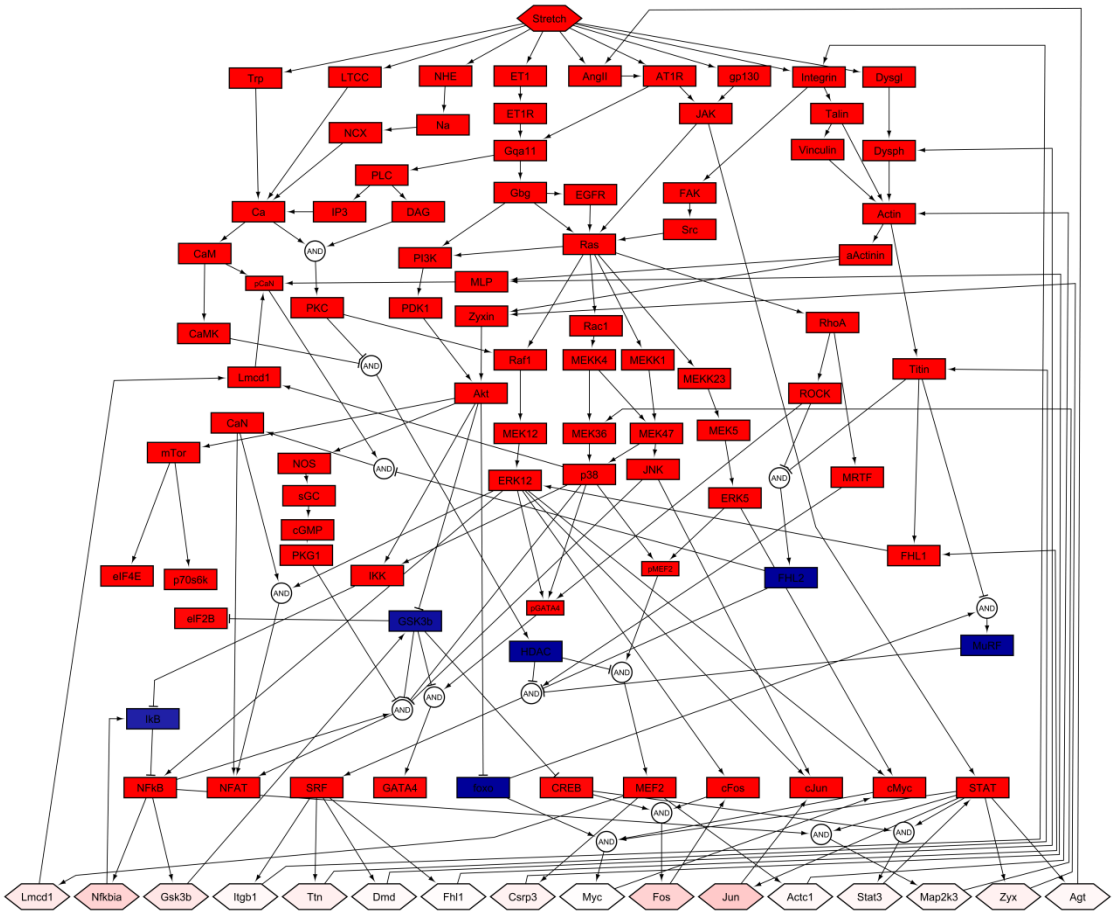

Figure 3.6| Node Activity Change After 30 Minutes of Stretch. The diagram above shows the change in activity of nodes in the MSN after 30 minutes of stretch. A stretch magnitude of 1 was applied. Red indicates an increase in activity, and blue indicates a decrease in activity.

After 4 hours of stretch, node activity has changed in the majority of target genes. The only genes that have not changed in activity are those with both activators and

inhibitors regulating them. Additionally, feedback loops start to play a role around 4 hours. The transcriptional activity of CREB and GATA4 notably decrease due to a feedback loop involving GSK3B (Figure 3.7).

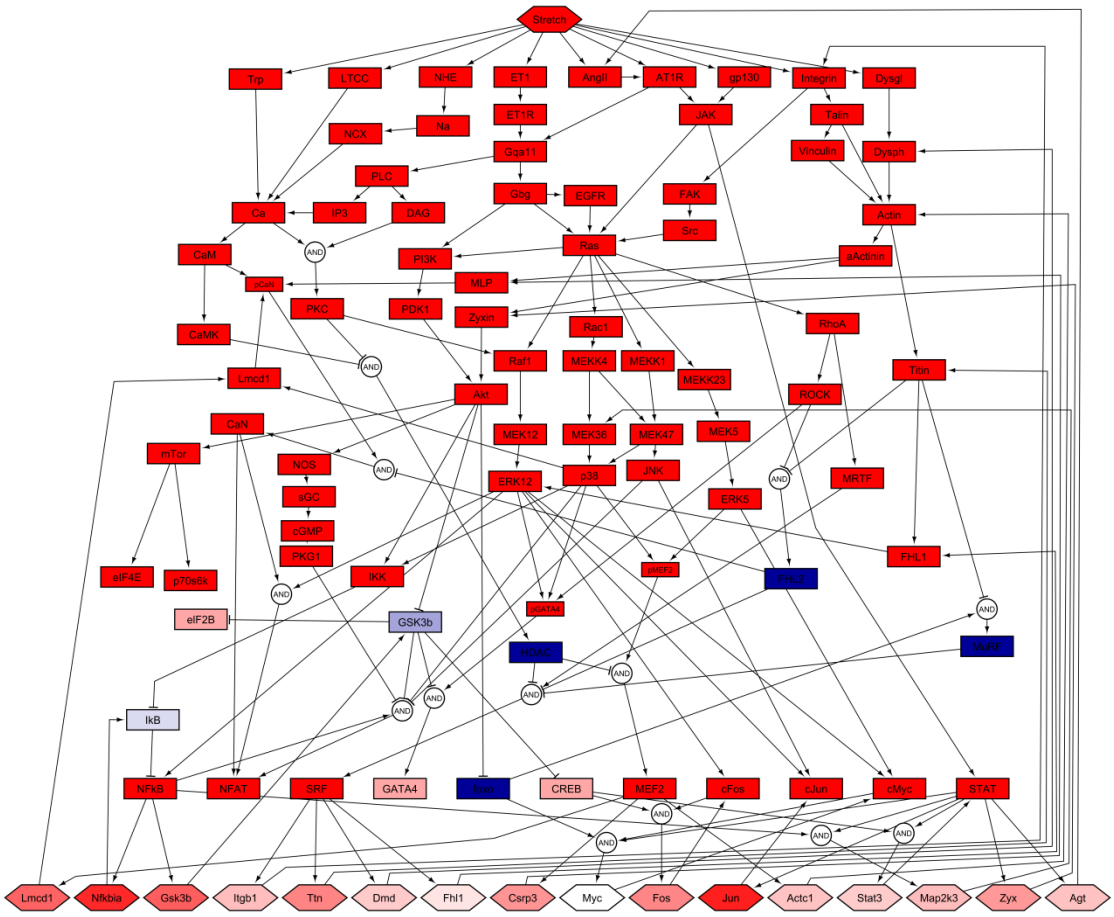

Figure 3.7| Node Activity Change After 4 Hours of Stretch. The diagram above shows the change in activity of nodes in the MSN after 4 hours of stretch. A stretch magnitude of 1 was applied. Red indicates an increase in activity, and blue indicates a decrease in activity.

The previous figures only displayed the change in activity of 16 of the 645 target genes. Figure 3.8 shows the change in activity of all 645 target genes after 12 hours of model simulation. Each row in Figure 3.8 corresponds to the expression profile of a

different target gene, and the rows are organized by the activity change at 12 hours. The majority of targets increase in activity with stretch, which are located at the top of the figure. At the bottom of the figure, several targets decrease in activity with stretch. In between these two groups of genes, there are some interesting behaviors. A group of 21 genes do not change in activity with stretch. These genes are both activated and inhibited by TFs, which prevents their change in activity. Lastly, there are genes that rapidly change in activity but are returning back to control levels by 12 hours. These genes are targets of CREB and GATA4, which are downstream of a negative feedback loop in the MSN.

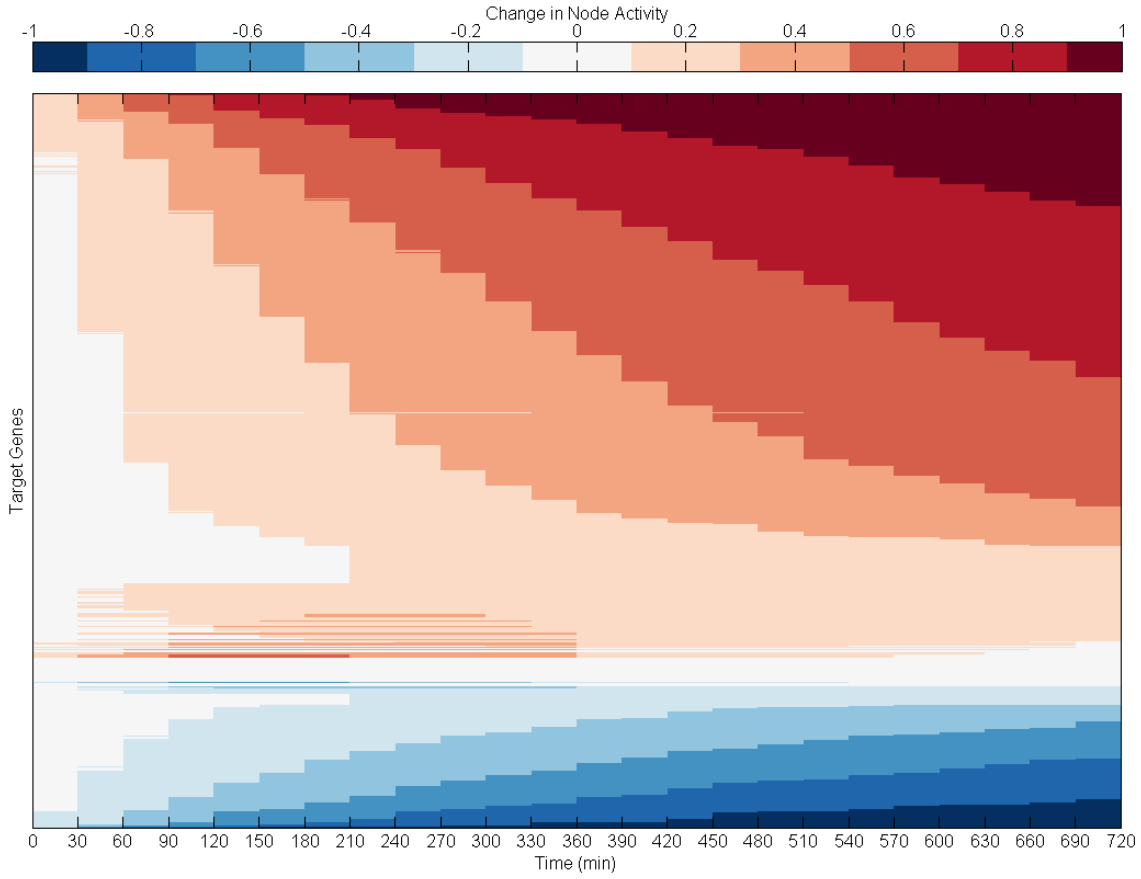

Figure 3.8| Change in Activity of All 645 Target Genes. The diagram above shows the change in activity of all 645 target genes after 12 hours of model simulation. Each row corresponds to a different target gene. Red indicates an increase in model activity, and blue indicates a decrease in model activity.

3.4. Discussion

Computational models of signaling networks are useful for understanding the mechanisms leading to downstream changes. In this chapter, a signaling network of cardiac myocyte stretch was developed based on prior to identify the receptors, signaling pathways, and TFs involved in mechanotransduction. This network includes 9 receptors

of stretch, 4 signaling pathways, and 11 TFs that convert the mechanical stimulus into a cellular response.

This portion of the network model was validated against independent data and accurately predicted the change in expression direction in 54 of the 61 (89%) experiments. This high percentage indicates the upstream signaling network is an accurate depiction of the events that occur in cardiac myocyte stretch signaling. Conversely, there were 7 instances where the model failed to correctly predict the effect of an inhibitor on the stretch response.

In 4 of these failures, the MSN did not predict a blunted response to stretch when the experiments did. These failures indicate that the MSN is missing interactions between existing nodes in the network. In 3 of these 4 failures, the experiments showed that inhibition of PI3K or Akt caused a blunted response of Ras or ERK1/2 to stretch [202]. This implies the PI3K-Akt signaling affects MAPK signaling. The other blunted response that was not predicted by the model was inhibition of NHE blunted the phosphorylation of STAT [73]. In our MSN, NHE leads to increased levels of the hub, calcium. However, we have not identified a direct connection between calcium and STAT. Future experiments should aim to investigate crosstalk between PI3K-Akt and MAPK and the effect of calcium on STAT.

The remaining 3 prediction failures were instances where the model predicted a blunted response that was not seen in the experimental data. In these 3 experiments, either Ras or epidermal growth factor receptor (EGFR) was inhibited, and the stretch-induced phosphorylation of ERK1/2 or JNK was unaffected by the inhibitor [202]. This

result is quite shocking since there is strong evidence that MAPKs are activated by Ras [210], which is downstream of EGFR [211]. This may imply that there is an alternative mechanism that allows for maximal stretch-induced activation of ERK1/2 or JNK in the presence of an inhibitor of Ras.

After the upstream MSN was validated, a transcriptional regulatory network of 645 target genes was added downstream of the TFs. By assigning a unique τ parameter to each gene, the model is able to predict different kinetics for the transcription of each gene. In general, the model predicts monotonic increase or decrease in the expression of target genes. However, the incorporation of negative feedback loops enables transient activation of target genes. This transient behavior is evident with targets of CREB and GATA4. The transcriptional regulation of the MSN will be validated in Chapter 4 using the RNA-Seq data.

3.5. Acknowledgements

Chapter 3, in part, is currently being prepared for submission for publication of the material. Tan, Philip; Buchholz, Kyle S; Omens, Jeffrey H; McCulloch, Andrew D; Saucerman, Jeffrey J. Reprinted with permission from all co-authors. The dissertation author was a primary investigator and author of this material.

Chapter 4: Analysis of RNA-Seq Data with Network Model

4.1. Introduction

To explore the mechanisms regulating gene expression changes observed from RNA-Seq data, we utilized a logic-based stretch signaling network model constructed from prior knowledge. The model correctly predicted the direction of gene expression changes in 95 of the 116 target genes observed to be DE in the RNA-Seq data. By performing GO term and sensitivity analyses, SRF and MEF2 were identified as longitudinal stretch-specific TFs that are mediated by calcium and PKC and upregulate genes that encode for sarcomeric and cytoskeletal proteins. In addition, CREB was determined to be an important regulator of transient activation of its target genes that are sensitive to both transverse and longitudinal stretch and then rapidly deactivated by GSK3B. This network model was successfully able to identify TFs and upstream regulators that modulate gene expression changes in response to anisotropic stretch of cardiac myocytes.

4.2. Methods

4.2.1. Sensitivity Analysis

A sensitivity analysis was performed by simulating individual knockdowns for each species in the network and then measuring the activation of all species in the network after 4 hours of stretch. A stretch stimulus was applied by increasing the input weight for the stretch node to 0.20. Results were displayed as an 82 by 82 sensitivity matrix in order to include all nodes from the MSN. Each value in the matrix is defined as:

$S_{i,j} = \Delta Y_i / \Delta P_j$, where $S_{i,j}$ is the sensitivity of species *i* to knockdown of species *j*, ΔY_i is the change in output of species *i* (control – knockdown), and $\Delta P_j = 1$, when species *j* is being knocked down.

4.2.2. Power Analysis

Power analysis was conducted on the RNA-Seq data. Count files were generated from mapped reads using HTSeq [127]. To filter out genes with low expression, only genes with greater than 1 count per million mapped reads in 3 or more samples were kept. The average number of counts per gene and the biological coefficient of variation for all genes were calculated in edgeR [130]. These values along with an FDR of 0.05 and a minimum log fold change of 0.5 were taken as inputs into the R package ssizeRNA, which was used to calculate power [212].

4.3. Results

4.3.1. Comparison of MSN Results with RNA-Seq Data

In order to compare model predictions and experimental data, the target gene list was reduced to the 570 genes that were expressed in the RNA-Seq data. A stretch stimulus was applied by increasing the input weight for the stretch node from 0 to 1. The number of genes that is defined as DE in the model depends on the threshold activity change. The more stringent the threshold, the fewer number of genes is predicted to be DE in the model. To assess the agreement between the data and model, a true positive rate (TPR) and a true negative rate (TNR) are defined.

$$TPR = \frac{DE\ in\ Data\ and\ Model}{DE\ in\ Data}$$

$$TNR = \frac{Not\ DE\ in\ Data\ and\ Model}{Not\ DE\ in\ Data}$$

Figure 4.1 shows that as the threshold is increased, the TPR decreases while the TNR increases. In order to determine the "optimal" threshold, the Youden Index was calculated at each threshold [213]. The Youden Index is maximal at a threshold of 0.088 for the 30 minute longitudinal data and 0.471 for the 4 hour longitudinal data. A DE threshold of 0.471 is too stringent and causes the model to predict 0 genes to be DE at 30 minutes. Therefore, a DE threshold of 0.088 was selected as the threshold for DE where the model predicts 96 genes to be DE at 30 minutes and 548 genes to be DE at 4 hours.

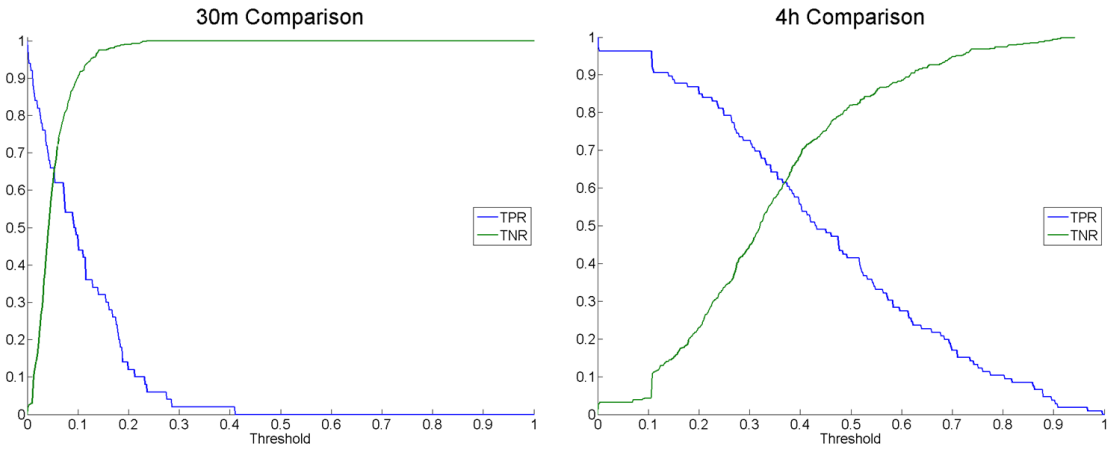

Figure 4.1| Effect of Threshold on Agreement Between Data and Model TPR represents the fraction of DE genes from the Data with an absolute activity change in the model greater than the threshold. TNR represents the fraction of non-DE genes from the Data with an absolute activity change in the model less than the threshold. At each time point, the transverse and longitudinal DE genes were pooled together. (A) 30 minutes (B) 4 hours

Table 4.1 indicates the number of genes that were correctly predicted as DE or not DE by the model in each stretch condition. Of the 95 genes predicted to be DE by the model at 30 minutes, 27 (28%) and 17 (18%) were DE after 30 minutes of longitudinal and transverse stretch, respectively. Conversely, 451 (95%) and 468 (99%) of the 474 genes predicted to be not DE by model matched the RNA-Seq data. There is a similar trend with the 4 hour predictions as well. The high fraction of genes predicted to change in the model that were not found to be DE in the data needs to be interpreted in the context of the statistical power of the RNA-Seq study, which only had three replicates per group and a power of 0.56. This means that the statistical confidence with which we could conclude from the measurements that any specific gene was not significantly changed from stretch is not much better than 50%. Those genes predicted to change in the

model but do not seem change in the data would be good candidates for further experiments with larger sample sizes.

Table 4.1| Agreement of DE Genes Between Data and Model Contingency matrices comparing DE vs. Not DE in the 570 target genes that were expressed in the RNA-Seq data. Genes were defined as DE in the RNA-Seq data for a given stretch condition with FDR < 0.05 and DE at that same time point in the model when Activity Change > 0.10. NC stands for No Change.

30m Long	Model DE	Model NC
Data DE	27	23
Data NC	69	451

4h Long	Model DE	Model NC
Data DE	102	4
Data NC	446	18

30m Trans	Model DE	Model NC
Data DE	17	6
Data NC	79	468

4h Trans	Model DE	Model NC
Data DE	6	0
Data NC	542	22

Table 4.2 indicates the agreement in expression direction for genes that were identified as DE by both the model and the data. At 30 minutes, the model correctly predicts the direction of change for 26 of 27 DE genes (96%) with longitudinal stretch and 16 of 17 DE genes (94%) with transverse stretch. The majority of these DE genes are identified as upregulated by both the model and in the data. At 4 hours, the model correctly predicts the change in direction for 87 of 102 DE genes (85%) with longitudinal stretch and 5 of 6 DE genes (83%) with transverse stretch. There are still a greater number of upregulated genes than downregulated genes at 4 hours. However, the disparity is not as great as at 30 minutes. Overall, the agreement in expression direction for genes that are DE in the model and the data is quite high. This indicates that the

model can accurately capture the regulatory mechanisms that induce expression changes in these genes.

Table 4.2| Agreement in Expression Direction Between Data and Model Contingency matrices comparing the change in expression direction of genes that were DE in the RNA-Seq data for a given stretch condition (FDR < 0.05) and DE at that same time point in the model (Activity Change > 0.10).

30m Long	Model Up	Model Down
Data Up	26	1
Data Down	0	0

4h Long	Model Up	Model Down
Data Up	84	7
Data Down	8	3

30m Trans	Model Up	Model Down
Data Up	16	1
Data Down	0	0

4h Trans	Model Up	Model Down
Data Up	5	1
Data Down	0	0

Specific examples can also illustrate the agreement between the model and the longitudinal stretch data (Figure 4.2). Ier2 is up 6.49-fold at 30 minutes and is only up 1.33-fold at 4 hours. The MSN is able to model this phasic temporal behavior due to a GSK3B feedback loop. GSK3B has a rapid decrease in activity due to phosphorylation by Akt. However, GSK3B gene expression increases over time, which leads to an increase in its protein activity. The net effect on Ier2 gene expression is a rapid increase in expression after stretch, followed by a decay back to control levels (Figure 4.2A). The time course of this behavior is a bit slower in the model than in the data. This indicates that the rate of gene transcription for Ier2 is much faster than the model prediction. Nevertheless, this phasic behavior of Ier2 could be explained by a GSK3B feedback loop. Another example illustrating the agreement between the data and the model can be seen

with Mafk gene expression. Mafk is up 1.83-fold at 30 minutes and is up 2.84-fold at 4 hours. The MSN models this steady climb in gene expression due to increases in activity of cFos and STAT (Figure 4.2B).

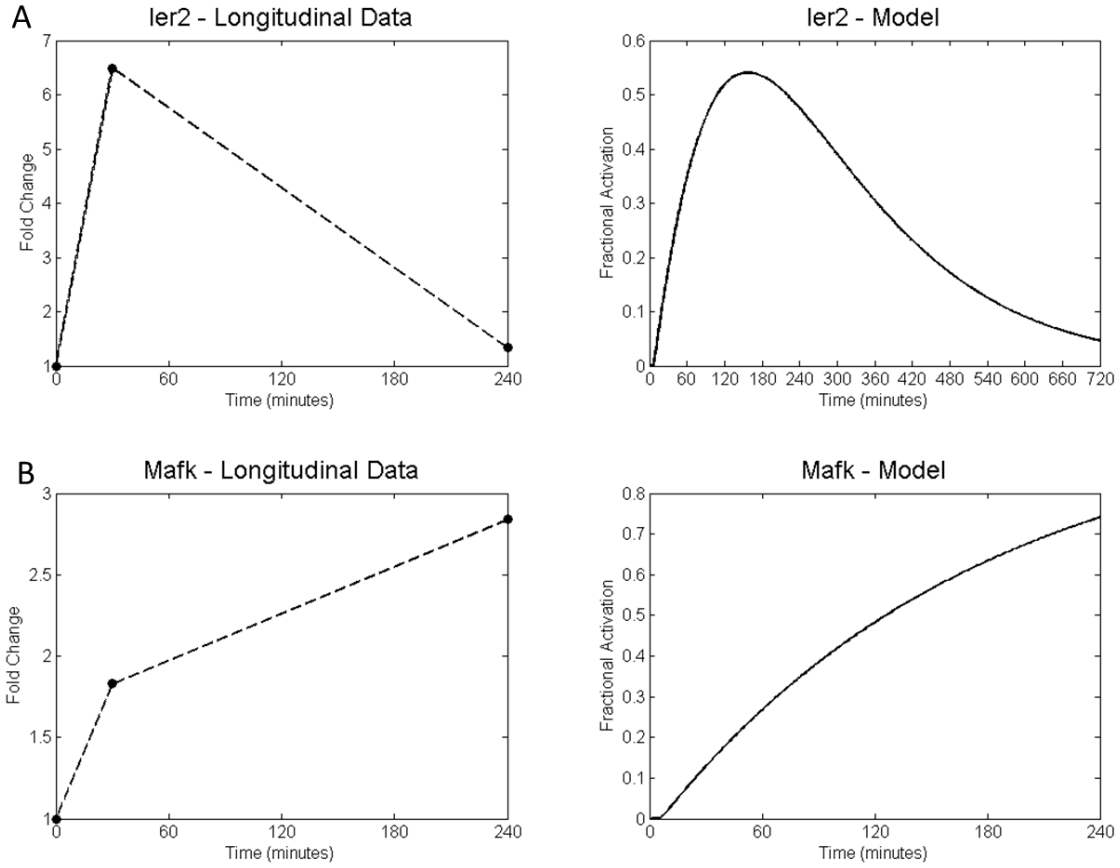

Figure 4.2| Temporal Behavior of Target Genes in the Data and Model Plots of gene expression over time of (A) Ier2 and (B) Mafk. The plots on the left show the fold change of each gene in response to longitudinal stretch. The plots on the right show the change in node activity after stretch is applied in the model.

There are 116 genes that are present in the model and DE in at least one of the 4 stretch conditions. GO Term enrichment analysis on these 116 DE genes that appear in

the MSN yields similar results to enrichment analysis on all 843 DE genes (Figure 4.3). The stretch axis-insensitive functions (TF activity, receptor binding, and growth factor activity) were all enriched with the 116 DE genes. Also, cytoskeletal protein binding, sarcomere, and adherens junction are functions and components that were specifically enriched with longitudinal stretch upregulated genes. These GO terms are also enriched with the 116 DE genes from the MSN. However, the third group of GO terms, which were specifically enriched with longitudinal stretch downregulated genes, was not enriched with the 116 DE genes from the MSN. These GO terms included potassium channel activity, sarcolemma, T-tubule, and potassium channel complex. This result indicates that potassium ion channel gene expression may be specifically modulated by longitudinal stretch and furthermore, the MSN does not yet capture the regulatory mechanisms that control expression of these genes.

Subsequently, the 116 DE genes were partitioned by TF and then enrichment analysis was performed to identify the functions regulated by each TF. The longitudinal stretch-specific GO terms (cytoskeletal protein binding, actin cytoskeleton organization, and adherens junction) appeared as enriched for targets of SRF and MEF2. This may be indicative that SRF and MEF2 are longitudinal-specific TFs. Multiple TFs have target genes enriched in the axis-insensitive GO term, TF activity. These TFs include CREB, forkhead box O (FoxO), nuclear factor of activated T-cells (NFAT), and STAT. This enrichment analysis of target genes might indicate that these 4 TFs are regulated by both transverse and longitudinal stretch.

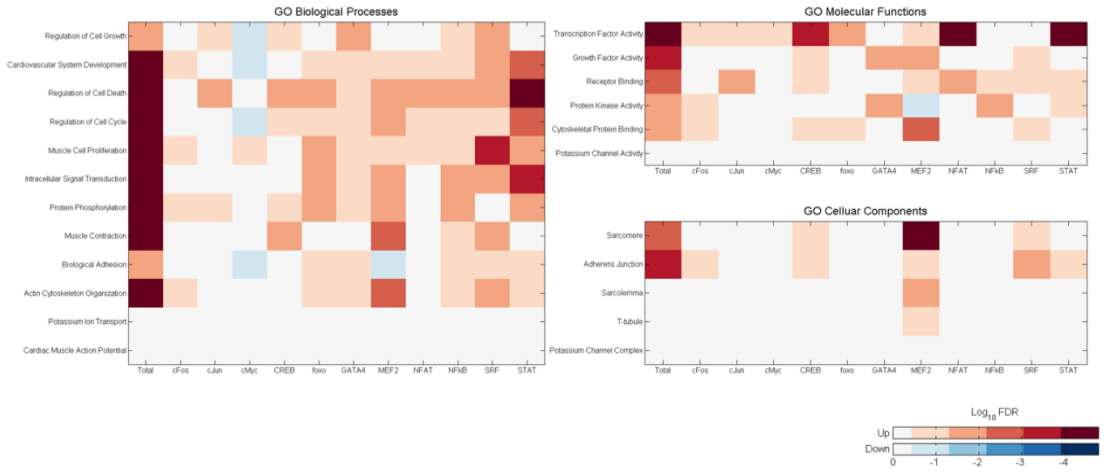

Figure 4.3| Enrichment Analysis of GO Terms of Target Genes of Each TF Heat maps showing select GO terms. DE genes were categorized as upregulated or downregulated for each TF. The shade of each element represents the $\log_{10}$ FDR of either the upregulated or downregulated genes of that TF. The color indicates whether the upregulated (red) or downregulated (blue) genes had a lower FDR.

4.3.2. Distribution of Targets of Each TF

In Figure 4.4, the prediction accuracy of the computational model for the target genes of each TF was determined. Of the 116 experimentally DE genes that are in the model, 95 (82%) are predicted to change in the correct direction, 15 (13%) are predicted to change but in the opposite direction as observed in the RNA-Seq data, and 6 (5%) are not predicted to change by the model. Although the model does not predict the targets of any TF significantly better or worse than expected, the change in expression is accurately predicted in targets of SRF, MEF2, and CREB.

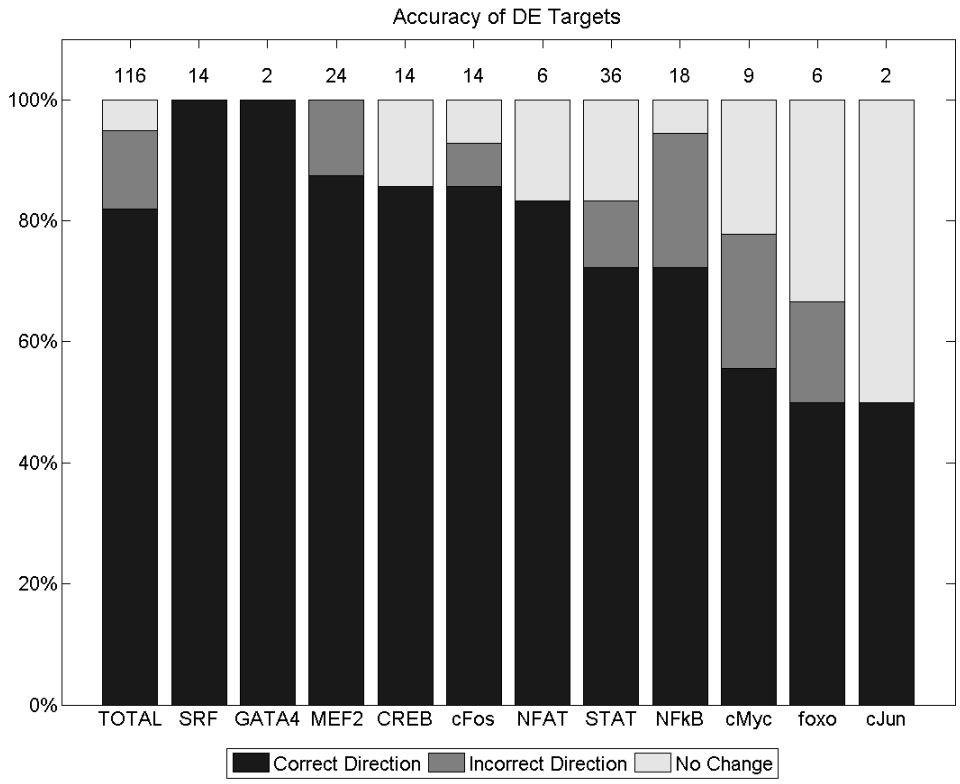

Figure 4.4| Accuracy of DE Target Genes of Each TF The 116 genes that were DE in the data and were targets of TFs in the model were broken down by TF for further analysis. The number of DE target genes of each TF is represented above the bar. A statistically significant difference between the total distribution and the distribution for a given TF is indicated by * $P < 0.05$. The bar graph indicates if the model predicts the target gene to change in the same direction as the data, the opposite direction of the data, or to not change.

In Figure 4.5, we investigated the number of target genes of each TF that are upregulated and downregulated in the RNA-Seq data. Of the 116 DE genes, 103 (89%) are upregulated and 13 (11%) are downregulated with stretch. Only five of the eleven TFs have target genes that are downregulated. A Fisher's exact test indicates that cMyc

(P = 0.009) has a significantly higher percentage of its DE genes downregulated with stretch than the expected fraction of 11%.

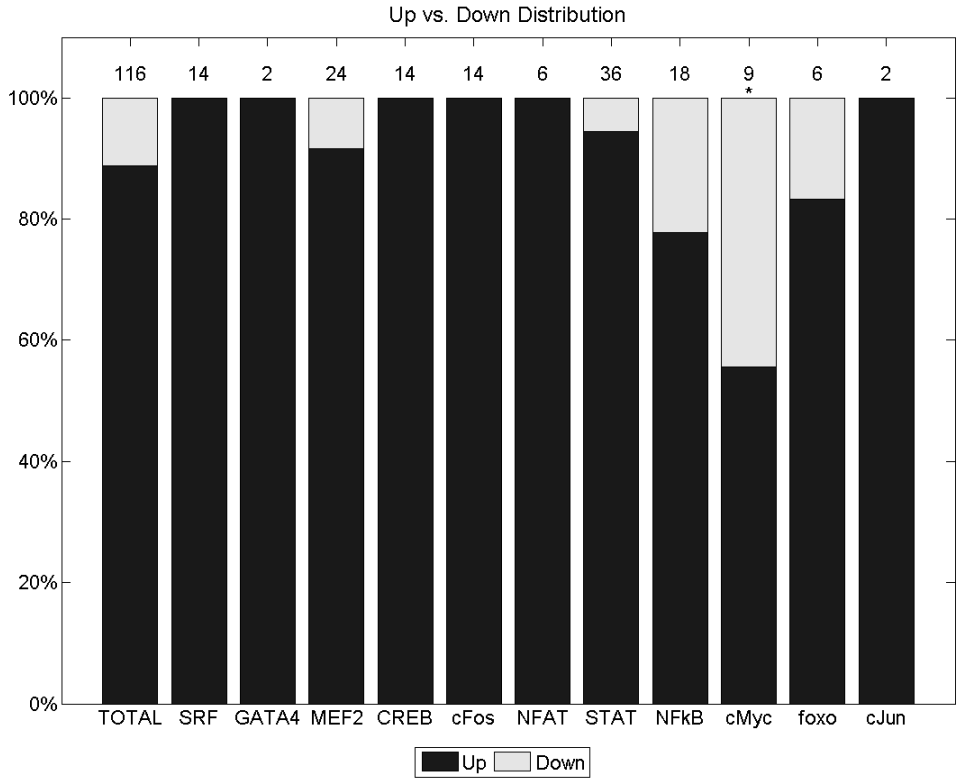

Figure 4.5| Up vs. Down Distribution of DE Target Genes of Each TF The 116 genes that were DE in the data and were targets of TFs in the model were broken down by TF for further analysis. The number of DE target genes of each TF is represented above the bar. A statistically significant difference between the total distribution and the distribution for a given TF is indicated by * P < 0.05. The bar graph indicates whether the target gene was upregulated or downregulated with stretch.

In order to investigate whether certain TFs are specifically activated by stretch along one axis, the distribution of target genes that are DE in transverse and/or longitudinal stretch for each TF was determined (Figure 4.6). Of these 116 DE genes, 116

(100%) are DE with longitudinal stretch and 27 (23%) are DE with transverse stretch. A Fisher's exact test indicates that CREB (P = 0.004) and NFkB (P = 0.012) have significantly different than expected fractions of genes induced by transverse stretch. CREB has the highest percentages (57%) of its DE target genes due to transverse stretch. This result may indicate that CREB is a stretch-responsive TF that is not sensitive to the stretch axis. In contrast, all 18 target genes of NFkB are only DE with longitudinal stretch, which indicates that NFkB may be specifically activated by longitudinal stretch.

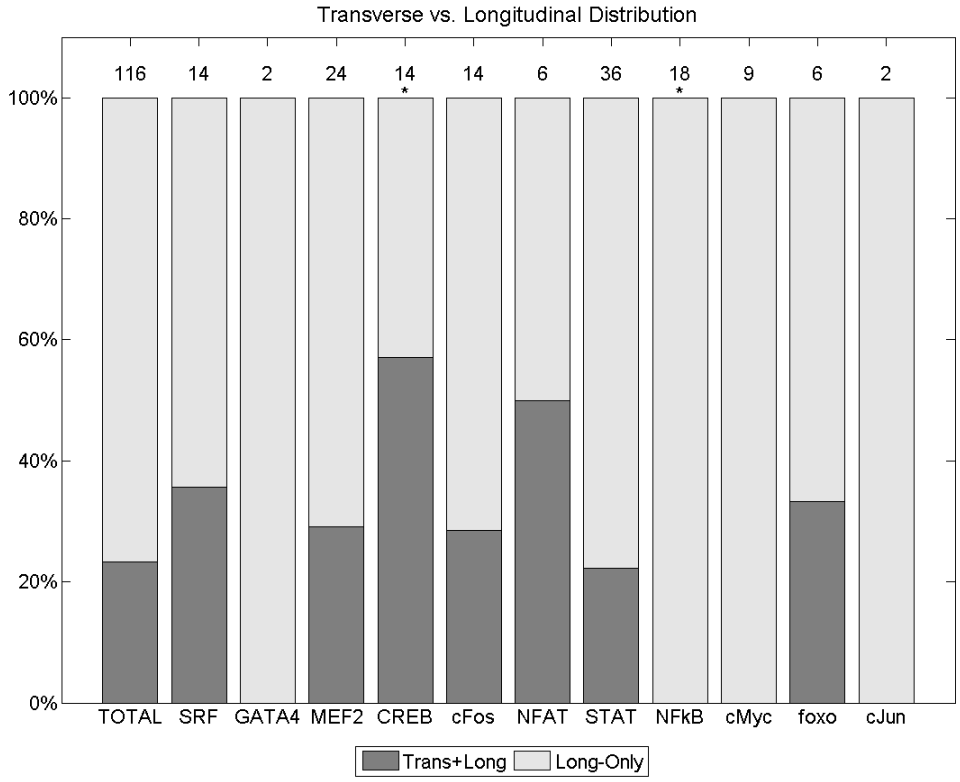

Figure 4.6| Transverse vs. Longitudinal Distribution of DE Target Genes of Each TF The 116 genes that were DE in the data and were targets of TFs in the model were broken down by TF for further analysis. The number of DE target genes of each TF is represented above the bar. A statistically significant difference between the total distribution and the distribution for a given TF is indicated by * $P < 0.05$. The bar graph indicates whether the target gene was changed with transverse and/or longitudinal stretch.

Furthermore, this transverse vs. longitudinal distribution can be partitioned at 30 minutes and 4 hours (Figure 4.7). Interestingly, a high percentage of CREB targets are DE with transverse stretch only at 30 minutes but not at 4 hours, which indicates that CREB regulates a rapid transcriptional response that appears to be insensitive to stretch axis. As for NFkB, all of its targets are only affected by longitudinal but not transverse

stretch at both time points. However, all 18 of them are DE at 4 hours, which may indicate that NFkB regulates a slower, longitudinal-specific response.

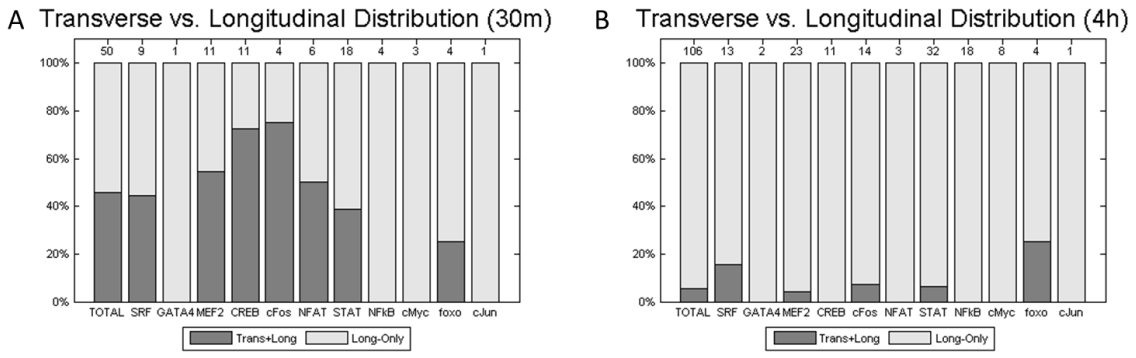

Figure 4.7| Transverse vs. Longitudinal Distribution of Targets at Each Time Point The number of DE target genes of each TF is represented above the bar. A statistically significant difference between the total distribution and the distribution for a given TF is indicated by * $P < 0.05$. The bar graph indicates whether the target gene was changed with transverse and/or longitudinal stretch at (A) 30 m or (B) 4h.

Temporal expression patterns seen in the data can be explained by certain TFs. Figure 4.8 examines the distribution of target genes that are DE at 30 minutes and/or 4 hours of stretch for each TF. Of the 116 DE genes, 50 (43%) are DE at 30 minutes and 106 (91%) are DE at 4 hours. NFAT ($P = 0.005$) and CREB ($P = 0.008$) both have a significantly higher percentage of their genes DE at 30 minutes than expected according to a Fisher's exact test.

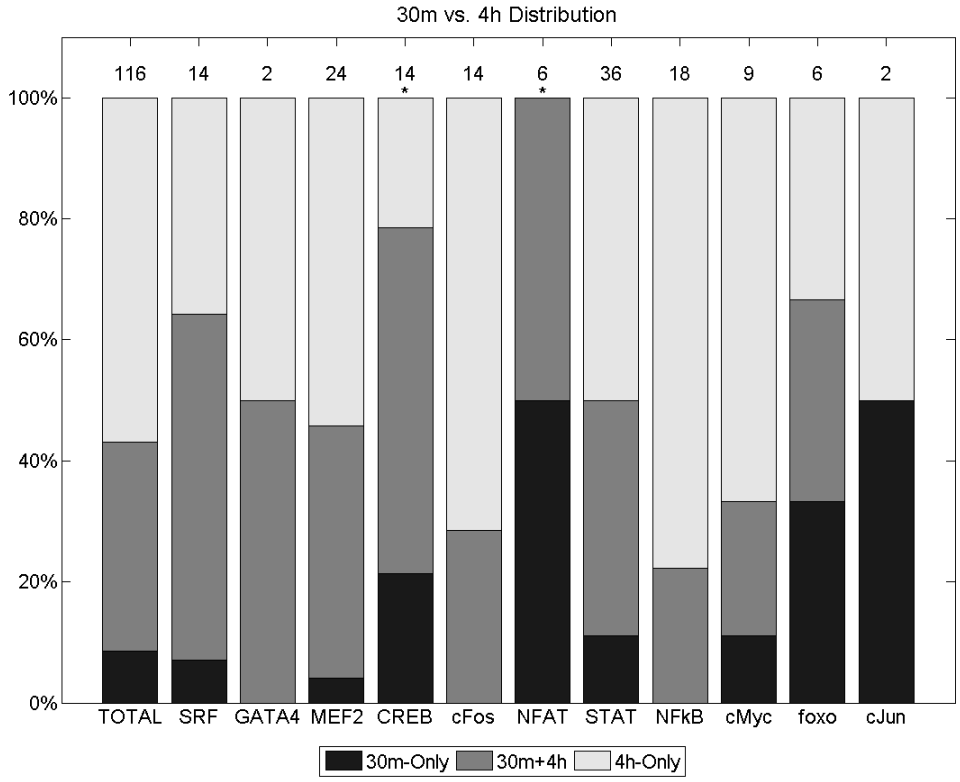

Figure 4.8| 30m vs. 4h Distribution of DE Target Genes of Each TF The 116 genes that were DE in the data and were targets of TFs in the model were broken down by TF for further analysis. The number of DE target genes of each TF is represented above the bar. A statistically significant difference between the total distribution and the distribution for a given TF is indicated by * $P < 0.05$. The bar graph indicates whether the target gene was changed at 30m and/or 4h of stretch.

Furthermore, this 30 minute vs. 4 hour distribution was partitioned into transverse and longitudinal stretch (Figure 4.9). In both stretches, CREB and NFAT have the highest percentage of their targets DE at 30 minutes. This may indicate that NFAT in addition to CREB is responsible for a rapid, axis-insensitive response.

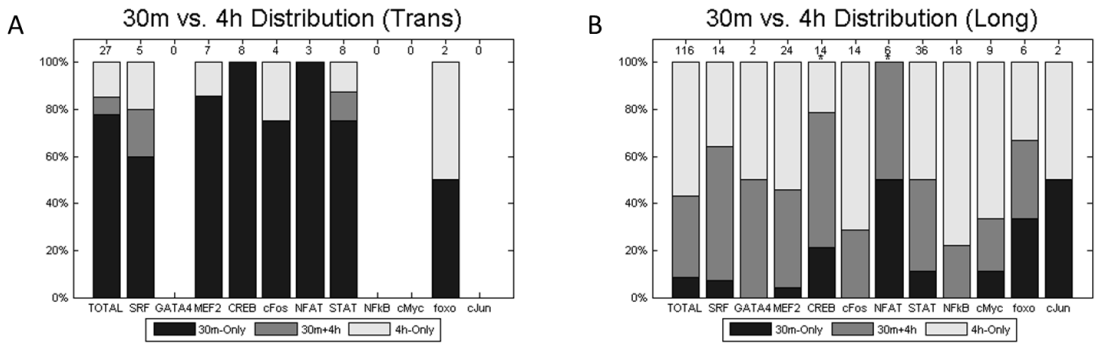

Figure 4.9| 30m vs. 4h Distribution of DE Target Genes in Each Stretch Axis The number of DE target genes of each TF is represented above the bar. A statistically significant difference between the total distribution and the distribution for a given TF is indicated by * $P < 0.05$. The bar graph indicates whether the target gene was changed at 30m and/or 4h of (C) transverse stretch or (D) longitudinal stretch.

4.3.3. Upstream Pathways of Each TF

Sensitivity analysis uncovers qualitative relationships between nodes in the MSN. Each simulation represents inhibiting the function of a specific node on the x-axis and determining the effect on each in the MSN by viewing up the corresponding column (Figure 4.10). By examining across a row in the sensitivity matrix, one can determine which upstream nodes have the greatest effect on the activity of that species.

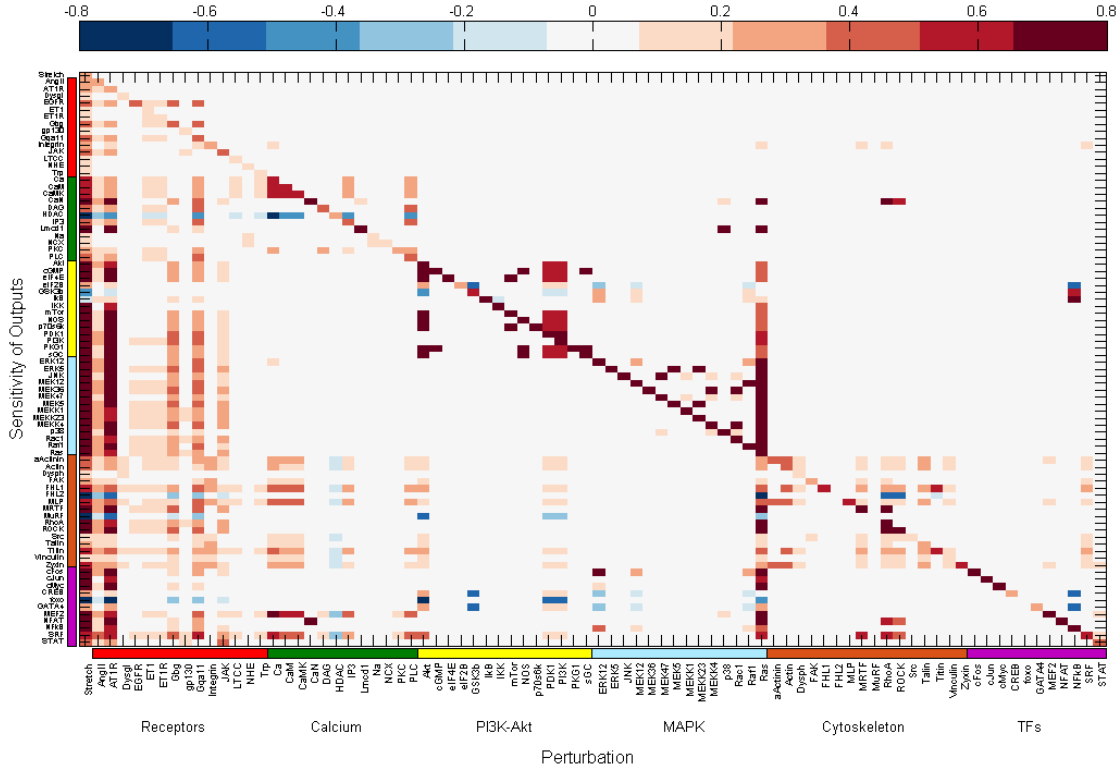

Figure 4.10| Sensitivity Analysis of MSN Model The full sensitivity matrix is displayed as a heat map. A column represents a computational experiment where the given species is knocked down and the effect on all other species' activity after 4h was measured. Sensitivity values indicate the change in activity after 4h of stretch (Control – Knockdown). The species are organized by signaling module.

Figure 4.11 is a subset of the full sensitivity matrix and displays the rows corresponding to the 11 TFs. AngII and AT1R are highly influential and affect activity of all 11 TFs. Ten of the 11 TFs are also highly sensitive to Ras with the lone exception being STAT.

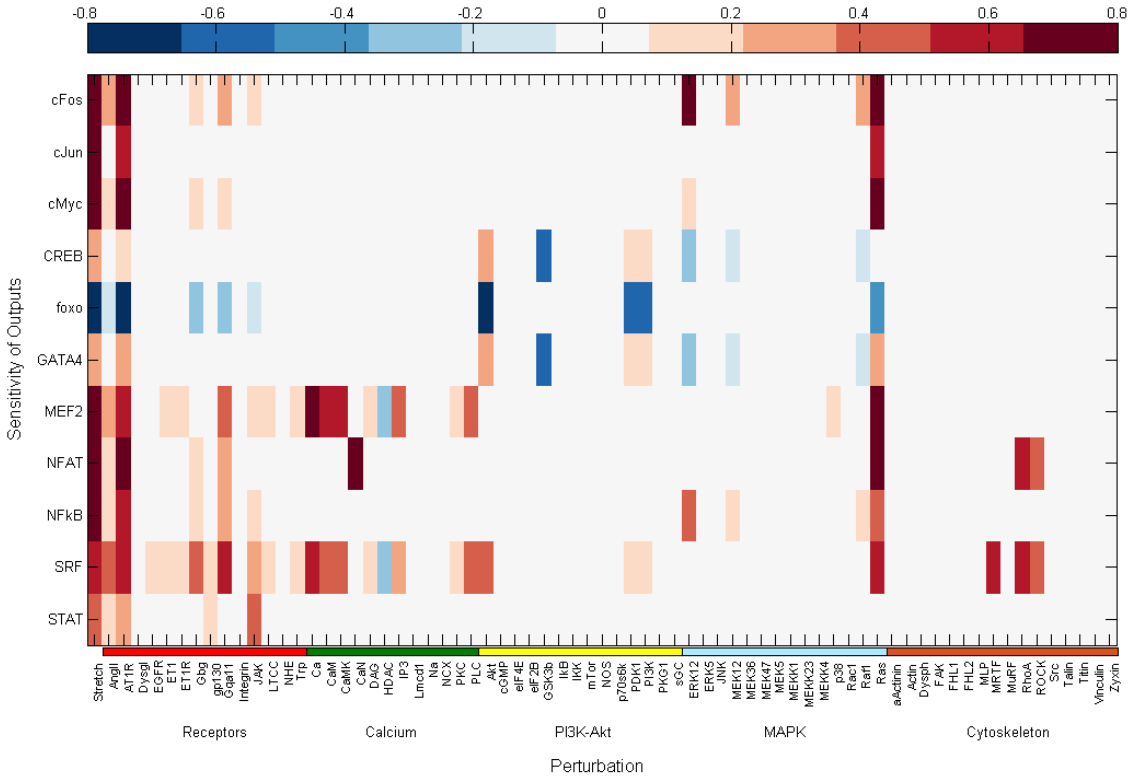

Figure 4.11| Sensitivity Analysis of MSN Model (Subset) A subset of the full sensitivity matrix is displayed as a heat map. A column represents a computational experiment where the given species is knocked down and the effect on all other species' activity after 4h was measured. Sensitivity values indicate the change in activity after 4h of stretch (Control – Knockdown). The species are organized by signaling module. Only the 11 TFs are displayed on the y-axis and the remaining species are displayed on the x-axis.

CREB and GATA4 are most sensitive to changes in GSK3B. Because targets of CREB were found to be insensitive to stretch axis, this could be an indication that GSK3B signaling is not sensitive to stretch axis. Another finding of particular interest is that SRF and MEF2 are very sensitive to changes in activity of nodes in the calcium signaling module. Two such nodes include PKC and CaMK. Since both SRF and MEF2 were found to regulate target genes involved in longitudinal stretch-specific GO terms,

this suggests that PKC and CaMK may be specifically activated by longitudinal stretch. Previous literature has shown that PKC is necessary for longitudinal stretch-induced sarcomere remodeling [163]. This finding supports previous literature because longitudinal stretch induced DE target genes of SRF and MEF2 that were enriched in cytoskeletal-related GO terms.

4.4. Discussion

This chapter describes how transcriptomic data can be combined with computational modeling in order to grasp a better understanding of the mechanisms leading to gene expression changes during mechanical loading of cardiac myocytes. Our computational model identifies the pathways and TFs regulating these gene expression changes. This analysis suggests that SRF and MEF2 are longitudinal-specific TFs that are controlled by calcium and PKC signaling. Target genes of SRF and MEF2 encode for sarcomeric proteins and are involved in actin cytoskeleton organization. On the other hand, CREB, which is located downstream of GSK3B, appears to rapidly activate its target genes in response to both longitudinal and transverse stretch. These two pathways are highlighted in Figure 4.12. Additionally, knowledge can be gained by identifying genes not in the model. Several genes encoding for potassium ion channels were downregulated with longitudinal stretch. However, none of these genes appeared in the MSN, signifying that future research could focus on transcriptional control of potassium ion channels.

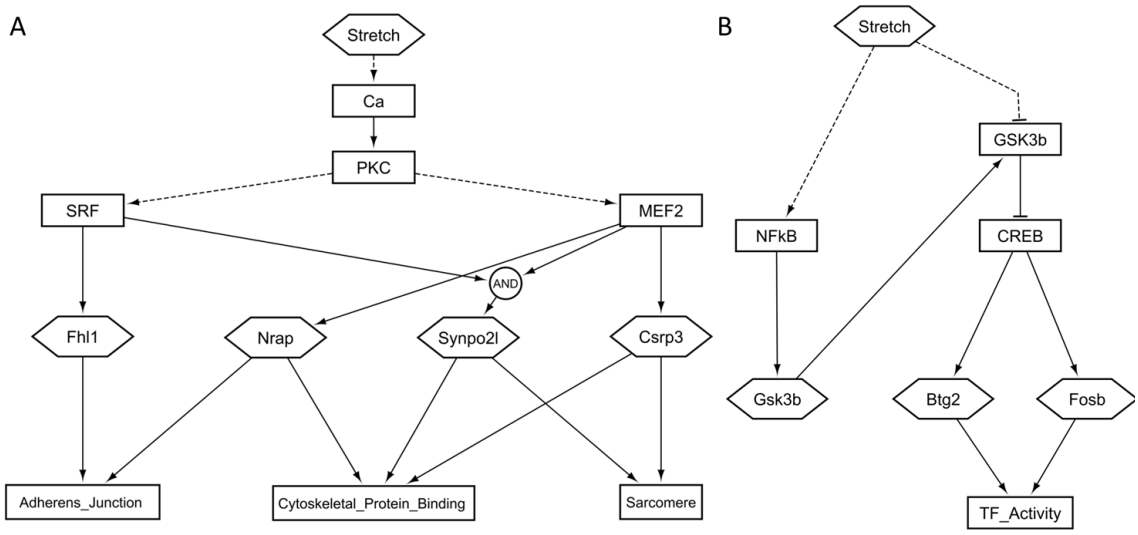

Figure 4.12| Schematic of Proposed Stretch-induced Pathways (A) Stretch leads to activation of calcium and PKC signaling. SRF and MEF2 are transcription factors downstream of these signaling molecules. Their target genes are enriched in GO terms related to cytoskeletal remodeling. (B) Stretch activates CREB via GSK3B. Target genes of CREB are enriched in the GO term, Transcription Factor Activity. CREB experiences a negative feedback loop through protein translation of GSK3B. This causes CREB target genes to be transiently activated with stretch.

4.4.1. SRF and MEF2

SRF and MEF2 are TFs that we propose to be specifically activated by longitudinal stretch. Based on network topology, calcium is the most influential node regulating SRF and MEF2-dependent transcription, which would indicate that elevated calcium levels are specific to longitudinal and not transverse stretch. Consistent with this result, one group showed that in diaphragm muscle, intracellular calcium antagonist TMB-8 blunts activation of ERK1/2 by longitudinal stretch but not by transverse stretch [116]. Another study showed that longitudinal stretch induces an increase in intracellular calcium in cardiac myocytes and that a Trpv4 antagonist prevented this increase [214].

Trp channels are non-selective cation channels that permit calcium influx through and are physically linked to the costamere via Homer proteins [215]. A potential mechanism could be for longitudinal stretch to apply force to the costamere, leading to the opening of Trp channels, and allowing calcium signaling to proceed.

Calcium signaling can activate CaMK, which leads to transcription activation by SRF [93] and MEF2 [69] via nuclear export of HDAC4. PKC can also regulate SRF and MEF2 via HDAC [68]. Furthermore, an *in vitro* experiment using micropatterned neonatal cardiac myocytes showed that in response to longitudinal strain, the sarcomeres acutely lengthen, but over the course of six hours, additional sarcomeres are added in series, which allows the sarcomeres to return to their resting length. However, inhibition of PKC prevented addition of sarcomeres in series, which indicates that PKC is necessary for longitudinal stretch-induced sarcomere remodeling [163]. Our model results are consistent this finding since SRF and MEF2 are downstream of PKC in the MSN and regulate expression of genes involved in sarcomere remodeling.

4.4.2. NFkB

NFkB is another TF identified as specific to longitudinal stretch. IkB and IKK control the transcriptional activity of NFkB by modulating its translocation to the nucleus [83]. Previous research in mouse diaphragm muscle showed that longitudinal stretch induced phosphorylation of IKK, IkB, and NFkB and that no induction of phosphorylation occurred after transverse stretch [117]. Our results support this conclusion since none of the target genes of NFkB in our MSN were DE with transverse stretch.

4.4.3. CREB

CREB is a TF that may be responsive to both longitudinal and transverse stretch. Akt indirectly activates CREB-dependent transcription via phosphorylation of GSK3B at serine-9 [58]. Our findings indicate that GSK3B is phosphorylated by both longitudinal and transverse stretch. Akt is the only kinase that directly regulates GSK3B activity in the MSN and therefore is implicated as an axis-insensitive kinase. However, this conflicts with a previous experiment in mouse diaphragm muscle, which showed that Akt is specifically phosphorylated by longitudinal stretch and not by transverse stretch [117]. Additionally, the PI3K-Akt signaling pathway was enriched with longitudinal but not transverse stretch in our RNA-Seq data. This contradictory result may imply that there is a second kinase that is activated by transverse stretch and phosphorylates GSK3B. One such kinase could be PKA, which is also able to phosphorylate GSK3B at serine-9 [216]. The PKA inhibitor H89 has been shown to blunt the stretch-induced increases of Atf3 and BNP mRNA in neonatal cardiac myocytes [217], which implies that PKA is involved in the stretch response of cardiac myocytes. In addition, PKA inhibitors, H-7 and KT5720, have been shown to blunt the activation of ERK1/2 in response to transverse stretch but not longitudinal stretch in diaphragm muscle [116]. These findings provide a mechanism where transverse stretch-induced phosphorylation of GSK3B could be mediated by PKA, which would lead to transcriptional activation of CREB. PKA will be added to a future version of the MSN by identifying upstream pathways linking PKA through a series of direct interactions to stretch.

4.4.4. Potassium Channel Downregulation

Potassium channel activity is a GO molecular function that was enriched in the RNA-Seq data but was not enriched in target genes of the MSN. Specific DE genes of this GO term, such as Kcnq1, Kcnj2, and Kcnh2, mediate I_{Ks}, the inward rectifier current (I_{K1}), and the repolarizing potassium current (I_{Kr}), respectively [170], and were downregulated by about 2-fold at 4 hours of longitudinal stretch but were not significantly changed with transverse stretch. Because these potassium channel genes are not present in the MSN, they may be regulated by stretch via an alternative mechanism than the pathways and TFs included in the MSN.

Androgen receptor functions as a TF [218] and could be involved in gene expression regulation of Kcnj2 and Kcnq1. In left atrium tissues with androgen receptor knockout, there was an increase in action potential duration and decreases in expression of proteins encoded by Kcnj2 and Kcnq1 as compared with wild type tissues [219]. Downregulation of ion channels could be due to microRNAs including miR-1 and miR-133, which are downstream targets of SRF. Overexpression of these microRNAs inhibits translation of Kcnj2 and Kcnj2 and reduces protein expression in healthy guinea pig hearts [220]. These findings indicate that androgen receptors and microRNAs-1 and -133 may downregulate potassium ion channels. However, additional experiments must be conducted to link the mechanisms to stretch of cardiac myocytes prior to their addition to a future MSN.

4.4.5. Limitations

There are multiple reasons why a large percentage of target genes in the MSN are not DE in the RNA-Seq data. Many of the references used to construct the relationships between TFs and target genes were not specific to cardiac myocytes, and none of these interactions were specific to stretch. It is likely that many of these interactions are specific to cell type or experimental conditions, and this would explain why many of the target genes in the MSN did not change in the data. Another contributing factor is the low power in the RNA-Seq data analysis. As with many RNA-Seq study designs, this study has a small number (3) of biological replicates. Furthermore, a major focus of the statistics for differential expression testing is to avoid incorrectly identifying a gene as DE. Using an adjusted p-value limits this by increasing the test's specificity. However, the trade-off is to decrease the test's sensitivity. The low sample size in conjunction with using a p-value correction for multiple comparisons drastically reduces the power. Therefore, although we can be confident of our claims that certain genes are DE, we cannot be confident in claiming that genes are not DE. This creates the possibility that some genes defined as not DE in this study could actually be DE with stretch.

4.4.6. Conclusion

The analysis presented in this chapter combines RNA-Seq data with a computational model in order to identify the pathways and TFs that regulate stretch-induced gene expression changes in cardiac myocytes. The results indicate that longitudinal stretch induces a more robust response in gene expression. Using the MSN, we identify that the TFs SRF, MEF2, and NFkB may be specifically activated with

longitudinal stretch, and in contrast, CREB appears to be activated by both longitudinal and transverse stretch. Sensitivity analysis of the computational model suggests that calcium and PKC are key regulators of SRF and MEF2 transcriptional activity. Enrichment analysis indicates that target genes of SRF and MEF2 are involved in cytoskeletal remodeling. The model also identifies that CREB is controlled by GSK3B and transiently activates immediate early genes.

4.5. Acknowledgements

Chapter 4, in part, is currently being prepared for submission for publication of the material. Buchholz, Kyle S; Tan, Philip; Zambon, Alexander C; Saucerman, Jeffrey J; McCulloch, Andrew D; Omens, Jeffrey H. Reprinted with permission from all co-authors. The dissertation author was the primary investigator and author of this material.

Chapter 5: Summary and Conclusion

5.1. Summary of Findings

The objective of this dissertation was to identify the genes, TFs, and pathways regulated by transverse and longitudinal stretch of cardiac myocytes. In Chapter 2, RNA-Seq was performed to identify DE genes in response to acute, mechanical stretch. In Chapter 3, a computational model of the mechanical stretch signaling network was constructed, and the upstream portion of the network was validated against independent data from the literature. In Chapter 4, the gene expression changes predicted by the model were compared against the RNA-Seq data in order to validate the transcriptional regulatory network. A sensitivity analysis was also performed to identify the most influential TFs and pathways regulating specific gene expression changes.

RNA-Seq analysis identified a more robust gene expression response to longitudinal stretch than to transverse stretch. Transverse stretch induced 53 and 35 genes to be DE at 30 minutes and 4 hours, respectively. In contrast, 168 and 795 genes were DE due to longitudinal stretch at these two time points. In addition, the genes DE in transverse stretch were predominantly a subset of the genes changed in longitudinal stretch, and only 13 genes were specifically DE in transverse stretch. Based on GO term analysis, longitudinal and transverse stretch both appear to induce a general stress response including intracellular signal transduction, activation of TFs, and regulation of cell growth. Additionally, certain processes were specifically enriched with genes only DE in longitudinal stretch. One set of these GO terms indicates that sarcomere remodeling is induced by longitudinal stretch. This finding is consistent with a previous

study, which showed that sarcomeres are added in series due to longitudinal stretch [163], and also indicates the specific genes that may be involved. A second set of terms shows that potassium ion channel genes are downregulated and may be an indication that electrical remodeling is regulated by longitudinal stretch. Previous results have shown that biaxial stretch can downregulate potassium ion channel genes in cardiac myocytes [170], but these results indicate that the longitudinal component of biaxial strain may be causing their downregulation.

Prior knowledge from published literature was used to integrate receptors, signaling pathways, and TFs into a cardiac myocyte MSN. Underlying this network was a computational model that utilized a normalized-Hill differential equation modeling approach. The upstream signaling portion of the MSN correctly predicted 54 of 61 independent, experimental data sets. For the downstream transcriptional regulatory network, the change in expression direction was correctly predicted by the model in 95 of the 116 target genes that were DE in the RNA-Seq data. After this model validation was performed, enrichment and sensitivity analyses were conducted to determine the TFs that regulate specific gene expression changes cellular functions and to identify the nodes and pathways upstream of these transcriptional changes. SRF and MEF2 were classified as regulators of gene involved cytoskeletal remodeling that were specifically upregulated by longitudinal stretch. Calcium and PKC are key nodes that regulate transcriptional activity of SRF and MEF2. CREB was identified as a TF activated by both longitudinal and transverse stretch that regulates immediate early genes with transient expression profiles. GSK3B is a mediator of CREB activity. Lastly, potassium ion channel genes were

enriched in longitudinal stretch but were not recognized as target genes of the TFs in the MSN. This may indicate that additional mechanisms are involved in the regulation of gene expression changes due to mechanical stretch signaling and provides motivation for expanding future versions of this MSN.

5.2. Future Work

5.2.1. Validation of Model Predictions

The conclusions drawn from combining the RNA-Seq data with the MSN model are derived from various sources and experimental conditions. These predictions based on the computational model should be confirmed experimentally.

One major conclusion is that PKC regulates target genes of SRF and MEF2 in response to longitudinal stretch. Bioinformatics analysis indicates the targets of SRF and MEF2 are involved in sarcomere remodeling. Previous literature has shown that PKC is necessary for longitudinal stretch-induced sarcomere remodeling [163]. PKC has also been shown to regulate SRF and MEF2 via HDAC [68]. However, a connection between PKC and SRF and MEF2 targets has not been shown experimentally.

This connection could be confirmed using an inhibitor of PKC and probing for target genes of SRF and MEF2 using PCR. Specific MEF2 target genes, such as Csrp3, Nrap, Lmod3, Sntb1, and Trim54, would be good candidates since they were upregulated 2-3-fold with 4 hours of longitudinal stretch. A potential inhibitor, Bisindolylmaleimide I (BIM-1), has previously been shown to inhibit PKC by pre-incubation for 45 minutes at a concentration of 5 μM BIM-1 prior to stretch [116]. The anticipated result of this

experiment would be a blunted response of MEF2 targets when stretched longitudinally in the presence of BIM-1 as compared with the 2-3-fold increase that is seen without the inhibitor.

Another main conclusion is that CREB targets are activated by both transverse and longitudinal stretch, which is negatively regulated by GSK3B. A potential experiment to link GSK3B to CREB target genes would be to induce constitutive activation of GSK3B. GSK3B is normally active in cardiac myocytes and is inhibited via phosphorylation at serine-9 [58]. Transgenic mice with a serine-to-alanine mutation at position 9 of GSK3B using an alpha-myosin heavy chain promoter have previously been generated, which makes GSK3B non-phosphorylatable and allows it to remain constitutively active in cardiac myocytes [58].

A connection between GSK3B and CREB target genes could be confirmed using cardiac myocytes isolated from these transgenic mice. Specific CREB target genes, such as Btg2, Ier2, Inhba, and Fosb, were all upregulated by at least 2-fold after 30 minutes of both transverse and longitudinal stretch and therefore would be suitable genes to examine using PCR. The anticipated result of this experiment would be a blunted stretch-induced response of CREB targets in cardiac myocytes from transgenic mice as compared to those from wildtype mice. The signaling pathway could be traced upstream of GSK3B to investigate where axis-dependent regulation of GSK3B may occur. In Chapter 4, we proposed that GSK3B inactivation may be regulated by PI3K and Akt in response to longitudinal stretch and by PKA in response to transverse stretch. Inhibitors of PI3K,

such as wortmannin, and PKA, such as H-7 or KT5720, could be used to test these hypotheses.

5.2.2. Connecting the MSN Model to Cardiac Growth Models

The MSN model identifies molecular changes at the cellular level, such as protein phosphorylation, TF activation, and gene transcription. To increase the clinical relevance of these molecular changes, multi-scale modeling approach should be taken in order to scale up the MSN model into an organ-level growth model. By integrating these two models, one could predict the effect of signaling network changes on the growth response of the heart. In addition, by separating the MSN model into separate models of the response to transverse stretch and the response to longitudinal stretch, it may be possible to correlate this with the type of *in vivo* hypertrophy.

Hemodynamic overload can result in either eccentric (volume-overload) hypertrophy or concentric (pressure-overload) hypertrophy, which is caused by increased pressure (afterload) [3,161,172]. In eccentric hypertrophy, cardiac myocytes grow by the addition of sarcomeres in series, which causes dilation of the ventricular chamber. In concentric hypertrophy, sarcomeres are added in parallel, results in thickening of the ventricular wall [172].

The biomechanical stimuli that lead to these divergent modes of hypertrophy are not well-understood. Sarcomere addition in series has been shown to occur *in vitro* in response to longitudinal strain over the course of six hours [163]. This finding suggests that cardiac myocytes have a preferred sarcomere length. Based on this knowledge, a strain-based cardiac growth law was developed where cardiac myocytes grow longer in

response to longitudinal strain to maintain their sarcomere length and grow thicker in response to transverse strain to maintain their interfilament lattice spacing [221]. A finite element model using this cardiac growth law was able to recapitulate the structural and functional changes that occur experimentally in canine models exposed to aortic stenosis in order to induce pressure-overload hypertrophy and mitral valve regurgitation to induce volume-overload hypertrophy [62,156,222]. These experimental and computational findings indicate that axis of stretch may regulate the mode of hypertrophy.

In a recent paper, one group has connected specific signaling pathways to the type of *in vivo* hypertrophy [223]. Their study determined that concentric remodeling was induced by ERK1/2 and that calcineurin stimulated a general growth response. This finding is supported by the RNA-Seq data and the MSN in conjunction with the strain-based growth law. ERK1/2 is a primary kinase in the MAPK signaling pathway, which was one of the few KEGG pathways enriched with genes DE in transverse stretch. Therefore, transverse stretch may promote concentric remodeling via ERK1/2. Secondly, NFAT was the most sensitive TF to changes in calcineurin activity, and a high percentage of its target genes were DE with both longitudinal and transverse stretch. This would support that calcineurin-NFAT signaling is activated by both stretch axes and therefore is a general growth response. Additional connections between the stretch and hypertrophy could be included based on the findings in this dissertation. PKC was identified as a longitudinal stretch-specific regulator of changes in SRF and MEF2 transcriptional activity, and therefore these three nodes may mediate eccentric remodeling.

5.3. Significance

The RNA-Seq data identified specific gene markers that are sensitive to mechanical stretch. The construction of the MSN model was an effort to summarize the signaling components involved in the response to mechanical loading. This stretch response can be characterized by hypertrophic growth and may eventually lead to decompensated heart failure. Analysis of the MSN model could be used to identify therapeutic targets with the long-term goal of developing drugs and compounds to prevent heart failure. A logic extension of the MSN model would be to integrate it with an organ-level growth model. In this situation, a stretch stimulus could be applied to the MSN in order to generate output values. These values would then be used as input parameters in the growth model to determine changes in cardiac morphology due to mechanical loading. Furthermore, the efficacy of pharmacological inhibitors could be tested by inhibiting the node of interest in the MSN model and observing the effect in the growth model. Overall, the acquisition of this RNA-Seq data and the construction of this MSN model can help understand the mechanisms leading to and identify preventative therapies of heart failure.

Appendix A: DE Genes from RNA-Seq Experiment

This table lists all 843 genes that were DE in at least 1 of the 4 stretch conditions. For each stretch condition, the logarithm to the base 2 of the fold change (log FC) and the adjusted p-value (q_val) are displayed.

	30m Trans		30m Long		4h Trans		4h Long	
Symbol	**log FC**	**q_val**	**log FC**	**q_val**	**log FC**	**q_val**	**log FC**	**q_val**
0610009O20Rik	-0.13	1.00	-0.16	1.00	-0.27	1.00	-0.54	0.05
1110032F04Rik	-0.36	1.00	-0.77	0.18	-0.50	1.00	-0.84	0.02
1110067D22Rik	0.03	1.00	0.41	0.62	-0.03	1.00	0.59	0.02
1190005I06Rik	-0.26	1.00	-0.46	1.00	-0.18	1.00	-1.10	0.02
1300014I06Rik	0.20	1.00	0.67	0.08	0.07	1.00	0.75	0.01
1810011O10Rik	0.35	1.00	0.74	0.28	0.30	1.00	0.87	0.02
1810049H13Rik	-0.41	1.00	-0.48	1.00	-0.23	1.00	-0.80	0.04
2010107G23Rik	-0.60	1.00	-0.48	1.00	-0.29	1.00	-1.60	0.01
2010111I01Rik	0.37	1.00	0.49	0.31	0.51	0.34	1.30	0.00
2210403K04Rik	0.81	0.21	0.96	0.00	0.55	0.52	1.19	0.00
2310028H24Rik	0.46	1.00	0.37	1.00	0.06	1.00	0.62	0.04
2310040G24Rik	-0.17	1.00	-0.66	1.00	-0.03	1.00	-1.10	0.03
2310044G17Rik	0.06	1.00	0.10	1.00	0.17	1.00	0.59	0.02
2310057M21Rik	0.66	1.00	0.67	0.28	0.20	1.00	1.17	0.00
2700023E23Rik	1.14	0.72	1.11	0.09	0.88	0.84	1.51	0.00
2810030E01Rik	-0.03	1.00	-0.24	1.00	-0.40	1.00	-0.85	0.02
2900026A02Rik	0.19	1.00	0.39	0.71	0.30	1.00	0.96	0.00
4930523C07Rik	0.49	1.00	0.72	0.04	0.26	1.00	1.53	0.00
4930555G01Rik	1.44	0.39	1.05	0.32	-0.06	1.00	1.20	0.03
6330439K17Rik	-0.02	1.00	-0.38	1.00	-0.44	1.00	-1.22	0.03
6430548M08Rik	0.39	1.00	0.36	0.98	0.00	1.00	0.99	0.00
6430573F11Rik	-0.26	1.00	-0.19	1.00	-0.54	1.00	-1.87	0.01
9030425E11Rik	0.02	1.00	-0.13	1.00	-0.50	0.98	-0.72	0.02
9430020K01Rik	0.14	1.00	0.34	1.00	0.30	1.00	0.78	0.00
AW551984	1.98	0.00	2.17	0.00	-0.36	1.00	1.85	0.00
Abcc8	-0.08	1.00	-0.09	1.00	-0.63	0.25	-0.79	0.00
Abce1	0.08	1.00	0.18	1.00	0.13	1.00	0.56	0.04
Abcg4	-0.09	1.00	-0.40	1.00	-0.83	1.00	-1.34	0.02
Abhd6	0.02	1.00	-0.26	1.00	-0.24	1.00	-0.93	0.01
Abhd8	-0.12	1.00	-0.31	1.00	-0.22	1.00	-0.69	0.01
Ablim2	0.02	1.00	-0.33	1.00	-0.19	1.00	-0.91	0.01
Abr	0.00	1.00	-0.07	1.00	-0.38	0.98	-0.60	0.01
Abra	2.63	0.00	3.27	0.00	1.29	0.00	3.22	0.00

Abtb1	-0.05	1.00	-0.40	0.81	0.10	1.00	-0.61	0.03
Acan	0.16	1.00	0.88	0.01	0.01	1.00	1.07	0.00
Acer2	-0.11	1.00	-0.27	1.00	-0.48	1.00	-1.15	0.00
Acot11	-0.12	1.00	-0.18	1.00	-0.45	1.00	-0.86	0.00
Acot9	0.06	1.00	0.33	1.00	0.11	1.00	0.68	0.01
Acta1	1.38	0.01	1.15	0.00	0.01	1.00	0.73	0.03
Acta2	0.23	1.00	0.79	0.52	0.06	1.00	0.91	0.02
Actb	0.41	1.00	0.78	0.32	0.32	1.00	0.78	0.05
Actg2	0.00	1.00	0.45	1.00	0.26	1.00	0.75	0.05
Actn1	0.39	1.00	0.41	1.00	-0.05	1.00	0.65	0.04
Actn4	0.32	1.00	0.53	0.63	0.16	1.00	0.91	0.00
Actr3	0.13	1.00	0.29	1.00	0.29	1.00	0.78	0.02
Acvr1b	-0.03	1.00	-0.19	1.00	-0.29	1.00	-0.64	0.01
Adamts1	0.99	0.00	1.39	0.00	0.54	0.16	1.26	0.00
Adamts14	0.33	1.00	0.14	1.00	-0.05	1.00	0.73	0.04
Adamts15	-0.20	1.00	-0.39	1.00	-0.72	0.17	-0.96	0.00
Adamts6	-0.04	1.00	-0.42	1.00	-0.14	1.00	-0.84	0.04
Adamts8	1.05	0.13	0.76	0.07	-0.28	1.00	1.06	0.00
Adcy5	-0.06	1.00	0.06	1.00	-0.23	1.00	-0.62	0.02
Adcyap1r1	-0.02	1.00	0.09	1.00	0.17	1.00	0.89	0.02
Add3	-0.02	1.00	-0.25	1.00	-0.19	1.00	-0.71	0.01
Adm	0.20	1.00	0.31	1.00	0.42	1.00	0.72	0.02
Adpgk	0.03	1.00	0.18	1.00	0.11	1.00	0.61	0.04
Adra1b	0.05	1.00	-0.50	0.32	-0.26	1.00	-1.30	0.00
Agfg1	0.11	1.00	0.18	1.00	0.25	1.00	0.81	0.00
Agtr1a	0.02	1.00	-0.33	1.00	-0.38	1.00	-1.14	0.00
Ahrr	-0.37	1.00	-0.06	1.00	-0.90	0.32	-1.12	0.00
Aif1l	0.13	1.00	0.26	1.00	0.16	1.00	0.76	0.02
Akap2	0.33	1.00	0.40	1.00	0.28	1.00	1.05	0.00
Akap5	0.21	1.00	0.97	0.20	0.28	1.00	1.12	0.01
Akap6	0.11	1.00	0.36	1.00	0.53	0.33	0.76	0.00
Aldh1a3	-0.41	1.00	0.81	0.38	-0.42	1.00	1.39	0.00
Aldh1b1	-0.19	1.00	-0.78	0.00	0.16	1.00	-0.92	0.00
Aldh3a1	-0.01	1.00	-0.43	1.00	0.07	1.00	-0.85	0.04
Aldh5a1	-0.15	1.00	-0.22	1.00	-0.22	1.00	-0.67	0.03
Alms1	-0.06	1.00	-0.24	1.00	-0.65	1.00	-0.99	0.01
Amotl2	0.49	1.00	0.71	0.01	0.42	0.74	0.79	0.00
Angpt1	-0.13	1.00	-0.42	1.00	0.00	1.00	-1.24	0.00
Ankrd23	0.39	1.00	0.65	0.13	0.43	0.99	1.22	0.00
Anxa1	-0.08	1.00	0.45	0.56	0.42	0.79	0.90	0.00

Aph1b	-0.04	1.00	-0.12	1.00	-0.33	1.00	-0.75	0.01
Aqp4	-0.43	1.00	-0.26	1.00	-0.18	1.00	-0.77	0.00
Arc	2.28	0.00	2.95	0.00	0.13	1.00	1.26	0.00
Arhgap23	0.37	1.00	0.37	0.85	0.43	0.59	1.21	0.00
Arhgap26	-0.25	1.00	-0.36	1.00	0.00	1.00	-0.80	0.00
Arhgap31	0.01	1.00	-0.25	1.00	-0.13	1.00	-0.83	0.00
Arhgef19	-0.03	1.00	-0.06	1.00	-0.83	0.14	-1.19	0.00
Arhgef3	-0.13	1.00	-0.26	1.00	-0.39	1.00	-1.12	0.00
Arid5a	0.80	0.44	1.46	0.00	0.80	0.14	1.67	0.00
Arid5b	0.34	1.00	0.44	0.43	0.38	0.99	0.93	0.00
Arpc5	0.05	1.00	0.24	1.00	0.23	1.00	0.62	0.01
Arrdc3	-0.31	1.00	-0.82	0.00	-0.26	1.00	-0.88	0.00
Asb10	0.08	1.00	-0.30	1.00	-0.32	1.00	-1.10	0.00
Asb5	0.28	1.00	0.55	1.00	0.66	1.00	1.89	0.00
Asrgl1	0.02	1.00	-0.38	1.00	-0.05	1.00	-0.70	0.02
Atf3	2.75	0.00	3.50	0.00	0.61	0.32	2.10	0.00
Atg14	-0.20	1.00	-0.44	0.67	-0.12	1.00	-0.63	0.04
Atp13a3	0.21	1.00	0.29	1.00	0.12	1.00	0.78	0.00
Atp8b1	-0.10	1.00	0.50	0.88	0.26	1.00	0.85	0.01
Avpi1	0.22	1.00	0.33	1.00	-0.03	1.00	0.66	0.04
Azi1	0.09	1.00	-0.36	1.00	-0.12	1.00	-0.80	0.01
Azin1	0.31	1.00	0.49	0.71	0.39	1.00	1.34	0.00
B3gnt5	0.62	1.00	0.88	0.38	0.27	1.00	1.21	0.01
BC031353	0.17	1.00	-0.16	1.00	-0.15	1.00	-0.81	0.01
BC057022	-0.31	1.00	-0.78	0.36	-1.17	0.07	-1.84	0.00
Baalc	0.41	1.00	0.53	1.00	0.04	1.00	1.38	0.00
Bach2	-0.05	1.00	0.07	1.00	1.12	0.00	1.78	0.00
Bag2	0.45	1.00	0.58	0.09	0.06	1.00	1.21	0.00
Bahcc1	0.01	1.00	-0.25	1.00	-0.41	0.99	-0.77	0.00
Bcl11b	-0.17	1.00	-0.58	1.00	-1.44	0.46	-2.17	0.00
Bcl2l11	-0.05	1.00	-0.94	0.01	-0.47	1.00	-1.62	0.00
Bcl7a	-0.04	1.00	-0.36	1.00	-0.12	1.00	-0.85	0.00
Bcr	0.42	1.00	0.85	0.00	0.43	0.71	1.60	0.00
Bdkrb2	-0.39	1.00	0.42	1.00	-0.16	1.00	1.20	0.04
Bdnf	0.46	1.00	0.85	0.29	0.66	1.00	1.35	0.00
Bend4	0.10	1.00	0.14	1.00	0.13	1.00	0.66	0.01
Bex1	0.46	1.00	0.60	0.31	-0.18	1.00	0.84	0.01
Bhlhe40	0.58	1.00	0.60	0.06	0.38	1.00	0.73	0.00
Bmf	-0.11	1.00	-0.68	0.03	-0.15	1.00	-1.21	0.00
Bmp10	1.04	1.00	1.13	0.11	0.46	1.00	1.19	0.02

Bmper	0.31	1.00	0.53	0.20	0.16	1.00	1.00	0.00
Btg2	2.81	0.00	3.01	0.00	0.62	0.06	1.02	0.00
C130080G10Rik	0.21	1.00	0.17	1.00	0.53	0.29	1.55	0.00
C2cd3	-0.04	1.00	-0.24	1.00	-0.15	1.00	-0.59	0.05
C2cd4b	0.17	1.00	-0.77	1.00	-0.29	1.00	-2.03	0.03
Cables1	-0.24	1.00	-0.73	0.22	-0.02	1.00	-0.81	0.02
Cacna1g	-0.08	1.00	-0.42	1.00	-0.10	1.00	-0.71	0.01
Cacna1h	0.09	1.00	-0.75	0.01	-0.36	1.00	-1.49	0.00
Cast	0.03	1.00	0.20	1.00	0.19	1.00	0.60	0.03
Cav1	-0.09	1.00	0.29	1.00	0.34	1.00	0.71	0.03
Cav2	-0.09	1.00	0.30	1.00	0.37	1.00	0.72	0.01
Cav3	0.09	1.00	0.23	1.00	0.34	1.00	0.66	0.01
Cby1	-0.07	1.00	-0.10	1.00	-0.28	1.00	-0.68	0.03
Cc2d2a	-0.02	1.00	-0.28	1.00	-0.46	1.00	-1.11	0.00
Ccdc85c	0.04	1.00	-0.19	1.00	-0.19	1.00	-0.75	0.04
Ccdc86	0.30	1.00	0.33	1.00	0.20	1.00	0.67	0.03
Ccl2	0.75	0.30	1.19	0.00	0.54	0.48	0.84	0.00
Ccl7	1.18	0.02	1.57	0.00	0.59	1.00	0.82	0.02
Ccng2	-0.10	1.00	-0.45	0.44	-0.10	1.00	-1.05	0.00
Ccnjl	-0.04	1.00	-0.34	1.00	0.03	1.00	-1.03	0.01
Ccnyl1	0.11	1.00	0.38	0.98	0.18	1.00	0.58	0.05
Ccrl2	-0.19	1.00	-0.72	0.64	-0.19	1.00	-1.14	0.01
Cct8	0.39	1.00	0.44	1.00	0.01	1.00	0.75	0.03
Cd44	0.33	1.00	0.71	0.01	-0.06	1.00	1.08	0.00
Cdc42ep1	0.22	1.00	0.40	0.67	0.32	1.00	0.78	0.00
Cdc42ep3	0.24	1.00	0.33	1.00	0.29	1.00	0.70	0.01
Cdc42se1	0.13	1.00	0.31	1.00	0.25	1.00	0.92	0.01
Cdh20	-0.29	1.00	-0.43	1.00	-0.24	1.00	-1.34	0.00
Cdk18	0.25	1.00	0.09	1.00	-0.04	1.00	0.65	0.02
Cdr2	0.52	1.00	0.82	0.00	0.31	1.00	1.17	0.00
Cdsn	-0.38	1.00	-0.22	1.00	-1.12	0.01	-0.45	0.36
Cdyl	0.12	1.00	0.14	1.00	0.26	1.00	0.59	0.04
Celsr1	-0.09	1.00	-0.18	1.00	-0.72	0.06	-1.18	0.00
Ces1d	-0.89	1.00	-1.82	0.00	1.18	0.07	-0.63	0.38
Ch25h	2.19	0.00	2.81	0.00	0.60	0.86	1.37	0.00
Chst3	0.76	1.00	1.06	0.01	0.26	1.00	1.70	0.00
Chsy3	0.19	1.00	0.71	0.73	0.46	1.00	0.94	0.05
Cited2	0.75	0.18	0.75	0.00	0.18	1.00	0.35	0.33
Ckap4	0.06	1.00	0.39	0.97	0.10	1.00	0.75	0.00
Ckmt2	-0.59	1.00	-0.20	1.00	-0.77	0.01	-0.55	0.06

Cldn25	0.12	1.00	0.24	1.00	0.35	1.00	0.56	0.03
Cldn4	1.12	1.00	0.44	1.00	0.87	1.00	2.88	0.00
Clic5	0.78	1.00	0.85	0.04	0.27	1.00	1.47	0.00
Cnn1	1.02	0.53	0.97	0.01	-0.34	1.00	0.45	0.27
Cnn2	0.13	1.00	0.55	0.22	0.19	1.00	0.80	0.00
Cnst	0.04	1.00	-0.11	1.00	0.04	1.00	-0.64	0.01
Col14a1	-0.13	1.00	-0.71	0.01	-0.15	1.00	0.02	1.00
Coq10b	0.08	1.00	0.31	1.00	0.33	1.00	0.67	0.01
Cpeb1	0.34	1.00	0.31	1.00	0.32	1.00	0.75	0.02
Cpeb3	0.05	1.00	-0.16	1.00	0.01	1.00	-0.70	0.01
Creb5	0.29	1.00	0.44	1.00	0.70	0.30	1.59	0.00
Crhr2	-0.44	1.00	-0.08	1.00	-0.65	0.45	-1.14	0.00
Crim1	0.18	1.00	0.18	1.00	0.36	1.00	0.76	0.00
Csf1	0.15	1.00	0.66	0.05	-0.07	1.00	0.49	0.13
Cspg4	0.48	1.00	0.62	0.12	-0.08	1.00	1.07	0.00
Csrnp1	1.55	0.00	2.01	0.00	0.45	1.00	1.54	0.00
Csrp3	0.86	1.00	0.79	0.69	0.18	1.00	1.68	0.00
Ctgf	1.75	1.00	2.21	0.00	1.25	0.03	2.66	0.00
Ctps	0.10	1.00	0.36	0.98	0.28	1.00	0.80	0.00
Cttnbp2nl	0.47	1.00	0.44	0.41	0.25	1.00	0.83	0.00
Cul9	-0.03	1.00	-0.28	1.00	-0.06	1.00	-0.55	0.05
Cx3cl1	0.13	1.00	0.46	0.37	0.03	1.00	0.70	0.00
Cxcl1	2.41	0.00	2.59	0.00	0.66	1.00	0.92	0.19
Cxxc4	0.21	1.00	-0.34	1.00	-0.65	1.00	-1.38	0.00
Cxxc5	-0.05	1.00	-0.14	1.00	-0.17	1.00	-0.54	0.04
Cyld	0.17	1.00	0.20	1.00	0.13	1.00	0.74	0.01
Cyp1b1	-0.23	1.00	-0.20	1.00	-0.74	0.01	-0.82	0.00
Cyp2j9	-0.16	1.00	-0.25	1.00	-0.66	1.00	-1.49	0.01
Cyr61	2.75	0.00	3.24	0.00	0.89	0.00	2.09	0.00
Cyth1	-0.08	1.00	-0.18	1.00	-0.12	1.00	-0.62	0.04
D430042O09Rik	-0.04	1.00	-0.12	1.00	-0.23	1.00	-0.81	0.00
D4Wsu53e	-0.21	1.00	-0.61	0.04	0.20	1.00	-0.11	0.92
D630037F22Rik	-0.05	1.00	-0.24	1.00	-0.24	1.00	-0.80	0.04
D830029L11	0.38	1.00	0.38	1.00	0.85	0.71	1.21	0.00
Dact3	0.01	1.00	-0.08	1.00	-0.23	1.00	-0.68	0.00
Dapk1	-0.13	1.00	-0.28	1.00	-0.10	1.00	-0.84	0.00
Dbp	-0.23	1.00	-0.60	0.63	-0.36	1.00	-1.36	0.00
Dbt	-0.02	1.00	-0.32	1.00	-0.26	1.00	-0.73	0.00
Ddah1	0.19	1.00	0.58	0.15	0.05	1.00	0.76	0.00
Ddit4	-0.02	1.00	-0.38	0.79	-0.20	1.00	-1.02	0.00

Ddx21	0.13	1.00	0.12	1.00	0.25	1.00	0.62	0.02
Ddx3y	0.16	1.00	0.22	1.00	0.38	1.00	0.62	0.01
Dgat2	-0.27	1.00	-0.59	0.25	-0.19	1.00	-0.76	0.01
Diras2	0.33	1.00	0.49	1.00	0.22	1.00	1.28	0.00
Dixdc1	-0.04	1.00	-0.43	0.75	-0.59	0.32	-1.03	0.00
Dlk2	0.22	1.00	0.96	1.00	0.74	1.00	2.30	0.05
Dnaja4	0.58	1.00	0.66	0.05	0.46	0.55	1.40	0.00
Dnajb4	0.60	1.00	0.71	0.01	0.56	0.14	1.12	0.00
Dnajb5	0.29	1.00	0.67	0.03	0.47	0.53	1.33	0.00
Dnajc28	-0.19	1.00	-0.65	0.08	-0.01	1.00	-0.92	0.00
Dock5	0.00	1.00	0.30	1.00	-0.04	1.00	0.70	0.04
Dok7	0.28	1.00	0.32	1.00	-0.48	1.00	0.82	0.01
Dot1l	0.24	1.00	0.16	1.00	0.16	1.00	0.83	0.00
Dpf3	0.01	1.00	-0.30	1.00	-0.53	1.00	-1.41	0.00
Dusp1	1.67	0.00	1.73	0.00	0.53	0.29	0.81	0.00
Dusp10	0.49	1.00	0.58	0.31	0.35	1.00	1.52	0.00
Dusp27	0.44	1.00	0.65	0.09	0.41	0.79	1.19	0.00
Dusp4	0.51	1.00	0.87	0.00	0.35	1.00	1.07	0.00
Dusp5	1.13	0.07	1.26	0.00	0.34	1.00	0.92	0.01
Dusp6	1.04	0.00	1.60	0.00	0.27	1.00	0.79	0.00
Dusp8	0.85	0.13	1.46	0.00	1.03	0.00	1.77	0.00
E330013P06	1.47	0.03	0.99	0.19	0.81	1.00	1.12	0.02
E330017L17Rik	-0.17	1.00	-0.52	1.00	0.05	1.00	-1.39	0.02
Ears2	0.57	1.00	0.70	0.03	0.34	1.00	1.20	0.00
Edn1	0.95	0.12	1.29	0.00	0.63	0.53	0.92	0.00
Ednra	-0.29	1.00	-0.58	0.07	-0.34	1.00	-1.52	0.00
Eef1e1	0.11	1.00	0.28	1.00	0.00	1.00	0.72	0.02
Efhd2	0.18	1.00	0.42	0.64	0.24	1.00	0.74	0.00
Efna2	-0.03	1.00	-0.28	1.00	-0.32	1.00	-0.92	0.04
Efnb2	0.27	1.00	0.40	0.73	0.15	1.00	0.78	0.00
Efnb3	0.04	1.00	-1.03	0.00	0.48	0.46	-0.88	0.00
Efr3b	0.21	1.00	0.27	1.00	0.25	1.00	1.06	0.00
Egr1	3.53	0.00	3.77	0.00	0.23	1.00	0.72	0.00
Egr2	2.72	0.00	3.17	0.00	0.08	1.00	0.70	0.11
Egr3	2.81	0.00	3.18	0.00	0.03	1.00	0.61	0.36
Eif1a	0.15	1.00	0.40	0.64	0.29	1.00	0.86	0.00
Ell2	0.03	1.00	0.25	1.00	0.06	1.00	0.66	0.02
Enah	0.56	1.00	0.60	0.50	0.33	1.00	1.51	0.00
Engase	-0.31	1.00	-0.50	1.00	-0.54	1.00	-0.99	0.01
Entpd5	-0.12	1.00	-0.41	0.88	-0.06	1.00	-0.71	0.00

Epha2	0.62	1.00	1.02	0.00	0.60	0.37	1.50	0.00
Epha4	-0.10	1.00	-0.33	1.00	-0.37	1.00	-0.96	0.00
Eppk1	0.60	1.00	0.64	0.30	0.32	1.00	2.17	0.00
Ereg	2.22	0.00	2.97	0.00	0.69	0.76	2.08	0.00
Errfi1	1.50	0.00	1.94	0.00	0.54	0.46	1.30	0.00
Esyt2	-0.07	1.00	0.20	1.00	0.24	1.00	0.58	0.03
Extl1	-0.10	1.00	-0.21	1.00	-0.69	0.10	-1.36	0.00
Extl3	-0.10	1.00	-0.24	1.00	-0.25	1.00	-0.84	0.00
Ezr	-0.07	1.00	-0.18	1.00	-0.09	1.00	-0.59	0.02
F2rl1	0.53	1.00	0.97	0.22	0.06	1.00	1.38	0.00
Fam105b	0.37	1.00	0.47	0.40	0.46	0.59	1.43	0.00
Fam107b	-0.02	1.00	0.22	1.00	0.16	1.00	0.63	0.05
Fam124a	0.00	1.00	0.30	1.00	0.06	1.00	0.66	0.04
Fam13a	0.03	1.00	-0.08	1.00	0.04	1.00	1.28	0.00
Fam161b	0.09	1.00	-0.20	1.00	-0.46	1.00	-1.00	0.01
Fam163b	-0.08	1.00	-0.15	1.00	-0.31	1.00	-1.50	0.04
Fam198b	0.27	1.00	0.59	0.29	0.39	1.00	1.33	0.00
Fam19a3	-0.10	1.00	-0.19	1.00	-0.71	1.00	-0.93	0.05
Fam19a5	0.23	1.00	0.26	1.00	-0.18	1.00	1.32	0.00
Fam20c	0.14	1.00	0.26	1.00	0.06	1.00	0.62	0.02
Fam46a	0.99	0.01	1.34	0.00	0.59	0.11	1.19	0.00
Fam46b	0.55	1.00	0.83	0.12	-0.04	1.00	1.81	0.00
Fbxo16	0.00	1.00	0.29	1.00	-0.74	1.00	-1.11	0.04
Fbxo21	-0.04	1.00	-0.13	1.00	-0.25	1.00	-0.65	0.01
Fbxo30	0.10	1.00	0.21	1.00	0.34	1.00	0.67	0.01
Fbxo31	0.00	1.00	-0.24	1.00	-0.23	1.00	-0.67	0.01
Fbxo32	0.05	1.00	-0.46	0.54	0.02	1.00	-1.09	0.00
Fbxo40	0.36	1.00	0.42	0.59	0.26	1.00	0.88	0.00
Fdps	0.23	1.00	0.69	0.03	-0.23	1.00	0.16	0.85
Fem1b	0.00	1.00	0.08	1.00	0.18	1.00	0.57	0.03
Fgd3	-0.09	1.00	0.49	1.00	0.17	1.00	0.84	0.02
Fgd4	-0.02	1.00	-0.33	1.00	-0.14	1.00	-0.82	0.00
Fgf1	-0.12	1.00	0.03	1.00	-0.27	1.00	-0.55	0.04
Fgf9	-0.08	1.00	0.01	1.00	-0.34	1.00	-1.12	0.04
Fgfr3	1.12	1.00	0.85	0.64	-0.11	1.00	2.01	0.00
Fhdc1	0.22	1.00	0.66	0.22	0.23	1.00	0.83	0.01
Fhl1	1.19	1.00	1.02	0.19	-0.38	1.00	1.40	0.00
Fhl3	0.11	1.00	0.50	0.40	0.13	1.00	0.83	0.00
Fign	-0.06	1.00	-0.42	1.00	-0.48	1.00	-1.16	0.00
Filip1	0.29	1.00	0.38	0.85	0.21	1.00	0.65	0.01

Flnb	0.03	1.00	0.34	1.00	-0.09	1.00	0.61	0.02
Flnc	0.37	1.00	0.23	1.00	0.06	1.00	1.54	0.00
Flt1	0.00	1.00	0.47	0.46	0.07	1.00	0.77	0.00
Fn3k	-0.18	1.00	-0.23	1.00	-0.27	1.00	-0.91	0.02
Fndc5	-0.25	1.00	-0.81	0.00	-0.24	1.00	-1.22	0.00
Fos	4.46	0.00	4.83	0.00	0.43	1.00	1.23	0.00
Fosb	4.03	0.00	4.54	0.00	-0.18	1.00	1.06	0.04
Fosl2	0.76	0.19	1.11	0.00	0.55	0.14	1.22	0.00
Foxo3	-0.08	1.00	-0.23	1.00	-0.05	1.00	-0.56	0.05
Foxo6	-0.18	1.00	-0.63	0.31	-0.51	1.00	-1.65	0.00
Foxs1	0.26	1.00	0.75	0.14	0.35	1.00	0.86	0.01
Frem2	-0.35	1.00	-0.34	1.00	-0.71	0.01	-1.09	0.00
Frmd5	0.35	1.00	0.41	0.66	0.18	1.00	0.81	0.00
Fscn1	0.13	1.00	0.46	0.39	0.46	0.46	0.85	0.00
Fsd1l	0.34	1.00	0.59	0.24	0.31	1.00	1.35	0.00
Fst	0.39	1.00	1.41	0.00	0.67	1.00	1.32	0.00
Fstl3	0.30	1.00	0.45	0.53	-0.15	1.00	0.69	0.01
Fzd4	-0.28	1.00	-0.27	1.00	-0.27	1.00	-0.67	0.02
Gabarapl1	0.09	1.00	-0.04	1.00	0.25	1.00	0.66	0.01
Gadd45a	-0.15	1.00	-0.43	0.97	-0.52	0.86	-0.88	0.00
Gadd45g	1.52	0.00	2.16	0.00	0.26	1.00	1.69	0.00
Gal3st3	-0.18	1.00	-0.59	0.52	-0.49	1.00	-1.56	0.00
Gbp10	0.14	1.00	-0.36	1.00	0.44	1.00	-1.13	0.05
Gbp6	0.07	1.00	-0.49	1.00	0.40	1.00	-1.18	0.00
Gcnt4	0.28	1.00	1.04	0.00	0.15	1.00	1.11	0.00
Gda	-0.20	1.00	-0.32	1.00	0.40	1.00	1.01	0.01
Gdf15	0.78	0.45	1.02	0.00	0.17	1.00	0.88	0.00
Gdf6	0.38	1.00	0.83	0.03	0.79	0.15	1.56	0.00
Gdnf	1.18	1.00	1.95	0.00	-0.03	1.00	1.58	0.00
Gdpd1	-0.06	1.00	-0.35	1.00	-0.26	1.00	-0.98	0.00
Gdpd5	-0.13	1.00	-0.43	0.89	-0.33	1.00	-0.81	0.01
Gja5	-0.20	1.00	-0.32	1.00	-0.04	1.00	-0.76	0.00
Glul	0.35	1.00	0.43	1.00	0.32	1.00	0.78	0.01
Gm10406	1.20	0.26	0.99	0.08	0.07	1.00	1.60	0.00
Gm1078	-0.31	1.00	-0.49	0.47	-0.34	1.00	-1.06	0.00
Gm12295	0.21	1.00	0.29	1.00	-1.03	0.01	-0.51	0.20
Gm13363	0.23	1.00	0.31	1.00	0.26	1.00	0.68	0.04
Gm1337	-0.47	1.00	-0.69	0.33	-0.53	1.00	-1.34	0.00
Gm13889	0.63	1.00	0.68	0.39	0.00	1.00	1.10	0.00
Gm16197	-0.05	1.00	-0.43	1.00	-0.12	1.00	-1.09	0.01

Gm16515	-0.06	1.00	-0.24	1.00	-0.16	1.00	-0.63	0.01
Gm19277	-0.20	1.00	-0.82	0.15	0.51	1.00	-0.91	0.02
Gm2897	1.18	0.83	0.89	0.45	0.06	1.00	1.38	0.00
Gm3002	0.97	0.45	0.60	0.67	0.53	1.00	1.75	0.00
Gm3264	1.15	1.00	1.16	0.39	0.28	1.00	1.70	0.00
Gm3383	1.10	1.00	0.91	1.00	0.01	1.00	1.62	0.04
Gm3696	0.97	1.00	0.65	0.97	-0.17	1.00	1.34	0.00
Gm5105	0.39	1.00	0.23	1.00	0.02	1.00	0.70	0.03
Gm5796	1.20	0.45	0.86	0.36	0.12	1.00	1.60	0.00
Gm5797	1.17	1.00	0.82	1.00	0.15	1.00	1.52	0.03
Gm6460	3.83	0.00	2.19	0.04	-0.37	1.00	2.81	0.00
Gm6682	0.16	1.00	0.70	0.02	-0.10	1.00	0.55	0.05
Gm8348	1.28	0.25	1.18	0.03	0.28	1.00	1.78	0.00
Gm8615	-0.24	1.00	-0.40	1.00	-7.59	0.00	-0.33	0.69
Gm889	-0.34	1.00	0.19	1.00	0.66	0.37	0.72	0.03
Gnai1	0.21	1.00	0.36	0.98	0.17	1.00	0.85	0.00
Gnb4	0.05	1.00	0.47	0.56	0.16	1.00	0.62	0.04
Gpatch4	0.21	1.00	0.26	1.00	0.13	1.00	0.73	0.05
Gpr155	-0.08	1.00	-0.29	1.00	-0.47	1.00	-1.29	0.00
Gpr176	-0.02	1.00	0.55	0.22	0.44	1.00	0.95	0.00
Gpr56	-0.05	1.00	-0.20	1.00	-0.31	1.00	-0.74	0.00
Gramd1b	-0.15	1.00	-0.23	1.00	-0.23	1.00	-0.99	0.00
Grb14	-0.11	1.00	-0.38	0.82	0.13	1.00	-0.82	0.00
Grem1	-0.14	1.00	0.87	0.18	-0.29	1.00	0.96	0.02
Grk5	0.18	1.00	0.24	1.00	0.40	0.86	0.57	0.03
Grwd1	0.34	1.00	0.36	1.00	0.22	1.00	0.90	0.00
Gsg1l	-0.08	1.00	-0.14	1.00	-0.37	1.00	-0.87	0.00
Gsto1	0.23	1.00	0.34	1.00	-0.02	1.00	0.91	0.00
Gucy1a3	-0.10	1.00	-0.69	0.01	0.24	1.00	-0.46	0.14
Gypc	-0.28	1.00	-0.27	1.00	-0.37	1.00	-0.68	0.01
Has2	0.49	1.00	1.16	0.02	0.11	1.00	0.91	0.06
Hbegf	1.38	0.01	1.83	0.00	0.99	0.00	2.48	0.00
Hcn2	-0.26	1.00	-0.60	0.38	0.06	1.00	-0.80	0.02
Hcn4	-0.11	1.00	-0.52	0.50	-0.36	1.00	-0.73	0.02
Hdac11	-0.23	1.00	-0.59	0.11	-0.45	0.81	-1.59	0.00
Heatr1	0.13	1.00	0.10	1.00	0.26	1.00	0.76	0.00
Heatr5a	0.10	1.00	0.17	1.00	0.06	1.00	0.62	0.02
Hectd2	0.24	1.00	0.62	0.91	0.57	1.00	1.16	0.01
Herc3	0.25	1.00	0.36	0.95	0.17	1.00	0.92	0.00
Hey2	-0.01	1.00	-0.61	0.31	-0.43	1.00	-1.51	0.00

Hfe2	-0.20	1.00	-0.11	1.00	-0.32	1.00	-0.60	0.02
Hist3h2a	-0.11	1.00	-0.27	1.00	-0.40	1.00	-0.82	0.00
Hk2	0.50	1.00	0.55	0.19	0.23	1.00	1.17	0.00
Hlf	-0.26	1.00	-0.88	0.00	-0.47	0.79	-1.69	0.00
Hmga2	0.07	1.00	0.68	0.02	0.04	1.00	0.56	0.05
Hmgcr	0.28	1.00	0.62	0.04	-0.04	1.00	0.73	0.00
Hmgcs2	-0.05	1.00	-0.72	1.00	-0.27	1.00	-1.50	0.03
Hmox1	0.01	1.00	-0.03	1.00	-0.14	1.00	1.23	0.00
Hr	0.29	1.00	0.45	0.54	-0.01	1.00	1.15	0.00
Hs6st1	0.14	1.00	0.31	1.00	0.27	1.00	0.63	0.02
Hsp90aa1	0.28	1.00	0.30	1.00	0.24	1.00	0.94	0.00
Hspa12a	-0.11	1.00	-0.09	1.00	-0.49	0.79	-0.64	0.03
Hspa1a	1.05	0.08	0.40	1.00	-0.01	1.00	2.07	0.00
Hspa1b	0.90	0.32	0.39	1.00	0.15	1.00	1.92	0.00
Hspa1l	0.66	1.00	0.79	0.02	0.30	1.00	1.53	0.00
Hspb1	1.21	1.00	0.86	0.07	-0.32	1.00	1.46	0.00
Hspb8	0.24	1.00	0.20	1.00	0.20	1.00	0.76	0.00
Hsph1	0.39	1.00	0.18	1.00	-0.03	1.00	0.58	0.03
Id1	0.67	1.00	1.11	0.00	-0.56	1.00	-0.22	0.84
Idi1	0.15	1.00	0.65	0.05	-0.31	1.00	0.39	0.25
Ier2	2.35	0.00	2.70	0.00	0.02	1.00	0.41	0.30
Ier3	1.16	0.00	1.51	0.00	0.59	0.11	1.49	0.00
Ier5	1.13	0.00	1.54	0.00	0.45	0.56	1.24	0.00
Ifit1	-0.67	1.00	0.44	1.00	1.37	0.00	-0.71	0.11
Ifit3	-0.48	1.00	0.26	1.00	1.03	0.01	-0.33	0.66
Ifrd1	0.40	1.00	0.42	0.53	0.14	1.00	0.74	0.00
Igf1r	0.13	1.00	0.07	1.00	0.18	1.00	0.68	0.01
Igf2bp2	0.20	1.00	0.23	1.00	0.29	1.00	0.83	0.00
Ildr2	1.43	0.00	1.00	0.00	-0.40	1.00	0.98	0.00
Inhba	1.27	0.01	1.49	0.00	0.75	0.05	2.03	0.00
Inpp4b	0.16	1.00	0.32	1.00	0.29	1.00	1.57	0.00
Insc	0.52	1.00	0.79	1.00	0.55	1.00	1.24	0.02
Irgm2	-0.16	1.00	-0.21	1.00	0.25	1.00	-0.70	0.02
Irs2	1.26	0.00	1.13	0.00	0.29	1.00	0.51	0.18
Irx4	-0.12	1.00	-0.36	0.85	-0.24	1.00	-0.92	0.00
Ism1	-0.03	1.00	0.36	1.00	0.52	1.00	0.92	0.05
Itga5	0.42	1.00	0.49	0.64	0.24	1.00	1.22	0.00
Itga7	0.38	1.00	0.55	0.19	-0.09	1.00	0.58	0.04
Itgb1bp3	1.25	0.02	1.46	0.00	-0.39	1.00	2.05	0.00
Jub	0.24	1.00	0.28	1.00	0.29	1.00	0.85	0.00

Jun	2.11	0.00	2.05	0.00	0.42	0.77	0.63	0.01
Junb	1.99	0.00	2.20	0.00	0.10	1.00	0.27	0.59
Jund	0.43	1.00	0.54	0.23	0.49	0.46	0.71	0.01
Kbtbd10	0.25	1.00	0.09	1.00	0.08	1.00	0.94	0.00
Kbtbd5	0.18	1.00	0.45	0.54	-0.25	1.00	1.17	0.00
Kcnb1	-0.41	1.00	-0.27	1.00	-0.43	0.72	-0.82	0.00
Kcnh2	-0.19	1.00	-0.37	0.94	-0.41	0.83	-1.01	0.00
Kcnj12	0.08	1.00	-0.08	1.00	-0.33	1.00	-1.06	0.00
Kcnj2	-0.49	1.00	-0.98	0.00	-0.29	1.00	-1.29	0.00
Kcnj3	-0.10	1.00	-0.37	1.00	-0.17	1.00	-1.08	0.00
Kcnj5	-0.26	1.00	-0.55	0.18	-0.39	1.00	-1.29	0.00
Kcnk2	0.14	1.00	1.03	0.20	0.31	1.00	1.17	0.03
Kcnn2	-0.35	1.00	-0.40	1.00	-0.49	1.00	-1.42	0.00
Kcnq1	-0.01	1.00	-0.10	1.00	-0.39	1.00	-0.91	0.00
Kctd10	0.22	1.00	0.48	0.40	0.30	1.00	0.71	0.01
Kctd9	0.23	1.00	0.40	0.64	0.04	1.00	0.67	0.01
Kif26b	-0.13	1.00	-0.08	1.00	-0.53	0.27	-0.97	0.00
Kif5b	0.13	1.00	0.28	1.00	0.25	1.00	0.69	0.03
Klc4	0.00	1.00	-0.22	1.00	-0.07	1.00	-0.55	0.05
Klf11	0.12	1.00	-0.17	1.00	0.01	1.00	-0.66	0.02
Klf2	1.10	0.00	1.52	0.00	0.11	1.00	0.37	0.41
Klf4	0.38	1.00	0.87	0.00	-0.05	1.00	0.53	0.08
Klf5	0.13	1.00	0.61	1.00	0.41	1.00	1.43	0.00
Klf6	0.95	0.01	1.30	0.00	0.48	0.37	0.96	0.00
Klhdc7a	-0.34	1.00	-0.28	1.00	-0.68	1.00	-1.41	0.00
Klhdc8b	-0.11	1.00	-0.31	1.00	-0.31	1.00	-0.78	0.02
Klhl29	0.05	1.00	0.30	1.00	0.69	0.86	1.47	0.00
Klhl3	0.01	1.00	-0.08	1.00	-0.53	1.00	-1.10	0.05
Klhl34	1.45	1.00	1.58	0.27	1.57	0.55	2.44	0.00
Klhl38	-0.25	1.00	-0.51	0.31	-0.04	1.00	-1.07	0.00
Klrg2	0.47	1.00	0.42	1.00	0.67	1.00	1.18	0.00
Kpna1	0.16	1.00	0.14	1.00	0.17	1.00	0.64	0.01
Kremen1	0.55	1.00	0.36	1.00	0.05	1.00	0.86	0.00
Krt18	0.65	1.00	0.37	0.97	0.15	1.00	1.05	0.00
Krt19	1.47	0.27	1.52	0.01	-0.06	1.00	1.76	0.00
Krt80	0.97	0.55	1.33	0.00	-0.27	1.00	0.86	0.02
Ky	-0.29	1.00	-0.59	0.07	-0.89	0.00	-2.21	0.00
Lama5	0.14	1.00	-0.36	1.00	0.00	1.00	-0.67	0.02
Lancl3	0.10	1.00	0.42	1.00	0.26	1.00	1.31	0.00
Ldlr	0.46	1.00	0.74	0.03	-0.10	1.00	1.02	0.00

Leprel1	0.89	0.32	0.65	0.18	-0.10	1.00	0.71	0.03
Letm2	-0.15	1.00	-0.59	0.71	-0.37	1.00	-0.81	0.05
Lgr6	-0.17	1.00	-0.26	1.00	-0.60	0.52	-0.70	0.03
Lif	1.76	0.01	2.52	0.00	0.23	1.00	1.25	0.00
Lims2	0.58	1.00	0.79	0.12	0.43	1.00	1.75	0.00
Lingo3	0.03	1.00	-0.86	0.51	-0.57	1.00	-2.10	0.00
Lmcd1	1.24	0.01	0.96	0.00	0.58	0.35	2.77	0.00
Lmod1	0.09	1.00	0.66	0.11	0.47	1.00	0.88	0.00
Lmod2	0.69	1.00	0.84	0.04	0.73	0.11	0.95	0.00
Lmod3	0.18	1.00	0.60	0.07	0.44	0.68	1.15	0.00
Lpar3	-0.10	1.00	-0.61	0.06	-0.15	1.00	-1.34	0.00
Lpin1	0.04	1.00	-0.32	1.00	0.08	1.00	-0.82	0.00
Lrig1	0.00	1.00	-0.34	1.00	-0.12	1.00	-0.62	0.02
Lrp8	0.37	1.00	0.92	0.00	-0.07	1.00	1.40	0.00
Lrrc14b	-0.11	1.00	-0.46	1.00	-0.26	1.00	-0.96	0.02
Lrrc17	-0.23	1.00	-0.40	1.00	-0.13	1.00	-0.99	0.00
Lrrc20	-0.01	1.00	-0.09	1.00	-0.28	1.00	-0.63	0.01
Lrrc32	-0.07	1.00	-0.21	1.00	0.40	1.00	0.76	0.00
Lrrc3b	0.54	1.00	0.96	0.00	0.07	1.00	0.54	0.14
Lrrc4b	-0.18	1.00	-0.36	1.00	-0.51	0.46	-1.30	0.00
Lypd6	1.34	0.25	1.21	0.03	-0.12	1.00	1.52	0.00
Lyst	0.06	1.00	-0.06	1.00	0.02	1.00	0.59	0.03
Maff	0.63	1.00	1.09	0.00	0.73	0.22	1.52	0.00
Mafg	0.32	1.00	0.35	1.00	0.35	1.00	0.68	0.01
Mafk	0.66	1.00	0.87	0.00	0.68	0.02	1.51	0.00
Map2k3	0.15	1.00	0.32	1.00	0.16	1.00	0.72	0.00
Map2k6	-0.02	1.00	-0.37	1.00	-0.66	0.83	-1.63	0.00
Map3k5	0.15	1.00	0.09	1.00	0.65	0.06	1.06	0.00
Map3k6	0.12	1.00	0.32	1.00	0.11	1.00	0.77	0.04
Mapk4	0.16	1.00	0.58	0.37	0.04	1.00	0.99	0.00
Mapk6	0.17	1.00	0.28	1.00	0.22	1.00	0.67	0.01
March3	0.29	1.00	0.62	0.17	0.63	0.32	1.05	0.00
Mbd5	0.07	1.00	-0.12	1.00	-0.49	0.62	-0.72	0.01
Mcam	0.37	1.00	0.38	1.00	0.05	1.00	0.71	0.02
Mcm7	-0.19	1.00	-0.12	1.00	-0.46	0.78	-0.64	0.02
Mdn1	-0.08	1.00	-0.17	1.00	0.06	1.00	0.64	0.02
Meox1	-0.14	1.00	0.32	1.00	0.02	1.00	0.77	0.02
Mettl7a1	-0.10	1.00	-0.31	1.00	-0.33	1.00	-0.91	0.00
Mfsd7c	-0.25	1.00	-0.62	0.70	-0.26	1.00	-1.56	0.00
Mllt11	0.54	1.00	0.61	0.10	0.05	1.00	0.80	0.00

Mmp11	-0.11	1.00	-0.50	0.25	-0.14	1.00	-0.85	0.00
Mmp15	-0.20	1.00	-0.20	1.00	-0.13	1.00	-0.99	0.00
Mob3a	0.27	1.00	0.57	0.16	0.25	1.00	0.87	0.00
Mospd1	-0.10	1.00	-0.30	1.00	-0.03	1.00	-0.60	0.02
Mphosph10	0.07	1.00	0.29	1.00	0.15	1.00	0.65	0.03
Mreg	-0.04	1.00	-0.57	0.63	-0.11	1.00	-0.94	0.01
Mrm1	-0.31	1.00	-0.52	0.50	-0.40	1.00	-0.74	0.02
Msrb2	-0.28	1.00	-0.29	1.00	-0.11	1.00	-0.72	0.01
Msrb3	0.11	1.00	0.32	1.00	0.20	1.00	0.70	0.01
Mt1	0.15	1.00	-0.29	1.00	0.12	1.00	0.89	0.00
Mt2	0.18	1.00	-0.36	1.00	0.12	1.00	1.44	0.00
Mterfd3	-0.19	1.00	-0.27	1.00	-0.15	1.00	-0.86	0.02
Mtfp1	-0.22	1.00	-0.12	1.00	-0.53	1.00	-0.93	0.01
Mtpn	0.18	1.00	0.35	1.00	0.33	1.00	1.07	0.00
Mum1l1	0.18	1.00	0.34	1.00	0.27	1.00	1.01	0.00
Murc	0.36	1.00	0.68	0.04	0.60	0.22	1.73	0.00
Mustn1	-0.23	1.00	0.32	1.00	-0.04	1.00	0.66	0.03
Mxd1	-0.14	1.00	-0.32	1.00	-0.20	1.00	-0.68	0.02
Myadml2	-0.17	1.00	-0.13	1.00	-0.39	1.00	-0.79	0.00
Mybpc2	-0.03	1.00	0.15	1.00	-1.08	0.00	-0.59	0.05
Myc	1.05	0.23	1.54	0.00	0.46	1.00	1.27	0.00
Myh9	0.20	1.00	0.31	1.00	0.13	1.00	0.73	0.02
Myl1	0.17	1.00	0.81	0.00	-0.28	1.00	0.06	0.98
Myl12a	0.10	1.00	0.35	1.00	0.03	1.00	0.75	0.04
Myo1c	0.12	1.00	0.36	1.00	0.26	1.00	0.81	0.01
Myo1e	0.19	1.00	0.10	1.00	0.21	1.00	0.71	0.00
Ncapd2	-0.13	1.00	-0.14	1.00	-0.51	0.37	-0.81	0.00
Nceh1	0.03	1.00	-0.23	1.00	-0.11	1.00	-0.68	0.01
Ndrg1	-0.03	1.00	0.18	1.00	0.07	1.00	0.76	0.01
Neat1	0.36	1.00	0.03	1.00	1.12	0.00	1.35	0.00
Negr1	-0.02	1.00	-0.38	1.00	1.40	0.01	0.46	0.61
Nes	0.76	1.00	0.75	0.04	-0.10	1.00	1.56	0.00
Neto2	0.41	1.00	0.54	0.78	0.33	1.00	1.63	0.00
Neurl1b	0.01	1.00	-0.15	1.00	-0.67	0.73	-0.96	0.01
Nfatc2	0.49	1.00	0.44	1.00	0.04	1.00	0.90	0.00
Nfia	-0.08	1.00	-0.12	1.00	-0.30	1.00	-0.79	0.00
Nfil3	1.02	0.00	1.27	0.00	0.67	0.05	1.23	0.00
Nfkbiz	1.18	0.01	1.35	0.00	0.03	1.00	0.47	0.41
Ngef	-0.14	1.00	0.81	0.38	0.37	1.00	1.55	0.00
Ngp	-0.03	1.00	0.06	1.00	-2.67	0.02	-1.00	0.22

Nhsl1	0.06	1.00	-0.31	1.00	-0.24	1.00	-1.13	0.00
Nipal3	-0.06	1.00	-0.26	1.00	-0.21	1.00	-0.72	0.00
Nkiras2	-0.11	1.00	-0.22	1.00	-0.22	1.00	-0.56	0.03
Nmt2	0.24	1.00	0.37	1.00	0.21	1.00	0.74	0.01
Nol10	0.17	1.00	0.26	1.00	0.33	1.00	0.69	0.02
Nolc1	0.11	1.00	0.25	1.00	0.26	1.00	0.70	0.03
Nop58	0.16	1.00	0.33	1.00	0.29	1.00	0.92	0.00
Nos2	-0.34	1.00	-1.47	0.04	0.23	1.00	-0.02	1.00
Nppb	2.21	0.72	2.48	0.00	1.22	0.00	3.17	0.00
Nptx1	-0.67	0.72	0.41	0.90	-0.15	1.00	0.73	0.01
Nr0b2	-0.34	1.00	-0.54	1.00	-0.34	1.00	-1.21	0.00
Nr3c2	-0.14	1.00	-0.60	0.40	-0.52	1.00	-1.48	0.00
Nr4a1	2.53	0.00	2.72	0.00	0.50	0.48	0.74	0.00
Nr4a2	0.33	1.00	0.89	0.03	-0.32	1.00	0.29	0.76
Nr4a3	1.55	0.20	2.07	0.00	1.19	0.52	1.99	0.00
Nrap	0.52	1.00	0.46	1.00	0.34	1.00	1.70	0.00
Nrip3	1.09	1.00	0.85	0.55	-0.32	1.00	2.23	0.00
Nt5c2	0.35	1.00	0.33	1.00	0.07	1.00	0.76	0.00
Nt5c3	0.04	1.00	-0.32	1.00	-0.05	1.00	-0.76	0.00
Nt5e	0.19	1.00	0.18	1.00	0.44	0.60	1.53	0.00
Ntn1	-0.07	1.00	-0.38	0.75	-0.22	1.00	-0.90	0.00
Ntn4	-0.17	1.00	-0.04	1.00	0.75	0.01	0.66	0.01
Nuak1	0.59	1.00	1.02	0.00	0.55	0.16	1.42	0.00
Nudt18	0.16	1.00	0.42	0.63	0.48	0.51	1.17	0.00
Nudt22	-0.15	1.00	-0.20	1.00	-0.56	0.79	-0.93	0.00
Numa1	0.06	1.00	-0.19	1.00	-0.16	1.00	-0.58	0.03
Nxph3	-0.25	1.00	0.35	1.00	0.16	1.00	1.44	0.00
ORF63	1.04	0.45	1.05	0.01	0.49	1.00	2.39	0.00
Olfml1	-0.23	1.00	-0.80	0.20	-0.42	1.00	-1.08	0.00
Olr1	0.36	1.00	0.68	1.00	0.70	1.00	1.33	0.00
Osbp2	-0.38	1.00	-0.37	1.00	-0.19	1.00	-1.19	0.01
Osmr	0.24	1.00	0.46	0.35	0.28	1.00	0.75	0.00
Otud1	1.98	0.00	2.67	0.00	1.09	0.00	1.92	0.00
P2rx5	0.19	1.00	0.38	1.00	0.04	1.00	0.76	0.00
P4htm	-0.14	1.00	-0.10	1.00	-0.47	1.00	-0.79	0.02
Pacsin3	0.29	1.00	0.51	0.29	-0.01	1.00	0.74	0.00
Pak6	-0.08	1.00	-0.20	1.00	-0.47	0.98	-0.76	0.02
Palm2	0.08	1.00	0.31	1.00	0.23	1.00	1.00	0.00
Pank1	-0.09	1.00	-0.07	1.00	-0.11	1.00	-0.67	0.03
Paqr7	-0.19	1.00	-0.30	1.00	-0.37	1.00	-0.97	0.00

Paqr8	0.64	1.00	0.67	0.30	0.03	1.00	1.23	0.00
Pard6b	0.03	1.00	0.31	1.00	0.27	1.00	0.72	0.04
Pawr	0.19	1.00	0.47	0.66	0.36	1.00	0.74	0.01
Pcgf5	0.22	1.00	0.34	1.00	0.30	1.00	0.64	0.01
Pdcl3	0.14	1.00	0.34	1.00	0.24	1.00	0.74	0.00
Pde7b	-0.04	1.00	-0.16	1.00	-0.32	1.00	-0.67	0.04
Pdgfb	-0.12	1.00	0.00	1.00	0.35	1.00	0.66	0.02
Pdgfc	0.39	1.00	0.95	0.00	0.44	1.00	1.37	0.00
Pdk2	0.00	1.00	-0.32	1.00	0.04	1.00	-0.61	0.02
Pdlim3	0.13	1.00	0.28	1.00	0.13	1.00	0.71	0.00
Pdpk1	0.12	1.00	0.14	1.00	0.09	1.00	0.61	0.02
Pdxp	0.07	1.00	0.05	1.00	-0.43	1.00	-0.83	0.02
Per3	-0.10	1.00	-0.31	1.00	-0.32	1.00	-1.09	0.00
Phactr2	0.00	1.00	-0.21	1.00	0.02	1.00	-0.66	0.04
Phlda1	0.66	0.64	1.19	0.00	0.29	1.00	0.82	0.00
Phyhip	-0.18	1.00	-0.29	1.00	-0.50	0.74	-0.60	0.05
Picalm	0.24	1.00	0.37	1.00	0.32	1.00	0.97	0.00
Pik3cb	0.45	1.00	0.40	0.81	0.23	1.00	1.14	0.00
Pik3ip1	-0.35	1.00	-0.88	0.00	-0.28	1.00	-1.26	0.00
Pik3r3	-0.23	1.00	-0.29	1.00	-0.40	0.81	-0.97	0.00
Pirt	0.14	1.00	0.03	1.00	-0.32	1.00	-0.54	0.05
Pitpnc1	-0.13	1.00	-0.30	1.00	-0.08	1.00	-0.80	0.00
Pkdrej	0.08	1.00	-0.20	1.00	-0.06	1.00	-1.07	0.02
Pla2g4a	0.06	1.00	0.50	0.42	0.16	1.00	1.00	0.00
Pla2g4e	-0.06	1.00	-0.22	1.00	-0.69	1.00	-1.46	0.00
Plcl2	-0.20	1.00	-0.30	1.00	-0.38	1.00	-0.75	0.02
Plcxd2	0.83	0.85	0.97	0.00	0.67	0.32	2.19	0.00
Plekha1	0.06	1.00	0.06	1.00	0.21	1.00	0.57	0.03
Plekha7	-0.15	1.00	0.00	1.00	-0.55	0.30	-0.96	0.00
Plekhh1	-0.73	1.00	-0.98	0.02	0.10	1.00	-1.42	0.00
Plin4	-0.04	1.00	-0.25	1.00	-0.44	1.00	-0.76	0.02
Plk2	1.77	0.00	2.10	0.00	0.66	0.04	1.75	0.00
Plk3	0.82	1.00	1.12	0.02	0.28	1.00	0.98	0.02
Plxnb1	-0.08	1.00	-0.20	1.00	-0.42	0.73	-0.86	0.00
Pold1	-0.09	1.00	-0.16	1.00	-0.47	1.00	-0.66	0.04
Polr1e	0.08	1.00	0.21	1.00	0.12	1.00	0.67	0.02
Polr3d	0.17	1.00	0.25	1.00	0.17	1.00	0.63	0.04
Popdc3	0.44	1.00	0.61	0.06	-0.04	1.00	0.67	0.01
Pou3f1	0.35	1.00	0.55	1.00	0.65	1.00	1.96	0.00
Ppap2a	0.04	1.00	0.32	1.00	0.10	1.00	0.76	0.02

Ppara	-0.23	1.00	-0.45	0.69	-0.22	1.00	-0.78	0.01
Ppargc1a	0.07	1.00	-0.03	1.00	-0.02	1.00	-0.64	0.03
Ppfibp2	-0.04	1.00	-0.33	1.00	-0.16	1.00	-1.20	0.00
Ppil1	-0.18	1.00	-0.29	1.00	-0.36	1.00	-0.75	0.00
Ppm1k	-0.15	1.00	-0.53	0.20	-0.42	0.93	-1.30	0.00
Ppme1	0.26	1.00	0.29	1.00	0.13	1.00	0.62	0.02
Ppp1r12a	0.44	1.00	0.38	0.82	0.18	1.00	0.85	0.00
Ppp1r13l	0.24	1.00	0.21	1.00	0.28	1.00	0.65	0.01
Ppp1r15a	1.14	0.00	1.21	0.00	0.20	1.00	0.94	0.00
Ppp1r1b	-0.18	1.00	-0.65	1.00	-0.38	1.00	-1.53	0.00
Ppp1r2	0.07	1.00	0.21	1.00	0.12	1.00	0.63	0.01
Ppp1r3a	0.10	1.00	-0.25	1.00	-0.02	1.00	-0.70	0.01
Pprc1	0.12	1.00	0.26	1.00	0.25	1.00	0.76	0.00
Prkab1	-0.08	1.00	-0.35	1.00	-0.17	1.00	-0.74	0.00
Prkag3	-0.06	1.00	0.17	1.00	0.02	1.00	1.06	0.00
Prkci	0.43	1.00	0.48	0.31	0.44	0.59	1.34	0.00
Prkg2	0.32	1.00	0.93	0.31	0.15	1.00	1.44	0.00
Ptbp2	-0.02	1.00	-0.13	1.00	0.36	1.00	0.60	0.02
Ptgs2	3.17	0.00	3.64	0.00	0.43	1.00	2.94	0.00
Ptp4a3	0.03	1.00	-0.23	1.00	-0.03	1.00	-0.58	0.04
Ptpn21	0.18	1.00	0.37	0.87	0.54	0.16	0.88	0.00
Rab27b	0.49	1.00	0.80	0.03	-0.09	1.00	1.36	0.00
Ralgds	-0.14	1.00	-0.24	1.00	-0.29	1.00	-0.67	0.03
Rap1gap2	-0.01	1.00	-0.31	1.00	-0.08	1.00	-0.61	0.03
Rapsn	-0.11	1.00	-0.12	1.00	-0.31	1.00	-0.71	0.04
Rasgef1b	0.44	1.00	0.88	0.03	0.57	1.00	0.86	0.03
Rasl11b	1.38	0.00	1.78	0.00	0.62	0.08	1.84	0.00
Rassf1	0.15	1.00	0.26	1.00	-0.07	1.00	0.67	0.02
Rcan1	1.45	0.14	1.46	0.00	0.66	0.10	1.92	0.00
Rcor2	-0.08	1.00	-0.35	1.00	-0.83	0.01	-1.49	0.00
Rec8	0.03	1.00	-0.61	0.30	-0.25	1.00	-1.31	0.00
Relt	0.50	1.00	0.72	0.70	-0.53	1.00	1.13	0.01
Rerg	-0.07	1.00	0.41	1.00	0.47	1.00	1.01	0.00
Rfx5	0.09	1.00	-0.14	1.00	-0.39	1.00	-0.62	0.04
Rgs12	-0.06	1.00	-0.55	0.31	-0.38	1.00	-1.14	0.00
Rgs16	1.64	0.00	2.37	0.00	0.48	1.00	1.16	0.00
Rhbdf1	0.14	1.00	0.20	1.00	0.25	1.00	0.54	0.05
Rhobtb1	0.12	1.00	0.42	1.00	0.71	0.11	0.80	0.00
Rimkla	0.08	1.00	-0.21	1.00	-0.64	1.00	-1.38	0.00
Rin1	0.11	1.00	0.26	1.00	-0.24	1.00	0.72	0.04

Ripk2	0.16	1.00	0.62	0.21	0.07	1.00	0.80	0.01
Rit1	-0.24	1.00	-0.48	0.44	-0.08	1.00	-0.63	0.01
Rnd1	0.38	1.00	0.77	0.03	0.32	1.00	1.13	0.00
Rnd3	0.41	1.00	0.78	0.00	0.23	1.00	0.80	0.00
Rnf103	0.30	1.00	0.26	1.00	0.18	1.00	0.85	0.00
Rnf115	0.31	1.00	0.23	1.00	0.09	1.00	0.94	0.00
Rnf19a	0.14	1.00	0.28	1.00	0.25	1.00	0.61	0.02
Rnft1	0.12	1.00	0.20	1.00	0.26	1.00	0.83	0.00
Ror1	-0.02	1.00	-0.17	1.00	-0.17	1.00	-0.68	0.01
Rorc	0.08	1.00	-0.37	1.00	0.03	1.00	-0.74	0.00
Rph3al	0.18	1.00	-0.91	0.18	-0.07	1.00	-1.39	0.00
Rps6ka5	-0.12	1.00	-0.39	1.00	-0.50	1.00	-1.14	0.00
Rras2	0.10	1.00	0.23	1.00	0.49	0.38	1.18	0.00
Rreb1	0.02	1.00	-0.42	0.64	-0.42	0.81	-1.20	0.00
Rrp12	0.49	1.00	0.49	0.50	0.29	1.00	1.52	0.00
Rrp15	-0.09	1.00	0.16	1.00	0.13	1.00	0.73	0.04
Rsad2	-1.41	0.19	-0.44	1.00	0.81	0.92	-1.31	0.01
Rtn4rl1	-0.08	1.00	-0.30	1.00	-0.91	0.01	-1.66	0.00
Rusc2	0.32	1.00	0.36	1.00	0.14	1.00	0.82	0.00
S100a10	0.09	1.00	0.45	0.37	0.03	1.00	0.76	0.00
S1pr3	0.06	1.00	0.20	1.00	0.32	1.00	0.63	0.02
Samd4	0.18	1.00	0.36	0.98	0.39	1.00	0.69	0.02
Sbk1	-0.12	1.00	-0.33	1.00	-0.40	0.89	-0.75	0.00
Sbk2	-0.23	1.00	-0.47	1.00	-0.10	1.00	-0.87	0.01
Sbno2	0.28	1.00	0.31	1.00	0.41	0.79	0.77	0.00
Sc4mol	0.19	1.00	0.63	0.05	-0.04	1.00	0.76	0.00
Scube2	0.37	1.00	0.39	0.92	-0.13	1.00	0.85	0.00
Selenbp1	-0.19	1.00	-0.48	0.40	-0.09	1.00	-0.61	0.03
Sema4b	0.06	1.00	-0.19	1.00	-0.21	1.00	-0.66	0.02
Sema6c	0.07	1.00	-0.13	1.00	-0.30	1.00	-0.80	0.04
Sema7a	-0.12	1.00	0.60	0.33	0.10	1.00	0.97	0.00
Serinc5	-0.10	1.00	-0.13	1.00	-0.16	1.00	-0.64	0.01
Serpinb1a	0.52	1.00	1.00	0.00	0.14	1.00	1.32	0.00
Serpine1	1.14	0.02	1.90	0.00	0.92	0.00	2.25	0.00
Sgk1	0.71	1.00	1.08	0.00	-0.02	1.00	0.32	0.61
Sgms2	-0.10	1.00	0.24	1.00	0.30	1.00	0.88	0.01
Sh3bp5l	0.08	1.00	0.09	1.00	0.11	1.00	0.76	0.02
Shb	0.37	1.00	0.46	0.36	0.70	0.01	1.15	0.00
Shisa3	1.81	0.18	1.84	0.00	1.23	0.60	3.04	0.00
Sik1	0.67	0.45	0.68	0.02	0.22	1.00	0.56	0.05

Six5	0.10	1.00	-0.17	1.00	-0.27	1.00	-0.62	0.04
Slain2	0.24	1.00	0.31	1.00	0.46	0.79	0.79	0.00
Slc16a3	0.62	1.00	0.81	0.03	-0.47	1.00	-0.33	0.55
Slc1a1	0.87	1.00	1.16	0.10	-0.54	1.00	1.87	0.00
Slc20a1	0.41	1.00	0.66	0.19	0.35	1.00	1.09	0.00
Slc22a4	1.11	0.20	0.96	0.04	-0.11	1.00	1.27	0.00
Slc25a24	-0.03	1.00	0.21	1.00	0.02	1.00	0.75	0.00
Slc25a25	0.47	1.00	0.84	0.02	0.37	1.00	0.65	0.06
Slc25a30	-0.11	1.00	-0.51	0.64	-0.17	1.00	-0.77	0.02
Slc25a42	-0.01	1.00	-0.41	0.79	-0.34	1.00	-1.31	0.00
Slc25a43	0.46	1.00	0.70	1.00	0.56	1.00	1.30	0.02
Slc26a6	-0.11	1.00	-0.33	1.00	-0.29	1.00	-0.78	0.03
Slc29a1	-0.05	1.00	0.03	1.00	-0.44	1.00	-0.73	0.02
Slc2a1	0.24	1.00	0.33	1.00	0.22	1.00	0.65	0.01
Slc2a4	-0.17	1.00	-0.14	1.00	-0.26	1.00	-0.62	0.01
Slc2a8	-0.02	1.00	-0.10	1.00	-0.16	1.00	-0.72	0.01
Slc30a1	-0.02	1.00	-0.15	1.00	0.07	1.00	0.64	0.03
Slc38a2	0.45	1.00	0.62	0.55	0.46	1.00	1.15	0.00
Slc38a3	0.17	1.00	-0.45	1.00	-0.71	1.00	-1.86	0.00
Slc39a6	0.32	1.00	0.30	1.00	-0.01	1.00	0.79	0.00
Slc40a1	-0.20	1.00	-0.71	0.02	0.14	1.00	-0.14	0.88
Slc46a3	0.01	1.00	-0.31	1.00	-0.09	1.00	-1.15	0.00
Slc6a6	0.16	1.00	0.39	1.00	0.41	1.00	0.84	0.01
Slc7a1	0.11	1.00	0.43	0.51	-0.09	1.00	0.65	0.01
Slco5a1	0.10	1.00	0.60	1.00	0.29	1.00	1.47	0.00
Slitrk4	0.46	1.00	0.73	0.01	0.38	1.00	1.32	0.00
Slitrk5	0.21	1.00	-0.65	0.64	-0.27	1.00	-1.60	0.00
Slk	0.22	1.00	0.27	1.00	0.11	1.00	0.70	0.02
Slmap	0.13	1.00	0.38	1.00	0.49	0.81	1.06	0.00
Smad1	0.20	1.00	0.41	0.76	0.33	1.00	0.94	0.00
Smad2	0.30	1.00	0.40	0.67	0.22	1.00	0.73	0.00
Smad7	0.30	1.00	0.68	0.03	0.04	1.00	0.38	0.32
Smtnl2	-0.22	1.00	-0.86	0.00	-0.70	0.02	-1.94	0.00
Sntb1	0.12	1.00	0.31	1.00	-0.09	1.00	0.91	0.00
Snx25	0.02	1.00	0.15	1.00	0.28	1.00	0.60	0.04
Snx9	0.11	1.00	0.26	1.00	0.16	1.00	0.64	0.01
Sobp	-0.15	1.00	-0.19	1.00	-0.58	0.59	-1.03	0.00
Sorbs3	0.54	1.00	0.52	0.19	-0.03	1.00	0.73	0.00
Sorcs2	-0.38	1.00	-0.33	1.00	-0.32	1.00	-0.66	0.01
Sox4	0.00	1.00	-0.50	0.39	-0.09	1.00	-1.27	0.00

Spata13	0.18	1.00	0.43	0.52	0.19	1.00	0.63	0.02
Spcs3	0.65	1.00	0.82	0.00	0.70	0.02	2.17	0.00
Speer4d	1.62	1.00	1.49	0.54	1.09	1.00	3.11	0.00
Speer4e	1.05	1.00	1.21	0.97	0.66	1.00	2.84	0.00
Sphkap	-0.07	1.00	0.19	1.00	-0.38	1.00	-0.86	0.00
Spon2	-0.24	1.00	-0.98	0.00	-0.38	1.00	-0.34	0.38
Sprr1a	0.84	1.00	1.00	0.00	0.54	0.46	2.20	0.00
Sprr2a2	0.51	1.00	1.20	0.00	-0.01	1.00	0.97	0.00
Spry4	0.85	0.05	1.13	0.00	0.31	1.00	0.47	0.15
Spsb4	0.21	1.00	0.95	0.00	0.67	0.07	1.47	0.00
Sqle	0.13	1.00	0.57	0.09	-0.17	1.00	0.66	0.01
Srf	0.39	1.00	0.47	0.38	0.05	1.00	0.70	0.01
Srm	0.06	1.00	0.28	1.00	0.27	1.00	0.91	0.00
Srsf3	0.11	1.00	0.38	1.00	0.02	1.00	0.61	0.03
Srsf5	0.87	0.22	0.91	0.00	0.26	1.00	0.34	0.45
Srxn1	0.18	1.00	0.10	1.00	-0.04	1.00	1.14	0.00
Ssbp3	-0.04	1.00	-0.18	1.00	-0.31	1.00	-0.63	0.01
Stat1	-0.20	1.00	-0.07	1.00	0.27	1.00	-0.58	0.03
Stat5a	-0.10	1.00	-0.25	1.00	-0.21	1.00	-0.76	0.04
Stc1	0.01	1.00	0.19	1.00	-0.26	1.00	0.79	0.05
Steap3	-0.10	1.00	-0.25	1.00	-0.19	1.00	-0.79	0.00
Stk38l	0.57	1.00	0.66	0.04	0.51	0.36	1.31	0.00
Stk40	0.06	1.00	0.17	1.00	0.26	1.00	0.63	0.01
Stxbp4	0.00	1.00	-0.19	1.00	-0.37	1.00	-0.92	0.00
Synpo2	1.30	0.00	0.72	0.02	-0.23	1.00	1.01	0.00
Synpo2l	1.08	1.00	1.26	0.02	0.61	0.77	1.87	0.00
Sypl2	0.62	1.00	0.70	0.07	-0.93	0.03	-0.09	0.97
Syt12	0.87	1.00	1.21	0.06	1.08	0.30	2.19	0.00
Sytl2	0.20	1.00	0.57	0.79	0.37	1.00	0.89	0.03
Tap1	-0.24	1.00	-0.15	1.00	-0.08	1.00	-0.72	0.04
Tbc1d30	-0.19	1.00	-0.40	1.00	-0.47	1.00	-1.29	0.03
Tbx15	0.40	1.00	0.20	1.00	0.09	1.00	1.39	0.01
Tcea3	-0.12	1.00	-0.28	1.00	0.08	1.00	-0.62	0.02
Tec	0.08	1.00	0.12	1.00	0.58	0.59	0.72	0.03
Tef	-0.13	1.00	-0.32	1.00	-0.30	1.00	-0.78	0.00
Tet1	-0.29	1.00	-0.47	0.36	-0.35	1.00	-1.07	0.00
Tfrc	0.15	1.00	0.25	1.00	-0.77	0.00	-0.08	0.97
Tgfb1i1	0.20	1.00	0.43	0.52	0.11	1.00	0.76	0.00
Tgfb2	1.05	0.19	0.95	0.00	0.59	0.11	2.06	0.00
Tgfb3	0.12	1.00	0.23	1.00	0.41	0.77	0.99	0.00

Tgfbr3	-0.03	1.00	-0.54	0.14	-0.48	0.46	-1.32	0.00
Tgm2	0.92	1.00	0.45	1.00	-0.25	1.00	0.93	0.02
Thbs1	0.70	1.00	1.27	0.08	0.50	1.00	1.37	0.00
Thrsp	-0.20	1.00	-0.35	1.00	0.06	1.00	-1.24	0.02
Tiam2	0.44	1.00	0.72	0.25	-0.02	1.00	1.47	0.00
Tigd4	1.04	1.00	1.38	0.03	1.61	0.02	1.98	0.00
Tlr4	-0.02	1.00	0.22	1.00	0.39	1.00	1.10	0.00
Tmem100	1.29	1.00	2.27	0.00	0.38	1.00	1.52	0.00
Tmem158	0.13	1.00	0.25	1.00	0.33	1.00	1.40	0.00
Tmem41a	-0.07	1.00	-0.41	0.75	-0.12	1.00	-0.98	0.00
Tmem41b	-0.01	1.00	0.19	1.00	0.10	1.00	0.57	0.03
Tmem44	0.05	1.00	-0.08	1.00	-0.07	1.00	-0.64	0.04
Tmem51	-0.04	1.00	-0.26	1.00	-0.25	1.00	-1.11	0.00
Tmem86a	-0.17	1.00	-0.82	0.00	-0.32	1.00	-1.43	0.00
Tmem90b	1.68	0.06	1.48	0.01	0.45	1.00	2.65	0.00
Tnfrsf11b	0.39	1.00	1.56	0.00	-0.04	1.00	0.98	0.11
Tnfrsf12a	0.62	1.00	1.06	0.06	0.66	0.97	1.83	0.00
Tnnt1	-0.24	1.00	-0.47	0.36	-0.72	0.01	-0.31	0.49
Tnxb	-0.31	1.00	-1.51	0.00	0.08	1.00	-0.30	0.56
Tox	-0.18	1.00	-0.57	1.00	-0.25	1.00	-1.37	0.00
Tpm4	-0.06	1.00	0.42	1.00	0.14	1.00	0.69	0.02
Trib1	1.14	0.00	1.53	0.00	0.48	1.00	1.78	0.00
Trim16	0.29	1.00	0.43	1.00	0.00	1.00	1.02	0.00
Trim35	0.11	1.00	0.25	1.00	0.28	1.00	0.80	0.01
Trim47	0.34	1.00	0.61	0.19	0.31	1.00	1.16	0.00
Trim54	0.21	1.00	0.21	1.00	0.22	1.00	1.06	0.00
Trio	0.18	1.00	0.15	1.00	0.25	1.00	0.81	0.00
Trove2	0.15	1.00	0.07	1.00	0.07	1.00	0.77	0.00
Trp53inp1	-0.01	1.00	-0.34	1.00	-0.16	1.00	-0.70	0.01
Trpc6	0.08	1.00	0.49	1.00	0.19	1.00	1.14	0.03
Tslp	0.47	1.00	1.39	0.73	0.66	1.00	2.23	0.00
Tspyl4	-0.02	1.00	0.09	1.00	-0.44	0.79	-0.58	0.04
Tspyl5	0.40	1.00	0.21	1.00	0.29	1.00	0.66	0.01
Ttc21b	0.00	1.00	-0.12	1.00	-0.34	1.00	-0.63	0.05
Ttc38	-0.14	1.00	-0.38	1.00	-0.18	1.00	-0.88	0.00
Ttc9	-0.12	1.00	0.25	1.00	0.33	1.00	0.88	0.00
Tuba1c	0.21	1.00	0.67	0.05	-0.07	1.00	0.64	0.02
Tubb2a	0.43	1.00	0.78	0.00	-0.02	1.00	1.13	0.00
Tubb2b	0.35	1.00	0.59	0.09	-0.08	1.00	0.64	0.01
Tubb4b	0.31	1.00	0.72	0.02	-0.10	1.00	0.61	0.02

Tubb6	0.22	1.00	0.52	0.19	0.06	1.00	0.93	0.00
Txnip	-0.86	1.00	-1.40	0.00	0.12	1.00	-0.54	0.26
Txnrd1	0.17	1.00	0.09	1.00	0.18	1.00	1.13	0.00
Ubash3b	0.24	1.00	0.61	0.16	0.26	1.00	1.21	0.00
Ube2d3	0.14	1.00	0.16	1.00	0.18	1.00	0.69	0.03
Uck2	0.49	1.00	0.65	0.03	0.35	1.00	1.90	0.00
Ucp2	-0.08	1.00	-0.39	0.66	0.65	0.03	-0.15	0.86
Ucp3	0.04	1.00	-1.44	0.00	-0.03	1.00	-2.50	0.00
Unc119	-0.15	1.00	-0.51	0.30	-0.20	1.00	-0.96	0.00
Usp28	0.20	1.00	0.13	1.00	0.28	1.00	1.03	0.00
Usp31	0.23	1.00	0.26	1.00	0.24	1.00	0.66	0.01
Vash2	0.48	1.00	0.46	0.64	-0.04	1.00	0.73	0.01
Vav2	-0.18	1.00	-0.27	1.00	-0.39	1.00	-0.67	0.02
Vcl	0.13	1.00	0.34	1.00	0.47	0.93	0.98	0.00
Vgll3	0.00	1.00	0.46	0.39	0.37	1.00	0.76	0.00
Vmp1	0.30	1.00	0.42	0.54	0.18	1.00	0.59	0.02
Wdr1	0.36	1.00	0.50	0.52	0.15	1.00	0.92	0.00
Wdr43	0.08	1.00	0.12	1.00	0.18	1.00	0.55	0.04
Wdr6	-0.02	1.00	-0.14	1.00	-0.49	0.55	-0.86	0.00
Wdr72	-0.32	1.00	-0.39	1.00	-0.45	1.00	-1.00	0.03
Wdr75	0.07	1.00	0.11	1.00	0.28	1.00	0.67	0.01
Wdr91	-0.03	1.00	-0.19	1.00	-0.24	1.00	-0.67	0.02
Wnk2	-0.12	1.00	-0.20	1.00	-0.54	1.00	-0.97	0.02
Wnt5b	0.17	1.00	0.14	1.00	0.30	1.00	0.80	0.02
Wnt9a	0.49	1.00	0.53	0.98	0.26	1.00	0.81	0.04
Wsb1	0.28	1.00	0.32	1.00	0.33	1.00	0.70	0.02
Wwc2	0.20	1.00	0.31	1.00	0.32	1.00	0.77	0.00
Xirp1	0.83	1.00	0.95	0.01	0.38	1.00	1.65	0.00
Xirp2	1.85	1.00	1.19	0.07	0.67	1.00	3.02	0.00
Xk	0.13	1.00	0.01	1.00	0.28	1.00	0.85	0.00
Ypel3	-0.10	1.00	-0.42	0.52	0.11	1.00	-0.56	0.04
Zbtb38	0.22	1.00	0.37	0.98	0.35	1.00	0.84	0.00
Zbtb40	-0.01	1.00	-0.29	1.00	-0.38	1.00	-0.71	0.02
Zdhhc20	0.06	1.00	0.17	1.00	0.17	1.00	0.54	0.05
Zfp157	-0.24	1.00	-0.78	0.03	-0.18	1.00	-0.86	0.00
Zfp322a	0.21	1.00	0.21	1.00	0.42	1.00	1.13	0.00
Zfp36	1.88	0.00	2.13	0.00	0.24	1.00	0.78	0.00
Zfp37	0.69	1.00	0.72	0.06	0.22	1.00	1.10	0.00
Zfp395	0.00	1.00	-0.20	1.00	-0.18	1.00	-0.74	0.00
Zfp503	-0.15	1.00	-0.24	1.00	-0.42	1.00	-0.84	0.03

Zfp521	-0.03	1.00	-0.10	1.00	-0.53	0.42	-1.01	0.00
Zfp568	0.47	1.00	0.69	0.08	0.31	1.00	1.20	0.00
Zfp697	0.03	1.00	0.19	1.00	0.28	1.00	0.96	0.00
Zfpm1	0.09	1.00	-0.27	1.00	-0.11	1.00	-0.60	0.02
Zim1	0.57	1.00	0.25	1.00	-0.05	1.00	1.19	0.00
Znrf2	0.20	1.00	0.11	1.00	0.13	1.00	0.69	0.01
Zscan2	-0.17	1.00	-0.69	0.22	-0.24	1.00	-0.92	0.01
Zswim4	0.29	1.00	0.31	1.00	0.36	1.00	0.64	0.01
Zwint	0.19	1.00	0.29	1.00	0.07	1.00	0.62	0.02
Zyx	0.32	1.00	0.42	0.84	0.15	1.00	0.66	0.02

Appendix B: Species in the Upstream MSN

ID	Name	Module
aActinin	alpha-actinin	Cytoskeleton
Actin	Actin	Cytoskeleton
Akt	Protein kinase B	PI3K-Akt
AngII	Angiotensin II	Receptor
AT1R	Antiotensin type 1 receptor	Receptor
Ca	Calcium	Calcium
CaM	Calmodulin	Calcium
CaMK	CaM kinase	Calcium
CaN	Calcineurin	Calcium
cFos	Proto-oncogene c-Fos	Transcription
cGMP	Cyclic guanosine monophosphate	PI3K-Akt
cJun	Proto-oncogene c-Jun	Transcription
cMyc	Proto-oncogene c-Myc	Transcription
CREB	Cyclic adenosine monophosphate response element binding	Transcription
DAG	Diacylglycerol	Calcium
Dysgl	Dystroglycans	Receptor
Dysph	Dystrophin	Cytoskeleton
EGFR	Epidermal growth factor receptor	Receptor
eIF4E	Eukaryotic translation initiation factor 4E	PI3K-Akt
elF2B	Eukaryotic translation initiation factor 2B	PI3K-Akt
ERK12	Extracellular signal-related kinases 1 or 2	MAPK
ERK5	Extracellular signal-related kinase 5	MAPK
ET1	Endothelin-1	Receptor
ET1R	Endothelin-1 receptor	Receptor
FAK	Focal adhesion kinase	Cytoskeleton
FHL1	Four-and-a-half LIM domains protein 1	Cytoskeleton
FHL2	Four-and-a-half LIM domains protein 2	Cytoskeleton
foxo	Forkhead box O	Transcription
GATA4	GATA-binding protein 4	Transcription
Gbg	G protein beta and gamma subunits	Receptor
gp130	Glycoprotein 130	Receptor
Gqa11	G protein alpha subunit q or 11	Receptor
GSK3b	Glycogen synthase kinase 3 beta	PI3K-Akt
HDAC	Histone deacetylase	Calcium
IkB	Nuclear factor of kappa light polypeptide gene enhancer in	PI3K-Akt

	B-cells inhibitor, alpha	
IKK	Inhibitor of kappa light polypeptide gene enhancer in B-cells, kinase beta	PI3K-Akt
Integrin	Integrin	Receptor
IP3	Inositol triphosphate	Calcium
JAK	Janus kinase 1 or 2	Receptor
JNK	c-Jun N-terminal kinase	MAPK
Lmcd1	LIM and cystein-rich domains 1	Calcium
LTCC	L-type calcium channel	Receptor
MEF2	Myocyte enhancer factor 2	Transcription
MEK12	MAPK/ERK kinase 1 or 2	MAPK
MEK36	MAPK/ERK kinase 3 or 6	MAPK
MEK47	MAPK/ERK kinase 4 or 7	MAPK
MEK5	MAPK/ERK kinase 5	MAPK
MEKK1	MAPK/ERK kinase kinase 1	MAPK
MEKK23	MAPK kinase kinase 2 or 3	MAPK
MEKK4	MAPK kinase kinase 4	MAPK
MLP	Muscle LIM protein	Cytoskeleton
MRTF	Myocardin-related transcription factor	Cytoskeleton
mTor	Mechanistic target of rapamycin	PI3K-Akt
MuRF	Muscle ring finger protein	Cytoskeleton
Na	Sodium	Calcium
NCX	Sodium-calcium exchanger	Calcium
NFAT	Nuclear factor of activated T-cells	Transcription
NFkB	Nuclear factor kappa-light-chain-enhancer of activated B cells	Transcription
NHE	Sodium-hydrogen exchanger	Receptor
NOS	Endothelial nitric oxide synthase	PI3K-Akt
p38	p38 mitogen-activated protein kinase	MAPK
p70s6k	70 kDa ribosomal protein S6 kinase 1	PI3K-Akt
pCaN	CaN phosphorylation	
PDK1	3-phosphoinositide dependent protein kinase 1	PI3K-Akt
pGATA4	GATA4 phosphorylation	
PI3K	Phosphatidyl inositol 3 kinase	PI3K-Akt
PKC	Protein kinase C	Calcium
PKG1	cGMP-dependent protein kinase 1	PI3K-Akt
PLC	Phospholipase C	Calcium
pMEF2	MEF2 phosphorylation	
Rac1	Ras-related C3 botulinum toxin substrate 1	MAPK

Raf1	Proto-oncogene c-Raf	MAPK
Ras	Rat sarcoma viral oncogene homolog	MAPK
RhoA	Ras homolog gene family, member A	Cytoskeleton
ROCK	Rho-associated protein kinase	Cytoskeleton
sGC	Soluble guanylyl cyclase	PI3K-Akt
Src	Proto-oncogene c-Src	Cytoskeleton
SRF	Serum response factor	Transcription
STAT	Signal transducers and activators of transcription	Transcription
Stretch	Stretch	
Talin	Talin	Cytoskeleton
Titin	Titin	Cytoskeleton
Trp	Transient receptor potential channel	Receptor
Vinculin	Vinculin	Cytoskeleton
Zyxin	Zyxin	Cytoskeleton

Appendix C: Reactions in the Upstream MSN

ID	Reaction Rule	References
i1	=> Stretch	
r1	!Akt => foxo	[105]
r2	!Akt => GSK3b	[4,224]
r3	!CaMK & !PKC => HDAC	[4,68,69]
r4	!FHL2 & !HDAC & !MuRF & MRTF => SRF	[93,225-228]
r5	!FHL2 & pCaN => CaN	[229]
r6	!GSK3b & !JNK & !p38 & !PKG1 & NFkB => NFAT	[4,230,231]
r7	!GSK3b & pGATA4 => GATA4	[232,233]
r8	!GSK3b => CREB	[234]
r9	!GSK3b => elF2B	[232]
r10	!HDAC & pMEF2 => MEF2	[4,69]
r11	!IkB => NFkB	[4,235]
r12	!IKK => IkB	[4,235]
r13	!ROCK & !Titin => FHL2	[236,237]
r14	!Titin & foxo => MuRF	[227,238-241]
r15	aActinin => MLP	[242]
r16	aActinin => Zyxin	[243]
r17	Actin => aActinin	[244]
r18	Actin => Titin	[244]
r19	Akt => IKK	[245]
r20	Akt => mTor	[4]
r21	Akt => NOS	[246]
r22	AngII => AT1R	[4,247]
r23	AT1R => Gqa11	[248]
r24	AT1R => JAK	[248]
r25	Ca & DAG => PKC	[4,249]
r26	Ca => CaM	[4,250]
r27	CaM => CaMK	[4,250]
r28	CaM => pCaN	[232,251]
r29	CaN & ERK12 => NFAT	[4,252]
r30	CaN => NFAT	[4,252]
r31	cGMP => PKG1	[4,230]
r32	Dysgl => Dysph	[43]
r33	Dysph => Actin	[43]
r34	EGFR => Ras	[4,211]
r35	ERK12 => cFos	[4,253]

r36	ERK12 => cJun	[254]
r37	ERK12 => cMyc	[255]
r38	ERK12 => NFkB	[84]
r39	ERK12 => pGATA4	[256,257]
r40	ERK5 => cMyc	[255]
r41	ERK5 => pMEF2	[88,256]
r42	ET1 => ET1R	[4,258]
r43	ET1R => Gqa11	[4,259]
r44	FAK => Src	[208]
r45	FHL1 => ERK12	[15]
r46	Gbg => EGFR	[260]
r47	Gbg => PI3K	[4,261]
r48	Gbg => Ras	[49]
r49	gp130 => JAK	[262]
r50	Gqa11 => Gbg	[263]
r51	Gqa11 => PLC	[264]
r52	Integrin => FAK	[208]
r53	Integrin => Talin	[39]
r54	IP3 => Ca	[4,265]
r55	JAK => Ras	[49]
r56	JAK => STAT	[49,266]
r57	JNK => cJun	[267,268]
r58	Lmcd1 => pCaN	[269]
r59	LTCC => Ca	[270]
r60	MEK12 => ERK12	[4,271]
r61	MEK36 => p38	[4,272]
r62	MEK47 => JNK	[4,273,274]
r63	MEK47 => p38	[267,275,276]
r64	MEK5 => ERK5	[4,277]
r65	MEKK1 => MEK47	[49,274]
r66	MEKK23 => MEK5	[49,278]
r67	MEKK4 => MEK36	[279]
r68	MEKK4 => MEK47	[4,279]
r69	MLP => pCaN	[13]
r70	mTor => eIF4E	[232,280]
r71	mTor => p70s6k	[232,280]
r72	Na => NCX	[281]
r73	NCX => Ca	[282]
r74	NHE => Na	[281]

r75	NOS => sGC	[283,284]
r76	p38 => IKK	[84]
r77	p38 => Lmcd1	[285]
r78	p38 => pGATA4	[256]
r79	p38 => pMEF2	[286,287]
r80	PDK1 => Akt	[4,288]
r81	PI3K => PDK1	[4,289]
r82	PKC => Raf1	[290]
r83	PLC => DAG	[4,291,292]
r84	PLC => IP3	[248,292]
r85	Rac1 => MEKK4	[293]
r86	Raf1 => MEK12	[267,281]
r87	Ras => MEKK1	[49,294]
r88	Ras => MEKK23	[295]
r89	Ras => PI3K	[49,210]
r90	Ras => Rac1	[47,49,296]
r91	Ras => Raf1	[267,297]
r92	Ras => RhoA	[49,298]
r93	RhoA => MRTF	[225,299]
r94	RhoA => ROCK	[76]
r95	ROCK => pGATA4	[300]
r96	sGC => cGMP	[301]
r97	Src => Ras	[2,302]
r98	Stretch => AngII	[303-305]
r99	Stretch => AT1R	[248]
r100	Stretch => Dysgl	[306]
r101	Stretch => ET1	[304,307]
r102	Stretch => gp130	[308]
r103	Stretch => Integrin	[309]
r104	Stretch => LTCC	[310]
r105	Stretch => NHE	[281]
r106	Stretch => Trp	[214]
r107	Talin => Actin	[39]
r108	Talin => Vinculin	[39]
r109	Titin => FHL1	[15]
r110	Trp => Ca	[214]
r111	Vinculin => Actin	[39]
r112	Zyxin => Akt	[311]

Appendix D: Target Genes of MSN

This table lists all 645 target genes of the 11 TFs in the MSN. For each gene, the columns indicate upstream TFs that regulate the target gene, whether the target gene is activated (Up) or inhibited (Down) by each TF, and the half-life in hours are displayed.

Symbol	HL	cFos	cJun	cMyc	CREB	foxo	GATA4	MEF2	NFAT	NFkB	SRF	STAT
3425401B19Rik	5.6							Up				
6430548M08Rik	6.7	Up										
9930013L23Rik	10.9							Up				
Abca1	5.7											Up
Abcc3	7.6			Down								
Abcd3	5.0											Down
Abcg2	5.2							Up				Down
Abl2	2.4			Down								
Acta1	23.1							Up			Up	
Actc1	10.0							Up				
Adamts6	3.7									Up		
Adamts9	4.1								Up			
Adamtsl1	2.0		Up									
Add1	18.8			Down								
Add2	9.3	Up										
Adm	2.3											Up
Aff3	3.4					Up						
Agt	10.0											Up
Agtpbp1	8.4											Up
Akap12	7.0			Down								
Akap2	3.7											Up
Akt3	7.3										Up	
Aldh1b1	5.3			Up								
Alg3	7.4			Up								
Amotl2	1.2											Up
Ampd3	8.4									Up		
Angptl4	3.2											Up
Ank3	4.8		Up									
Ankrd1	5.7							Up			Up	
Ankrd6	5.6										Up	
Apln	3.3	Up										
Aqp3	24.0	Up										Down
Arfgef2	4.4									Up		
Arhgap8	11.6			Up								

Arhgdib	21.1								Up			
Arnt2	3.7		Down									
Arntl	4.0			Down								
Arntl2	9.7			Down					Up			Up
Atf3	2.2						Up					Up
Atic	6.4			Up								
Atp13a3	7.5	Up							Up			
Atp1a2	9.4						Up					
Atp2a2	4.4									Up		
Atp2b1	5.2								Up			Down
Atp2b4	3.9			Down								Up
Atp6v0b	8.8					Up						
Axl	8.4									Up		
B4galt1	9.2	Up							Up			
Bach1	2.1											Up
Bach2	2.3					Up						
Bag3	4.6				Up							
Baiap2l1	3.2						Up					
Bcl2	6.0					Up						
Bcl2l13	6.5											Down
Bcl3	8.4											Up
Bcl6	1.3											Up
Bdkrb1	12.0								Up			
Bdkrb2	3.2								Up			
Bdnf	1.9		Up									
Bet1	13.5											Down
Bex1	7.5								Up			
Blcap	3.7	Up										
Bmp2	2.3							Up				
Bmp7	11.0		Up									
Btg2	2.5				Up							
Btn2a2	1.4								Up			
Bves	16.1									Up		
C1s	12.5											Up
C3	11.5											Up
Cacna1s	24.0						Up					
Cacng1	4.6						Up					
Cant1	5.3								Up			
Cartpt	24.0				Up							
Cask	5.4								Up			

Casp4	10.2								Up			
Casq1	16.8						Up					
Casq2	5.8						Up					
Cast	10.2											Down
Ccl2	6.8											Up
Ccl20	3.4								Up			
Ccl3	24.0								Up			
Ccnd1	8.6				Up							
Ccnf	8.7				Up							
Ccng2	1.4		Down									
Ccr7	4.0				Up							
Cd46	3.7								Up			
Cd83	3.7							Up				
Cdc42ep3	1.9				Down							
Cdcp1	3.3								Up			
Cdh1	8.0	Down										
Cdh11	1.6								Up			
Cdk2	13.5		Down									
Cdk4	8.5		Up									
Cdkn1a	2.0			Up								
Cdkn1c	23.8				Down							
Cdkn2c	7.3				Down							
Cdv3	4.9								Up			
Ceacam1	8.7											Up
Cfl2	7.4										Up	
Cgn	5.3		Down									
Chd1	2.4											Up
Chn1	10.4						Up					
Chrna1	12.9			Up			Up					
Chst11	5.6											Up
Chst2	4.7								Up			
Chst8	2.8	Up										
Cirh1a	5.3		Up									
Cited2	1.0											Up
Ckb	15.7						Up					
Ckm	24.0						Up				Up	
Cldn1	3.3								Up			
Clmn	12.9											Up
Cnn1	9.3			Up							Up	
Cnr1	2.6						Up					

Col14a1	9.4			Down							
Col1a1	24.0			Down							
Col1a2	11.5			Down							
Col2a1	6.8					Down					
Col4a6	14.1						Down				
Col5a1	24.0			Down							
Col6a1	24.0								Up		
Col8a1	24.0								Up		
Col8a2	11.4			Down							
Cpeb4	4.7	Up									
Crem	4.8				Up						
Crhbp	5.2				Up						
Crim1	6.9					Up					
Cryab	24.0						Up				
Csda	16.1										Up
Csdc2	23.7		Down				Up				
Csrp2	6.6									Up	
Csrp3	4.9						Up				
Ctgf	1.3						Up				
Ctsb	24.0										Up
Ctsl	6.5										Up
Cxcl12	11.6					Up					
Cxcl14	15.8				Down						
Cxcl5	3.5								Up		
Cxcr4	1.4				Up	Up			Up		
Cxcr7	2.6							Up			
Cyfip2	9.4				Up						
Dapk2	7.6	Up									
Ddx10	4.3			Up							
Ddx18	6.1			Up							
Des	24.0						Up			Up	
Dhodh	6.7			Up							
Dicer1	6.4										Up
Dio2	5.3								Up		
Dmd	11.6									Up	
Dnajb4	4.1										Down
Dnajb5	2.8						Up				
Dnajc10	8.5								Up		
Dok7	3.1						Up				
Dpp4	24.0								Up		

Dtna	10.7											Up	
Dusp1	1.8				Up								Up
Dusp22	14.4			Down									
Dusp27	3.3							Up					
Dusp4	2.4										Up		
Dusp5	1.7												Up
Dusp6	0.8							Down					
Ecel1	12.2				Up								
Efna1	2.1												Up
Efnb2	2.1												Up
Egfr	3.0												Up
Egln3	3.7											Up	
Egr1	1.2											Up	
Egr2	1.3							Up	Up				
Ehf	4.0										Up		Down
Eif4a1	6.3			Up							Up		
Elf3	4.2												Up
Ell2	3.7										Up		Up
Emd	5.8				Up								
Eml1	5.9										Up		
Emp1	24.0			Down				Down					
Enah	5.6	Up										Up	
Eomes	2.2					Up							
Epas1	10.3												Up
Erbb3	5.9			Down									
Esd	8.3				Up								
Esm1	8.9										Up		
Ets2	3.4												Up
Evi5	7.7										Up		
Ext2	8.3										Up		
Fancl	6.9												Down
Fblim1	6.2	Up											
Fbln2	10.6			Down									
Fbn2	6.1		Up										
Fbxl3	2.8											Up	
Fem1c	3.0												Up
Fgb	7.0												Up
Fgf10	2.7							Down					
Fgf11	13.8			Down									
Fgfr2	3.0				Up								

Fgfr3	8.0						Up					
Fgg	5.1											Up
Fhl1	24.0										Up	
Fhod1	7.0	Up										
Fkbp3	9.0											Down
Flnb	5.0											Up
Flrt1	3.9					Up						
Flrt3	2.0											Up
Fn1	5.8			Down	Up							
Fnbp1	7.7										Up	
Fos	1.3	Up			Up							
Fosb	7.3				Up							
Fosl1	2.6											Up
Fosl2	1.6									Up		Up
Foxc1	1.2					Down						
Foxp4	10.3				Up							
Foxq1	1.9									Up		
Frmpd1	6.0						Up					
Fst	2.6						Up					
Fstl1	8.6									Up		
Fyn	4.5						Up					
Fzd5	2.4					Up						
Fzd8	2.7		Up									
G0s2	2.1											Up
Gadd45b	1.2											Up
Gadd45g	0.5				Down		Up					
Gal	4.1									Up		
Gata1	9.8					Up						
Gata6	1.8											Up
Gch1	8.7									Up		
Gclc	3.5											Down
Gem	2.8				Up				Up			
Gfpt2	8.5									Up		
Gfra1	4.6				Up							
Gjb2	6.2				Down							
Gpr3	16.3				Up							
Gramd3	7.2									Up		
Grasp	3.3				Up							
Grb10	7.9											Up
Grik2	11.5		Down									

Grin1	4.4											Up
Grip2	24.0							Up				
Grpel1	5.7											Up
Gsk3b	2.7									Up		
Gtf2i	5.4											Down
Gys1	9.9							Up				
Hbegf	2.2										Up	
Heatr3	5.6									Up		
Hfe2	3.0							Up				
Hhex	2.1											Down
Hk1	24.0											Up
Hk2	4.4			Up								Up
Hmga1	10.8		Up									
Hmox1	8.3	Up										
Homer1	6.4				Up							
Hook1	8.6	Up										
Hoxa10	5.2						Up					
Hpgd	4.8											Down
Hps1	24.0					Up						
Hrc	16.2							Up				
Hs3st1	2.2	Up										
Hs6st2	7.0			Up								
Hsd3b6	14.4	Down										
Hspb2	12.2							Up				
Hspb7	6.9							Up				
Hspb8	4.2	Down										
Hspd1	6.4			Up								
Htr2c	5.8				Up							
Htra1	11.7									Up		
Icam1	4.9									Up		Up
Id3	1.6											Down
Ier2	1.4				Up							
Ifi44	24.0											Down
Ikzf2	2.9					Down						
Ikzf5	6.8					Up						
Il15	2.3					Up						
Il1r1	7.5											Up
Inadl	5.3							Up				
Inhba	10.5				Up							
Ipo4	9.7			Up								

Iqgap2	7.2											Down
Irak2	2.6									Up		
Irf1	1.2											Up
Itga9	9.5										Up	
Itgb1	8.9										Up	
Itgb1bp2	6.6										Up	
Itgb6	20.6							Up				
Jak2	4.0											Up
Jph2	6.6							Up			Up	
Jun	1.3											Up
Junb	1.8											Up
Kcnd3	8.3		Up									
Kcnj10	3.0		Down				Down					
Kcnj15	10.6									Up		
Kcnn4	12.9	Up										
Kctd11	6.0									Up		
Kctd8	3.9						Up					
Klf3	1.4	Up										
Klf4	1.9					Up						Up
Klf6	1.4	Up										
Klf7	2.8					Up						
Krt18	4.8										Up	
Lama2	4.6							Up				
Lamb3	12.4			Down								
Lamc2	9.6			Down				Up				
Lamp3	15.5											Down
Lancl1	13.9											Down
Lap3	7.7											Down
Large	3.4	Up										
Layn	7.7				Up							
Lbh	7.2							Down			Up	Up
Lbp	15.0											Up
Ldb3	4.9										Up	
Lef1	3.1					Up						
Lfng	3.2					Down						
Lhfpl2	4.7					Up						
Lhx9	24.0						Down					
Lin7c	9.5										Up	
Litaf	13.2				Up							
Lix1	5.4							Up				

Lman1	6.9		Up								
Lmcd1	2.8						Up				
Lmod3	17.9						Up				
Lnpep	7.1								Up		
Loxl2	10.1										Up
Lpin1	3.6								Up		
Lrig1	2.4								Up		
Lrp1	9.4					Down					
Lrrc2	8.4						Up				
Lsr	11.9					Up					
Ltbp2	14.4			Down							
Ltbp3	11.6	Down									
Lyn	5.8								Up		Up
Maff	5.6										Up
Mafk	2.0	Up									Up
Magi1	4.2							Up			
Map2k3	8.8								Up		Up
Map3k8	2.0							Up			
Mapk6	8.6	Up									
Mapkap1	5.8								Up		
Mapre2	6.0									Up	
Mapt	24.0					Down					
Mb	24.0						Up				
Mbnl2	8.9										Up
Mboat2	6.7						Up				
Mcoln2	7.9			Up							
Met	3.9	Up									
Mettl1	8.0			Up							
Mid1	24.0										Down
Mknk1	7.1			Down							
Mlh1	8.4	Down									
Mllt10	2.3				Up						
Mmp12	8.9								Up		
Mreg	24.0								Up		
Mrpl14	5.4				Up						
Mrpl45	8.0				Up						
Mrpl47	5.6								Up		
Mrps14	10.6				Up						
Mrvi1	5.1				Down		Up				
Msn	11.0								Up	Up	

Mtcp1	6.3				Up					Down
Myc	1.0		Up		Up					Up
Myh3	24.0					Up				
Myh6	9.3								Up	
Myh7	11.0					Up			Up	
Myh9	5.5	Up								
Myl3	13.6								Up	
Myl4	24.0								Up	
Myl9	9.7		Down						Up	
Mylpf	24.0					Up				
Myo10	5.4							Up		
Myo18b	19.4					Up				
Myo1b	7.7							Up	Up	
Myog	15.4					Up				
Myom1	7.1					Up			Up	
Myom2	16.5					Up				
Myom3	5.1					Up				
Mypn	5.2					Up				
Nab1	6.8							Up		
Nap1l5	3.9			Up						
Napa	23.7									Down
Nav3	5.0							Up		
Ncald	6.2									Down
Ncl	8.5		Up							
Nde1	4.5		Down							
Nebl	3.9								Up	
Nedd4l	7.0							Up		
Nefl	24.0							Up		
Nefm	7.4							Up		
Nexn	6.8					Up				
Nfil3	1.9	Down		Up						Up
Nfkb2	6.4		Down							
Nfkbia	1.5							Up		
Nfkbiz	2.2						Up			
Ngfr	8.1		Down							
Nnmt	14.1									Up
Nog	1.3							Up		
Nol6	11.7		Up							
Npas4	5.9			Up						
Npm1	6.0		Up							

Npnt	5.7					Up				
Nppb	24.0								Up	
Nptx1	8.6	Up								
Nptx2	10.4			Up						
Npy	8.4			Up						
Nr1d1	3.7									Up
Nr4a1	2.5			Up			Up			
Nr4a2	5.8		Down	Up			Up			Down
Nr4a3	13.9						Up			
Nrap	6.4					Up				
Nrg1	2.3							Up		
Nrip1	1.1							Up		
Nrsn1	5.0			Up						
Nuak1	3.5					Up				
Nub1	5.5							Up		
Nudt6	2.8							Up		
Obscn	12.1					Up				
Ociad2	18.6			Up						
Ocln	3.0				Up					
Olig1	4.4		Up							
Optn	8.4							Up		
Osbp2	6.0		Down							
Osr1	5.6					Down				
Ostf1	8.0			Up						
Pa2g4	5.6		Up							
Pabpc1	4.6							Up		
Padi2	21.7					Up				
Paics	6.8		Up							
Panx1	2.5							Up		
Pard6b	2.8								Up	
Paxip1	5.7		Up							
Pcdh18	2.3								Up	
Pcdh7	3.0								Up	
Pcolce2	12.8		Up							
Pdcd2	3.0									Down
Pdgfb	2.5					Up				
Pdgfrl	9.4									Down
Pdlim4	5.6	Down								
Pdzd8	4.1							Up		
Peg10	14.9			Up						

Peli2	2.9										Up
Per1	3.7			Up							
Pfkfb3	5.1										Up
Pfkm	8.6		Up								
Pfn1	24.0	Up									
Pgrmc2	6.6										Down
Phb	11.7		Up								
Phyhipl	2.9				Up						
Pik3cb	2.8	Up									
Pik3r1	2.7					Down					
Pip5k1b	3.4					Up					
Pitpnc1	3.1										Up
Pkia	11.3						Up				
Pla2g4a	9.5								Up		Down
Plagl1	4.4										Up
Plau	24.0										Up
Plaur	6.8										Up
Plcb4	5.3										Down
Plekha1	6.2								Up		
Plekha7	3.2						Up				
Plod2	11.5								Up		Up
Plscr1	5.9										Down
Pmaip1	8.3										Up
Pnrc2	2.3										Down
Ppap2b	2.9										Up
Ppapdc3	2.9						Up				
Ppard	5.4								Up		
Ppif	5.2								Up		
Ppp1r9b	24.0					Down					
Prpf4b	4.3										Down
Prrx1	4.4						Down				
Psme2	6.9								Up		
Ptgs2	6.1									Up	
Ptprf	9.8										Up
Ptprn	14.2			Up							
Pxmp3	3.5										Down
Pygm	15.4						Up				
Qpct	24.0								Up		
Rab11fip1	5.1	Up									
Rab27a	13.7				Up						Up

Rae1	4.4								Up			
Ranbp9	3.1	Up										
Rarres1	7.3											Up
Rars	6.6			Up								
Rasgef1b	1.3				Up							
Rasgrp3	5.1					Down						
Rassf8	3.7								Up			
Rbms1	5.7											Up
Rbp1	12.3	Up										
Rcan1	6.9							Up		Up		
Rcl1	5.5			Up								
Rfx4	5.7				Up							
Rgs2	4.6								Up			
Rhbdd1	9.1								Up			
Rhbdf1	6.5			Down								
Rhobtb1	4.3											Down
Ripk2	4.0								Up			
Rpl19	8.3								Up			
Rps19	7.4								Up			
Runx1	2.6	Up		Down								
Runx2	6.1		Up									
Rusc2	3.7	Up										
S100a10	9.5								Up			
Saa2	24.0											Up
Samd4	3.5											Up
Sat1	7.5				Up							
Scel	6.4									Up		
Scg2	5.4				Up							
Scg5	8.3								Up			
Scn4a	12.4						Up					
Sdc2	8.4									Up		
Sdc4	24.0											Up
Sema3b	11.8	Down										
Sema3e	5.3		Up									
Sema4a	6.2			Down								
Serpinb7	4.1								Up			
Serpine1	24.0											Up
Serpine2	13.2											Up
Serpinh1	11.4			Down								
Sez6	6.3		Up									

Sgca	9.8						Up				
Sgcb	9.9									Up	
Sh2b3	8.5								Up		
Sirpa	4.1	Down									
Slc12a8	5.9		Up								
Slc19a1	6.6		Up								
Slc19a3	2.8										Up
Slc22a4	6.9								Up		
Slc25a37	10.7								Up		
Slc2a3	6.6										Up
Slc35b3	4.0								Up		
Slc39a8	7.1										Up
Slc40a1	3.6				Up						
Slc45a3	3.6	Down									
Slc7a1	5.1										Up
Slitrk6	1.8		Down								
Smad1	2.3								Up		
Smoc1	6.4					Down					
Smtn	13.6		Down								
Smurf1	3.8								Up		
Sntb1	10.6						Up				
Socs3	1.2										Up
Sod2	10.4								Up		Up
Sorbs1	5.2				Down						
Sorbs2	4.5						Up				
Sord	23.9		Up								
Sorl1	7.2		Down								
Sort1	7.3						Up				
Sox11	2.7						Up				
Sox9	4.3										Down
Sp100	24.0										Down
Sparc	9.6		Down								
Spred3	6.2			Up							
Sqrdl	9.9								Up		
Srl	3.8						Up				
Srm	5.8		Up								
Srxn1	5.5			Up							
Sst	10.3			Up							
Stat1	7.4										Down
Stat3	7.1			Up							Up

Stat5b	9.3				Up						
Stc1	4.7			Up							
Stc2	5.2								Up		
Stmn3	24.0		Down								
Stom	24.0										Up
Supv3l1	5.3		Up								
Svil	4.4									Up	
Synj2	4.1			Up							
Synpo2l	3.4						Up			Up	
Tac1	2.5			Up							
Tagln	7.0									Up	
Tagln2	6.8			Up					Up		
Tanc2	13.1								Up		
Tank	4.4								Up		
Taok1	4.4	Up									
Tbx21	3.7				Down						
Tbx3	3.1					Down					
Tcam1	4.1									Up	
Tcap	7.0						Up			Up	
Tcof1	6.4		Up								
Tead4	4.4						Up				Up
Tfb2m	5.4		Up								
Tfdp1	7.7		Up								
Tgfb2	5.1					Down			Up	Up	
Tgfb3	9.9						Up				
Tgm2	24.0									Up	
Thbd	5.5										Up
Thbs1	4.8										Up
Thbs2	17.9		Down								
Tiam1	6.0										Up
Tinf2	13.8			Up							
Tjp1	4.0									Up	
Tlr3	2.4										Down
Tmbim1	17.7			Up							
Tmed8	6.0								Up		
Tmem2	7.5										Up
Tmod3	19.3									Up	
Tnfaip2	10.9		Down								
Tnfrsf21	3.9								Up		
Tnip1	7.5								Up		

Tnnc1	16.6							Up			Up	
Tnnc2	24.0							Up				
Tnni1	24.0							Up				
Tnnt3	24.0			Down				Up				
Top1	6.9											Up
Tpm1	6.5	Up									Up	
Tpm2	20.3							Up			Up	
Tpm4	7.3				Up							
Traf4	2.7											Up
Trib2	1.8							Down				
Trim54	8.7							Up				
Trim63	5.9							Up				
Trim9	8.0						Down					
Trio	3.7											Up
Trpm3	6.0		Down									
Tst	12.1											Down
Ttn	4.1										Up	
Tubb3	24.0						Up					
Ubap1	4.1	Up										
Ube2l6	13.9											Down
Ube2q2	20.9	Up										
Ube3a	3.4									Up		
Ugcg	7.2											Up
Unc45b	4.4							Up				
Usp12	6.9											Up
Usp18	8.1											Down
Utrn	4.6	Up										
Vav3	3.5					Up						
Vcam1	8.6								Up			
Vdr	11.1						Up					
Vegfa	2.7										Up	
Vgf	10.7				Up							
Vgll2	3.6							Up				
Vldlr	4.4						Down					
Vrk2	3.8									Up		
Wdr12	6.2			Up								
Wfdc1	10.6							Up				
Wnk4	6.8						Up					
Wnt7b	4.2					Up						
Wnt9a	1.8							Up				

Wsb1	6.5		Down				Up
Wtap	3.1					Up	
Xpo5	7.8		Up				
Ywhaz	20.6	Up					
Zfand5	2.1			Up			
Zfp36	1.2						Up
Zfp46	1.5	Up					
Zhx2	4.5	Up					
Zic3	2.3				Up		
Zmiz2	17.2					Up	
Zyx	5.3						Up

References

[1] Lyon RC, Zanella F, Omens JH, Sheikh F. Mechanotransduction in cardiac hypertrophy and failure. Circ Res. 2015;116:1462-76.

[2] Jaalouk DE, Lammerding J. Mechanotransduction gone awry. Nat Rev Mol Cell Biol. 2009;10:63-73.

[3] Sugden PH. Mechanotransduction in cardiomyocyte hypertrophy. Circulation. 2001;103:1375-7.

[4] Heineke J, Molkentin JD. Regulation of cardiac hypertrophy by intracellular signalling pathways. Nat Rev Mol Cell Biol. 2006;7:589-600.

[5] Mozaffarian D, Benjamin EJ, Go AS, Arnett DK, Blaha MJ, Cushman M, Das SR, de Ferranti S, Despres JP, Fullerton HJ, Howard VJ, Huffman MD, Isasi CR, Jimenez MC, Judd SE, Kissela BM, Lichtman JH, Lisabeth LD, Liu S, Mackey RH, Magid DJ, McGuire DK, Mohler ER, 3rd, Moy CS, Muntner P, Mussolino ME, Nasir K, Neumar RW, Nichol G, Palaniappan L, Pandey DK, Reeves MJ, Rodriguez CJ, Rosamond W, Sorlie PD, Stein J, Towfighi A, Turan TN, Virani SS, Woo D, Yeh RW, Turner MB. Heart Disease and Stroke Statistics-2016 Update: A Report From the American Heart Association. Circulation. 2016;133:e38-60.

[6] Gautel M. The sarcomeric cytoskeleton: who picks up the strain? Curr Opin Cell Biol. 2011;23:39-46.

[7] Spudich JA. The myosin swinging cross-bridge model. Nat Rev Mol Cell Biol. 2001;2:387-92.

[8] Frank D, Frey N. Cardiac Z-disc signaling network. J Biol Chem. 2011;286:9897-904.

[9] Granzier HL, Labeit S. The giant protein titin: a major player in myocardial mechanics, signaling, and disease. Circ Res. 2004;94:284-95.

[10] Anderson BR, Granzier HL. Titin-based tension in the cardiac sarcomere: molecular origin and physiological adaptations. Prog Biophys Mol Biol. 2012;110:204-17.

[11] Hoshijima M. Mechanical stress-strain sensors embedded in cardiac cytoskeleton: Z disk, titin, and associated structures. Am J Physiol Heart Circ Physiol. 2006;290:H1313-25.

[12] Knoll R, Hoshijima M, Hoffman HM, Person V, Lorenzen-Schmidt I, Bang ML, Hayashi T, Shiga N, Yasukawa H, Schaper W, McKenna W, Yokoyama M,

Schork NJ, Omens JH, McCulloch AD, Kimura A, Gregorio CC, Poller W, Schaper J, Schultheiss HP, Chien KR. The cardiac mechanical stretch sensor machinery involves a Z disc complex that is defective in a subset of human dilated cardiomyopathy. Cell. 2002;111:943-55.

[13] Heineke J, Ruetten H, Willenbockel C, Gross SC, Naguib M, Schaefer A, Kempf T, Hilfiker-Kleiner D, Caroni P, Kraft T, Kaiser RA, Molkentin JD, Drexler H, Wollert KC. Attenuation of cardiac remodeling after myocardial infarction by muscle LIM protein-calcineurin signaling at the sarcomeric Z-disc. Proc Natl Acad Sci U S A. 2005;102:1655-60.

[14] Crabtree GR, Olson EN. NFAT signaling: choreographing the social lives of cells. Cell. 2002;109 Suppl:S67-79.

[15] Sheikh F, Raskin A, Chu PH, Lange S, Domenighetti AA, Zheng M, Liang X, Zhang T, Yajima T, Gu Y, Dalton ND, Mahata SK, Dorn GW, 2nd, Brown JH, Peterson KL, Omens JH, McCulloch AD, Chen J. An FHL1-containing complex within the cardiomyocyte sarcomere mediates hypertrophic biomechanical stress responses in mice. J Clin Invest. 2008;118:3870-80.

[16] Raskin A, Lange S, Banares K, Lyon RC, Zieseniss A, Lee LK, Yamazaki KG, Granzier HL, Gregorio CC, McCulloch AD, Omens JH, Sheikh F. A novel mechanism involving four-and-a-half LIM domain protein-1 and extracellular signal-regulated kinase-2 regulates titin phosphorylation and mechanics. J Biol Chem. 2012;287:29273-84.

[17] Miller MK, Bang ML, Witt CC, Labeit D, Trombitas C, Watanabe K, Granzier H, McElhinny AS, Gregorio CC, Labeit S. The muscle ankyrin repeat proteins: CARP, ankrd2/Arpp and DARP as a family of titin filament-based stress response molecules. J Mol Biol. 2003;333:951-64.

[18] Barash IA, Mathew L, Ryan AF, Chen J, Lieber RL. Rapid muscle-specific gene expression changes after a single bout of eccentric contractions in the mouse. Am J Physiol Cell Physiol. 2004;286:C355-64.

[19] Lun AS, Chen J, Lange S. Probing muscle ankyrin-repeat protein (MARP) structure and function. Anat Rec (Hoboken). 2014;297:1615-29.

[20] Yoshida M, Sho E, Nanjo H, Takahashi M, Kobayashi M, Kawamura K, Honma M, Komatsu M, Sugita A, Yamauchi M, Hosoi T, Ito Y, Masuda H. Weaving hypothesis of cardiomyocyte sarcomeres: discovery of periodic broadening and narrowing of intercalated disk during volume-load change. Am J Pathol. 2010;176:660-78.

[21] Sheikh F, Ross RS, Chen J. Cell-cell connection to cardiac disease. Trends Cardiovasc Med. 2009;19:182-90.

[22] Mezzano V, Sheikh F. Cell-cell junction remodeling in the heart: possible role in cardiac conduction system function and arrhythmias? Life Sci. 2012;90:313-21.

[23] Michaelson JE, Huang H. Cell-cell junctional proteins in cardiovascular mechanotransduction. Ann Biomed Eng. 2012;40:568-77.

[24] Chopra A, Tabdanov E, Patel H, Janmey PA, Kresh JY. Cardiac myocyte remodeling mediated by N-cadherin-dependent mechanosensing. Am J Physiol Heart Circ Physiol. 2011;300:H1252-66.

[25] Kostetskii I, Li J, Xiong Y, Zhou R, Ferrari VA, Patel VV, Molkentin JD, Radice GL. Induced deletion of the N-cadherin gene in the heart leads to dissolution of the intercalated disc structure. Circ Res. 2005;96:346-54.

[26] Sheikh F, Chen Y, Liang X, Hirschy A, Stenbit AE, Gu Y, Dalton ND, Yajima T, Lu Y, Knowlton KU, Peterson KL, Perriard JC, Chen J. alpha-E-catenin inactivation disrupts the cardiomyocyte adherens junction, resulting in cardiomyopathy and susceptibility to wall rupture. Circulation. 2006;114:1046-55.

[27] Lyon RC, Mezzano V, Wright AT, Pfeiffer E, Chuang J, Banares K, Castaneda A, Ouyang K, Cui L, Contu R, Gu Y, Evans SM, Omens JH, Peterson KL, McCulloch AD, Sheikh F. Connexin defects underlie arrhythmogenic right ventricular cardiomyopathy in a novel mouse model. Hum Mol Genet. 2014;23:1134-50.

[28] Salameh A, Karl S, Djilali H, Dhein S, Janousek J, Daehnert I. Opposing and synergistic effects of cyclic mechanical stretch and alpha- or beta-adrenergic stimulation on the cardiac gap junction protein Cx43. Pharmacol Res. 2010;62:506-13.

[29] Zhuang J, Yamada KA, Saffitz JE, Kleber AG. Pulsatile stretch remodels cell-to-cell communication in cultured myocytes. Circ Res. 2000;87:316-22.

[30] Peter AK, Cheng H, Ross RS, Knowlton KU, Chen J. The costamere bridges sarcomeres to the sarcolemma in striated muscle. Prog Pediatr Cardiol. 2011;31:83-8.

[31] Danowski BA, Imanaka-Yoshida K, Sanger JM, Sanger JW. Costameres are sites of force transmission to the substratum in adult rat cardiomyocytes. J Cell Biol. 1992;118:1411-20.

[32] Carter WG, Wayner EA, Bouchard TS, Kaur P. The role of integrins alpha 2 beta 1 and alpha 3 beta 1 in cell-cell and cell-substrate adhesion of human epidermal cells. J Cell Biol. 1990;110:1387-404.

[33] Babbitt CJ, Shai SY, Harpf AE, Pham CG, Ross RS. Modulation of integrins and integrin signaling molecules in the pressure-loaded murine ventricle. Histochem Cell Biol. 2002;118:431-9.

[34] Li R, Wu Y, Manso AM, Gu Y, Liao P, Israeli S, Yajima T, Nguyen U, Huang MS, Dalton ND, Peterson KL, Ross RS. beta1 integrin gene excision in the adult murine cardiac myocyte causes defective mechanical and signaling responses. Am J Pathol. 2012;180:952-62.

[35] Traister A, Li M, Aafaqi S, Lu M, Arab S, Radisic M, Gross G, Guido F, Sherret J, Verma S, Slorach C, Mertens L, Hui W, Roy A, Delgado-Olguin P, Hannigan G, Maynes JT, Coles JG. Integrin-linked kinase mediates force transduction in cardiomyocytes by modulating SERCA2a/PLN function. Nat Commun. 2014;5:4533.

[36] Kostin S, Scholz D, Shimada T, Maeno Y, Mollnau H, Hein S, Schaper J. The internal and external protein scaffold of the T-tubular system in cardiomyocytes. Cell Tissue Res. 1998;294:449-60.

[37] Israeli-Rosenberg S, Manso AM, Okada H, Ross RS. Integrins and integrin-associated proteins in the cardiac myocyte. Circ Res. 2014;114:572-86.

[38] Zemljic-Harpf AE, Ponrartana S, Avalos RT, Jordan MC, Roos KP, Dalton ND, Phan VQ, Adamson ED, Ross RS. Heterozygous inactivation of the vinculin gene predisposes to stress-induced cardiomyopathy. Am J Pathol. 2004;165:1033-44.

[39] Manso AM, Li R, Monkley SJ, Cruz NM, Ong S, Lao DH, Koshman YE, Gu Y, Peterson KL, Chen J, Abel ED, Samarel AM, Critchley DR, Ross RS. Talin1 has unique expression versus talin 2 in the heart and modifies the hypertrophic response to pressure overload. J Biol Chem. 2013;288:4252-64.

[40] Critchley DR. Biochemical and structural properties of the integrin-associated cytoskeletal protein talin. Annu Rev Biophys. 2009;38:235-54.

[41] Kovacic-Milivojevic B, Roediger F, Almeida EA, Damsky CH, Gardner DG, Ilic D. Focal adhesion kinase and p130Cas mediate both sarcomeric organization and activation of genes associated with cardiac myocyte hypertrophy. Mol Biol Cell. 2001;12:2290-307.

[42] Ervasti JM, Campbell KP. Dystrophin-associated glycoproteins: their possible roles in the pathogenesis of Duchenne muscular dystrophy. Mol Cell Biol Hum Dis Ser. 1993;3:139-66.

[43] Jung D, Yang B, Meyer J, Chamberlain JS, Campbell KP. Identification and characterization of the dystrophin anchoring site on beta-dystroglycan. J Biol Chem. 1995;270:27305-10.

[44] Towbin JA, Hejtmancik JF, Brink P, Gelb B, Zhu XM, Chamberlain JS, McCabe ER, Swift M. X-linked dilated cardiomyopathy. Molecular genetic evidence of linkage to the Duchenne muscular dystrophy (dystrophin) gene at the Xp21 locus. Circulation. 1993;87:1854-65.

[45] Emery AE. Duchenne muscular dystrophy--Meryon's disease. Neuromuscul Disord. 1993;3:263-6.

[46] Lynch GS, Hinkle RT, Chamberlain JS, Brooks SV, Faulkner JA. Force and power output of fast and slow skeletal muscles from mdx mice 6-28 months old. J Physiol. 2001;535:591-600.

[47] Ruwhof C, van der Laarse A. Mechanical stress-induced cardiac hypertrophy: mechanisms and signal transduction pathways. Cardiovasc Res. 2000;47:23-37.

[48] Sadoshima J, Izumo S. The cellular and molecular response of cardiac myocytes to mechanical stress. Annu Rev Physiol. 1997;59:551-71.

[49] Molkentin JD, Dorn GW, 2nd. Cytoplasmic signaling pathways that regulate cardiac hypertrophy. Annu Rev Physiol. 2001;63:391-426.

[50] Bueno OF, De Windt LJ, Tymitz KM, Witt SA, Kimball TR, Klevitsky R, Hewett TE, Jones SP, Lefer DJ, Peng CF, Kitsis RN, Molkentin JD. The MEK1-ERK1/2 signaling pathway promotes compensated cardiac hypertrophy in transgenic mice. Embo J. 2000;19:6341-50.

[51] Wang Y, Huang S, Sah VP, Ross J, Jr., Brown JH, Han J, Chien KR. Cardiac muscle cell hypertrophy and apoptosis induced by distinct members of the p38 mitogen-activated protein kinase family. J Biol Chem. 1998;273:2161-8.

[52] Wang Y, Su B, Sah VP, Brown JH, Han J, Chien KR. Cardiac hypertrophy induced by mitogen-activated protein kinase kinase 7, a specific activator for c-Jun NH2-terminal kinase in ventricular muscle cells. J Biol Chem. 1998;273:5423-6.

[53] Oudit GY, Sun H, Kerfant BG, Crackower MA, Penninger JM, Backx PH. The role of phosphoinositide-3 kinase and PTEN in cardiovascular physiology and disease. J Mol Cell Cardiol. 2004;37:449-71.

[54] Cantley LC. The phosphoinositide 3-kinase pathway. Science. 2002;296:1655-7.

[55] DeBosch B, Treskov I, Lupu TS, Weinheimer C, Kovacs A, Courtois M, Muslin AJ. Akt1 is required for physiological cardiac growth. Circulation. 2006;113:2097-104.

[56] Shiojima I, Sato K, Izumiya Y, Schiekofer S, Ito M, Liao R, Colucci WS, Walsh K. Disruption of coordinated cardiac hypertrophy and angiogenesis contributes to the transition to heart failure. J Clin Invest. 2005;115:2108-18.

[57] Proud CG. Ras, PI3-kinase and mTOR signaling in cardiac hypertrophy. Cardiovasc Res. 2004;63:403-13.

[58] Antos CL, McKinsey TA, Frey N, Kutschke W, McAnally J, Shelton JM, Richardson JA, Hill JA, Olson EN. Activated glycogen synthase-3 beta suppresses cardiac hypertrophy in vivo. Proc Natl Acad Sci U S A. 2002;99:907-12.

[59] Ruwhof C, van Wamel JT, Noordzij LA, Aydin S, Harper JC, van der Laarse A. Mechanical stress stimulates phospholipase C activity and intracellular calcium ion levels in neonatal rat cardiomyocytes. Cell Calcium. 2001;29:73-83.

[60] Gerdes AM, Capasso JM. Structural remodeling and mechanical dysfunction of cardiac myocytes in heart failure. J Mol Cell Cardiol. 1995;27:849-56.

[61] Limbu S, Hoang-Trong TM, Prosser BL, Lederer WJ, Jafri MS. Modeling Local X-ROS and Calcium Signaling in the Heart. Biophys J. 2015;109:2037-50.

[62] Kerckhoffs RC, Omens J, McCulloch AD. A single strain-based growth law predicts concentric and eccentric cardiac growth during pressure and volume overload. Mech Res Commun. 2012;42:40-50.

[63] Allen DG, Kentish JC. The cellular basis of the length-tension relation in cardiac muscle. J Mol Cell Cardiol. 1985;17:821-40.

[64] Kurihara S, Komukai K. Tension-dependent changes of the intracellular Ca2+ transients in ferret ventricular muscles. J Physiol. 1995;489 (Pt 3):617-25.

[65] Nishizuka Y, Kikkawa U. Early studies of protein kinase C: a historical perspective. Methods Mol Biol. 2003;233:9-18.

[66] Toischer K, Rokita AG, Unsold B, Zhu W, Kararigas G, Sossalla S, Reuter SP, Becker A, Teucher N, Seidler T, Grebe C, Preuss L, Gupta SN, Schmidt K, Lehnart SE, Kruger M, Linke WA, Backs J, Regitz-Zagrosek V, Schafer K, Field LJ, Maier LS, Hasenfuss G. Differential cardiac remodeling in preload versus afterload. Circulation. 2010;122:993-1003.

[67] Bullard TA, Hastings JL, Davis JM, Borg TK, Price RL. Altered PKC expression and phosphorylation in response to the nature, direction, and magnitude of mechanical stretch. Can J Physiol Pharmacol. 2007;85:243-50.

[68] Vega RB, Harrison BC, Meadows E, Roberts CR, Papst PJ, Olson EN, McKinsey TA. Protein kinases C and D mediate agonist-dependent cardiac hypertrophy through nuclear export of histone deacetylase 5. Mol Cell Biol. 2004;24:8374-85.

[69] Lu J, McKinsey TA, Nicol RL, Olson EN. Signal-dependent activation of the MEF2 transcription factor by dissociation from histone deacetylases. Proc Natl Acad Sci U S A. 2000;97:4070-5.

[70] Wang Y, De Keulenaer GW, Weinberg EO, Muangman S, Gualberto A, Landschulz KT, Turi TG, Thompson JF, Lee RT. Direct biomechanical induction of endogenous calcineurin inhibitor Down Syndrome Critical Region-1 in cardiac myocytes. Am J Physiol Heart Circ Physiol. 2002;283:H533-9.

[71] Sussman MA, Lim HW, Gude N, Taigen T, Olson EN, Robbins J, Colbert MC, Gualberto A, Wieczorek DF, Molkentin JD. Prevention of cardiac hypertrophy in mice by calcineurin inhibition. Science. 1998;281:1690-3.

[72] Kunisada K, Hirota H, Fujio Y, Matsui H, Tani Y, Yamauchi-Takihara K, Kishimoto T. Activation of JAK-STAT and MAP kinases by leukemia inhibitory factor through gp130 in cardiac myocytes. Circulation. 1996;94:2626-32.

[73] Pan J, Fukuda K, Saito M, Matsuzaki J, Kodama H, Sano M, Takahashi T, Kato T, Ogawa S. Mechanical stretch activates the JAK/STAT pathway in rat cardiomyocytes. Circ Res. 1999;84:1127-36.

[74] Uozumi H, Hiroi Y, Zou Y, Takimoto E, Toko H, Niu P, Shimoyama M, Yazaki Y, Nagai R, Komuro I. gp130 plays a critical role in pressure overload-induced cardiac hypertrophy. J Biol Chem. 2001;276:23115-9.

[75] Zhang SJ, Truskey GA, Kraus WE. Effect of cyclic stretch on beta1D-integrin expression and activation of FAK and RhoA. Am J Physiol Cell Physiol. 2007;292:C2057-69.

[76] Peters SL, Michel MC. The RhoA/Rho kinase pathway in the myocardium. Cardiovasc Res. 2007;75:3-4.

[77] Kimura K, Ito M, Amano M, Chihara K, Fukata Y, Nakafuku M, Yamamori B, Feng J, Nakano T, Okawa K, Iwamatsu A, Kaibuchi K. Regulation of myosin phosphatase by Rho and Rho-associated kinase (Rho-kinase). Science. 1996;273:245-8.

[78] Nobes CD, Hall A. Rho, rac, and cdc42 GTPases regulate the assembly of multimolecular focal complexes associated with actin stress fibers, lamellipodia, and filopodia. Cell. 1995;81:53-62.

[79] Morita T, Mayanagi T, Sobue K. Reorganization of the actin cytoskeleton via transcriptional regulation of cytoskeletal/focal adhesion genes by myocardin-related transcription factors (MRTFs/MAL/MKLs). Exp Cell Res. 2007;313:3432-45.

[80] Marttila M, Hautala N, Paradis P, Toth M, Vuolteenaho O, Nemer M, Ruskoaho H. GATA4 mediates activation of the B-type natriuretic peptide gene expression in response to hemodynamic stress. Endocrinology. 2001;142:4693-700.

[81] Liang Q, De Windt LJ, Witt SA, Kimball TR, Markham BE, Molkentin JD. The transcription factors GATA4 and GATA6 regulate cardiomyocyte hypertrophy in vitro and in vivo. J Biol Chem. 2001;276:30245-53.

[82] Oka T, Maillet M, Watt AJ, Schwartz RJ, Aronow BJ, Duncan SA, Molkentin JD. Cardiac-specific deletion of Gata4 reveals its requirement for hypertrophy, compensation, and myocyte viability. Circ Res. 2006;98:837-45.

[83] Wan F, Lenardo MJ. Specification of DNA binding activity of NF-kappaB proteins. Cold Spring Harb Perspect Biol. 2009;1:a000067.

[84] Craig R, Wagner M, McCardle T, Craig AG, Glembotski CC. The cytoprotective effects of the glycoprotein 130 receptor-coupled cytokine, cardiotrophin-1, require activation of NF-kappa B. J Biol Chem. 2001;276:37621-9.

[85] Li Y, Ha T, Gao X, Kelley J, Williams DL, Browder IW, Kao RL, Li C. NF-kappaB activation is required for the development of cardiac hypertrophy in vivo. Am J Physiol Heart Circ Physiol. 2004;287:H1712-20.

[86] Czubryt MP, Olson EN. Balancing contractility and energy production: the role of myocyte enhancer factor 2 (MEF2) in cardiac hypertrophy. Recent Prog Horm Res. 2004;59:105-24.

[87] Han J, Molkentin JD. Regulation of MEF2 by p38 MAPK and its implication in cardiomyocyte biology. Trends Cardiovasc Med. 2000;10:19-22.

[88] Kato Y, Zhao M, Morikawa A, Sugiyama T, Chakravortty D, Koide N, Yoshida T, Tapping RI, Yang Y, Yokochi T, Lee JD. Big mitogen-activated kinase regulates multiple members of the MEF2 protein family. J Biol Chem. 2000;275:18534-40.

[89] Nadruz W, Jr., Corat MA, Marin TM, Guimaraes Pereira GA, Franchini KG. Focal adhesion kinase mediates MEF2 and c-Jun activation by stretch: role in the activation of the cardiac hypertrophic genetic program. Cardiovasc Res. 2005;68:87-97.

[90] Xu J, Gong NL, Bodi I, Aronow BJ, Backx PH, Molkentin JD. Myocyte enhancer factors 2A and 2C induce dilated cardiomyopathy in transgenic mice. J Biol Chem. 2006;281:9152-62.

[91] Boxer LM, Prywes R, Roeder RG, Kedes L. The sarcomeric actin CArG-binding factor is indistinguishable from the c-fos serum response factor. Mol Cell Biol. 1989;9:515-22.

[92] Treisman R. Ternary complex factors: growth factor regulated transcriptional activators. Curr Opin Genet Dev. 1994;4:96-101.

[93] Davis FJ, Gupta M, Camoretti-Mercado B, Schwartz RJ, Gupta MP. Calcium/calmodulin-dependent protein kinase activates serum response factor transcription activity by its dissociation from histone deacetylase, HDAC4. Implications in cardiac muscle gene regulation during hypertrophy. J Biol Chem. 2003;278:20047-58.

[94] Kuwahara K, Kinoshita H, Kuwabara Y, Nakagawa Y, Usami S, Minami T, Yamada Y, Fujiwara M, Nakao K. Myocardin-related transcription factor A is a common mediator of mechanical stress- and neurohumoral stimulation-induced cardiac hypertrophic signaling leading to activation of brain natriuretic peptide gene expression. Mol Cell Biol. 2010;30:4134-48.

[95] Zhang X, Azhar G, Chai J, Sheridan P, Nagano K, Brown T, Yang J, Khrapko K, Borras AM, Lawitts J, Misra RP, Wei JY. Cardiomyopathy in transgenic mice with cardiac-specific overexpression of serum response factor. Am J Physiol Heart Circ Physiol. 2001;280:H1782-92.

[96] Parlakian A, Charvet C, Escoubet B, Mericskay M, Molkentin JD, Gary-Bobo G, De Windt LJ, Ludosky MA, Paulin D, Daegelen D, Tuil D, Li Z. Temporally controlled onset of dilated cardiomyopathy through disruption of the SRF gene in adult heart. Circulation. 2005;112:2930-9.

[97] Finsen AV, Lunde IG, Sjaastad I, Ostli EK, Lyngra M, Jarstadmarken HO, Hasic A, Nygard S, Wilcox-Adelman SA, Goetinck PF, Lyberg T, Skrbic B, Florholmen

G, Tonnessen T, Louch WE, Djurovic S, Carlson CR, Christensen G. Syndecan-4 is essential for development of concentric myocardial hypertrophy via stretch-induced activation of the calcineurin-NFAT pathway. PLoS One. 2011;6:e28302.

[98] Molkentin JD, Lu JR, Antos CL, Markham B, Richardson J, Robbins J, Grant SR, Olson EN. A calcineurin-dependent transcriptional pathway for cardiac hypertrophy. Cell. 1998;93:215-28.

[99] Blaeser F, Ho N, Prywes R, Chatila TA. Ca(2+)-dependent gene expression mediated by MEF2 transcription factors. J Biol Chem. 2000;275:197-209.

[100] Wang TL, Yang YH, Chang H, Hung CR. Angiotensin II signals mechanical stretch-induced cardiac matrix metalloproteinase expression via JAK-STAT pathway. J Mol Cell Cardiol. 2004;37:785-94.

[101] Kunisada K, Tone E, Fujio Y, Matsui H, Yamauchi-Takihara K, Kishimoto T. Activation of gp130 transduces hypertrophic signals via STAT3 in cardiac myocytes. Circulation. 1998;98:346-52.

[102] Bailey J, Phillips RJ, Pollard AJ, Gilmore K, Robson SC, Europe-Finner GN. Characterization and functional analysis of cAMP response element modulator protein and activating transcription factor 2 (ATF2) isoforms in the human myometrium during pregnancy and labor: identification of a novel ATF2 species with potent transactivation properties. J Clin Endocrinol Metab. 2002;87:1717-28.

[103] Anderson MJ, Viars CS, Czekay S, Cavenee WK, Arden KC. Cloning and characterization of three human forkhead genes that comprise an FKHR-like gene subfamily. Genomics. 1998;47:187-99.

[104] Brunet A, Bonni A, Zigmond MJ, Lin MZ, Juo P, Hu LS, Anderson MJ, Arden KC, Blenis J, Greenberg ME. Akt promotes cell survival by phosphorylating and inhibiting a Forkhead transcription factor. Cell. 1999;96:857-68.

[105] Skurk C, Izumiya Y, Maatz H, Razeghi P, Shiojima I, Sandri M, Sato K, Zeng L, Schiekofer S, Pimentel D, Lecker S, Taegtmeyer H, Goldberg AL, Walsh K. The FOXO3a transcription factor regulates cardiac myocyte size downstream of AKT signaling. J Biol Chem. 2005;280:20814-23.

[106] Rosenzweig A, Halazonetis TD, Seidman JG, Seidman CE. Proximal regulatory domains of rat atrial natriuretic factor gene. Circulation. 1991;84:1256-65.

[107] Mammoto A, Mammoto T, Ingber DE. Mechanosensitive mechanisms in transcriptional regulation. J Cell Sci. 2012;125:3061-73.

[108] Komuro I, Kaida T, Shibazaki Y, Kurabayashi M, Katoh Y, Hoh E, Takaku F, Yazaki Y. Stretching cardiac myocytes stimulates protooncogene expression. J Biol Chem. 1990;265:3595-8.

[109] Sadoshima J, Izumo S. Mechanotransduction in stretch-induced hypertrophy of cardiac myocytes. J Recept Res. 1993;13:777-94.

[110] O'Connell BC, Cheung AF, Simkevich CP, Tam W, Ren X, Mateyak MK, Sedivy JM. A large scale genetic analysis of c-Myc-regulated gene expression patterns. J Biol Chem. 2003;278:12563-73.

[111] Olson AK, Ledee D, Iwamoto K, Kajimoto M, O'Kelly Priddy C, Isern N, Portman MA. C-Myc induced compensated cardiac hypertrophy increases free fatty acid utilization for the citric acid cycle. J Mol Cell Cardiol. 2013;55:156-64.

[112] Torsoni AS, Constancio SS, Nadruz W, Jr., Hanks SK, Franchini KG. Focal adhesion kinase is activated and mediates the early hypertrophic response to stretch in cardiac myocytes. Circ Res. 2003;93:140-7.

[113] Gopalan SM, Flaim C, Bhatia SN, Hoshijima M, Knoell R, Chien KR, Omens JH, McCulloch AD. Anisotropic stretch-induced hypertrophy in neonatal ventricular myocytes micropatterned on deformable elastomers. Biotechnol Bioeng. 2003;81:578-87.

[114] Simpson DG, Majeski M, Borg TK, Terracio L. Regulation of cardiac myocyte protein turnover and myofibrillar structure in vitro by specific directions of stretch. Circ Res. 1999;85:e59-69.

[115] Senyo SE, Koshman YE, Russell B. Stimulus interval, rate and direction differentially regulate phosphorylation for mechanotransduction in neonatal cardiac myocytes. FEBS Lett. 2007;581:4241-7.

[116] Kumar A, Chaudhry I, Reid MB, Boriek AM. Distinct signaling pathways are activated in response to mechanical stress applied axially and transversely to skeletal muscle fibers. J Biol Chem. 2002;277:46493-503.

[117] Mohamed JS, Lopez MA, Cox GA, Boriek AM. Anisotropic regulation of Ankrd2 gene expression in skeletal muscle by mechanical stretch. FASEB journal : official publication of the Federation of American Societies for Experimental Biology. 2010;24:3330-40.

[118] Wang Z, Gerstein M, Snyder M. RNA-Seq: a revolutionary tool for transcriptomics. Nat Rev Genet. 2009;10:57-63.

[119] Auer PL, Doerge RW. Statistical design and analysis of RNA sequencing data. Genetics. 2010;185:405-16.

[120] Trapnell C, Roberts A, Goff L, Pertea G, Kim D, Kelley DR, Pimentel H, Salzberg SL, Rinn JL, Pachter L. Differential gene and transcript expression analysis of RNA-seq experiments with TopHat and Cufflinks. Nat Protoc. 2012;7:562-78.

[121] Liu L, Li Y, Li S, Hu N, He Y, Pong R, Lin D, Lu L, Law M. Comparison of next-generation sequencing systems. J Biomed Biotechnol. 2012;2012:251364.

[122] Andrews SR. FastQC: a quality control tool for high throughput sequence data. 2010. http://www.bioinformatics.bbsrc.ac.uk/projects/fastqc/, (accessed on May 20, 2016).

[123] FASTX-Toolkit: FASTQ/A short-reads pre-processing tools. 2009. http://hannonlab.cshl.edu/fastx_toolkit/index.html, (accessed on May 20, 2016).

[124] Langmead B, Trapnell C, Pop M, Salzberg SL. Ultrafast and memory-efficient alignment of short DNA sequences to the human genome. Genome Biol. 2009;10:R25.

[125] Trapnell C, Pachter L, Salzberg SL. TopHat: discovering splice junctions with RNA-Seq. Bioinformatics. 2009;25:1105-11.

[126] Li H, Handsaker B, Wysoker A, Fennell T, Ruan J, Homer N, Marth G, Abecasis G, Durbin R. The Sequence Alignment/Map format and SAMtools. Bioinformatics. 2009;25:2078-9.

[127] Anders S, Pyl PT, Huber W. HTSeq--a Python framework to work with high-throughput sequencing data. Bioinformatics. 2015;31:166-9.

[128] Trapnell C, Williams BA, Pertea G, Mortazavi A, Kwan G, van Baren MJ, Salzberg SL, Wold BJ, Pachter L. Transcript assembly and quantification by RNA-Seq reveals unannotated transcripts and isoform switching during cell differentiation. Nat Biotechnol. 2010;28:511-5.

[129] Roberts A, Trapnell C, Donaghey J, Rinn JL, Pachter L. Improving RNA-Seq expression estimates by correcting for fragment bias. Genome Biol. 2011;12:R22.

[130] Robinson MD, McCarthy DJ, Smyth GK. edgeR: a Bioconductor package for differential expression analysis of digital gene expression data. Bioinformatics. 2010;26:139-40.

[131] Anders S, Huber W. Differential expression analysis for sequence count data. Genome Biol. 2010;11:R106.

[132] Oshlack A, Robinson MD, Young MD. From RNA-seq reads to differential expression results. Genome Biol. 2010;11:220.

[133] Bullard JH, Purdom E, Hansen KD, Dudoit S. Evaluation of statistical methods for normalization and differential expression in mRNA-Seq experiments. BMC Bioinformatics. 2010;11:94.

[134] Robinson MD, Oshlack A. A scaling normalization method for differential expression analysis of RNA-seq data. Genome Biol. 2010;11:R25.

[135] Trapnell C, Hendrickson DG, Sauvageau M, Goff L, Rinn JL, Pachter L. Differential analysis of gene regulation at transcript resolution with RNA-seq. Nat Biotechnol. 2013;31:46-53.

[136] Seyednasrollah F, Laiho A, Elo LL. Comparison of software packages for detecting differential expression in RNA-seq studies. Brief Bioinform. 2015;16:59-70.

[137] Emig D, Salomonis N, Baumbach J, Lengauer T, Conklin BR, Albrecht M. AltAnalyze and DomainGraph: analyzing and visualizing exon expression data. Nucleic Acids Res. 2010;38:W755-62.

[138] Huang DW, Sherman BT, Tan Q, Collins JR, Alvord WG, Roayaei J, Stephens R, Baseler MW, Lane HC, Lempicki RA. The DAVID Gene Functional Classification Tool: a novel biological module-centric algorithm to functionally analyze large gene lists. Genome Biol. 2007;8:R183.

[139] Chen J, Bardes EE, Aronow BJ, Jegga AG. ToppGene Suite for gene list enrichment analysis and candidate gene prioritization. Nucleic Acids Res. 2009;37:W305-11.

[140] Zambon AC, Gaj S, Ho I, Hanspers K, Vranizan K, Evelo CT, Conklin BR, Pico AR, Salomonis N. GO-Elite: a flexible solution for pathway and ontology over-representation. Bioinformatics. 2012;28:2209-10.

[141] Szklarczyk D, Franceschini A, Wyder S, Forslund K, Heller D, Huerta-Cepas J, Simonovic M, Roth A, Santos A, Tsafou KP, Kuhn M, Bork P, Jensen LJ, von Mering C. STRING v10: protein-protein interaction networks, integrated over the tree of life. Nucleic Acids Res. 2015;43:D447-52.

[142] Warde-Farley D, Donaldson SL, Comes O, Zuberi K, Badrawi R, Chao P, Franz M, Grouios C, Kazi F, Lopes CT, Maitland A, Mostafavi S, Montojo J, Shao Q,

Wright G, Bader GD, Morris Q. The GeneMANIA prediction server: biological network integration for gene prioritization and predicting gene function. Nucleic Acids Res. 2010;38:W214-20.

[143] Morris MK, Saez-Rodriguez J, Sorger PK, Lauffenburger DA. Logic-based models for the analysis of cell signaling networks. Biochemistry. 2010;49:3216-24.

[144] Blais A, Dynlacht BD. Constructing transcriptional regulatory networks. Genes Dev. 2005;19:1499-511.

[145] Janky R, Verfaillie A, Imrichova H, Van de Sande B, Standaert L, Christiaens V, Hulselmans G, Herten K, Naval Sanchez M, Potier D, Svetlichnyy D, Kalender Atak Z, Fiers M, Marine JC, Aerts S. iRegulon: from a gene list to a gene regulatory network using large motif and track collections. PLoS Comput Biol. 2014;10:e1003731.

[146] Blais A, Tsikitis M, Acosta-Alvear D, Sharan R, Kluger Y, Dynlacht BD. An initial blueprint for myogenic differentiation. Genes Dev. 2005;19:553-69.

[147] Gong W, Koyano-Nakagawa N, Li T, Garry DJ. Inferring dynamic gene regulatory networks in cardiac differentiation through the integration of multi-dimensional data. BMC Bioinformatics. 2015;16:74.

[148] Dahlquist KD, Fitzpatrick BG, Camacho ET, Entzminger SD, Wanner NC. Parameter Estimation for Gene Regulatory Networks from Microarray Data: Cold Shock Response in Saccharomyces cerevisiae. Bull Math Biol. 2015;77:1457-92.

[149] Ropers D, de Jong H, Page M, Schneider D, Geiselmann J. Qualitative simulation of the carbon starvation response in Escherichia coli. Biosystems. 2006;84:124-52.

[150] McAdams HH, Arkin A. Stochastic mechanisms in gene expression. Proc Natl Acad Sci U S A. 1997;94:814-9.

[151] Bernot G, Comet JP, Faverney CR. Regulatory networks. Methods Mol Biol. 2013;930:215-34.

[152] Ryall KA, Holland DO, Delaney KA, Kraeutler MJ, Parker AJ, Saucerman JJ. Network reconstruction and systems analysis of cardiac myocyte hypertrophy signaling. J Biol Chem. 2012;287:42259-68.

[153] Kraeutler MJ, Soltis AR, Saucerman JJ. Modeling cardiac beta-adrenergic signaling with normalized-Hill differential equations: comparison with a biochemical model. BMC Syst Biol. 2010;4:157.

[154] Zeigler AC, Richardson WJ, Holmes JW, Saucerman JJ. A computational model of cardiac fibroblast signaling predicts context-dependent drivers of myofibroblast differentiation. J Mol Cell Cardiol. 2016;94:72-81.

[155] Bhalla US, Iyengar R. Emergent properties of networks of biological signaling pathways. Science. 1999;283:381-7.

[156] Nagatomo Y, Carabello BA, Hamawaki M, Nemoto S, Matsuo T, McDermott PJ. Translational mechanisms accelerate the rate of protein synthesis during canine pressure-overload hypertrophy. Am J Physiol. 1999;277:H2176-84.

[157] Saucerman JJ, Brunton LL, Michailova AP, McCulloch AD. Modeling beta-adrenergic control of cardiac myocyte contractility in silico. J Biol Chem. 2003;278:47997-8003.

[158] Covert MW, Schilling CH, Palsson B. Regulation of gene expression in flux balance models of metabolism. J Theor Biol. 2001;213:73-88.

[159] Covert MW, Xiao N, Chen TJ, Karr JR. Integrating metabolic, transcriptional regulatory and signal transduction models in Escherichia coli. Bioinformatics. 2008;24:2044-50.

[160] Park J, Ogunnaike B, Schwaber J, Vadigepalli R. Identifying functional gene regulatory network phenotypes underlying single cell transcriptional variability. Prog Biophys Mol Biol. 2015;117:87-98.

[161] Lammerding J, Kamm RD, Lee RT. Mechanotransduction in cardiac myocytes. Ann N Y Acad Sci. 2004;1015:53-70.

[162] Grossman W, Paulus WJ. Myocardial stress and hypertrophy: a complex interface between biophysics and cardiac remodeling. J Clin Invest. 2013;123:3701-3.

[163] Mansour H, de Tombe PP, Samarel AM, Russell B. Restoration of resting sarcomere length after uniaxial static strain is regulated by protein kinase Cepsilon and focal adhesion kinase. Circ Res. 2004;94:642-9.

[164] Cingolani HE, Ennis IL, Aiello EA, Perez NG. Role of autocrine/paracrine mechanisms in response to myocardial strain. Pflugers Arch. 2011;462:29-38.

[165] Camelliti P, Gallagher JO, Kohl P, McCulloch AD. Micropatterned cell cultures on elastic membranes as an in vitro model of myocardium. Nat Protoc. 2006;1:1379-91.

[166] Pfeiffer ER, Wright AT, Edwards AG, Stowe JC, McNall K, Tan J, Niesman I, Patel HH, Roth DM, Omens JH, McCulloch AD. Caveolae in ventricular

myocytes are required for stretch-dependent conduction slowing. J Mol Cell Cardiol. 2014;76:265-74.

[167] Schneider CA, Rasband WS, Eliceiri KW. NIH Image to ImageJ: 25 years of image analysis. Nat Methods. 2012;9:671-5.

[168] Oliveros JC. Venny: An interactive tool for comparing lists with Venn's diagrams. 2007-2015. http://bioinfogp.cnb.csic.es/tools/venny/index.html, (accessed on May 22, 2016).

[169] Lal H, Verma SK, Smith M, Guleria RS, Lu G, Foster DM, Dostal DE. Stretch-induced MAP kinase activation in cardiac myocytes: differential regulation through beta1-integrin and focal adhesion kinase. J Mol Cell Cardiol. 2007;43:137-47.

[170] De Jong AM, Maass AH, Oberdorf-Maass SU, De Boer RA, Van Gilst WH, Van Gelder IC. Cyclical stretch induces structural changes in atrial myocytes. J Cell Mol Med. 2013;17:743-53.

[171] Nattel S, Maguy A, Le Bouter S, Yeh YH. Arrhythmogenic ion-channel remodeling in the heart: heart failure, myocardial infarction, and atrial fibrillation. Physiol Rev. 2007;87:425-56.

[172] McCain ML, Parker KK. Mechanotransduction: the role of mechanical stress, myocyte shape, and cytoskeletal architecture on cardiac function. Pflugers Arch. 2011;462:89-104.

[173] Potier D, Davie K, Hulselmans G, Naval Sanchez M, Haagen L, Huynh-Thu VA, Koldere D, Celik A, Geurts P, Christiaens V, Aerts S. Mapping gene regulatory networks in Drosophila eye development by large-scale transcriptome perturbations and motif inference. Cell Rep. 2014;9:2290-303.

[174] Durchdewald M, Guinea-Viniegra J, Haag D, Riehl A, Lichter P, Hahn M, Wagner EF, Angel P, Hess J. Podoplanin is a novel fos target gene in skin carcinogenesis. Cancer Res. 2008;68:6877-83.

[175] Arthur-Farraj PJ, Latouche M, Wilton DK, Quintes S, Chabrol E, Banerjee A, Woodhoo A, Jenkins B, Rahman M, Turmaine M, Wicher GK, Mitter R, Greensmith L, Behrens A, Raivich G, Mirsky R, Jessen KR. c-Jun reprograms Schwann cells of injured nerves to generate a repair cell essential for regeneration. Neuron. 2012;75:633-47.

[176] Bild AH, Yao G, Chang JT, Wang Q, Potti A, Chasse D, Joshi MB, Harpole D, Lancaster JM, Berchuck A, Olson JA, Jr., Marks JR, Dressman HK, West M,

Nevins JR. Oncogenic pathway signatures in human cancers as a guide to targeted therapies. Nature. 2006;439:353-7.

[177] Frye M, Gardner C, Li ER, Arnold I, Watt FM. Evidence that Myc activation depletes the epidermal stem cell compartment by modulating adhesive interactions with the local microenvironment. Development. 2003;130:2793-808.

[178] Benito E, Valor LM, Jimenez-Minchan M, Huber W, Barco A. cAMP response element-binding protein is a primary hub of activity-driven neuronal gene expression. J Neurosci. 2011;31:18237-50.

[179] Tejera MM, Kim EH, Sullivan JA, Plisch EH, Suresh M. FoxO1 controls effector-to-memory transition and maintenance of functional CD8 T cell memory. J Immunol. 2013;191:187-99.

[180] Greer EL, Oskoui PR, Banko MR, Maniar JM, Gygi MP, Gygi SP, Brunet A. The energy sensor AMP-activated protein kinase directly regulates the mammalian FOXO3 transcription factor. J Biol Chem. 2007;282:30107-19.

[181] Chen SR, Tang JX, Cheng JM, Li J, Jin C, Li XY, Deng SL, Zhang Y, Wang XX, Liu YX. Loss of Gata4 in Sertoli cells impairs the spermatogonial stem cell niche and causes germ cell exhaustion by attenuating chemokine signaling. Oncotarget. 2015;6:37012-27.

[182] Wales S, Hashemi S, Blais A, McDermott JC. Global MEF2 target gene analysis in cardiac and skeletal muscle reveals novel regulation of DUSP6 by p38MAPK-MEF2 signaling. Nucleic Acids Res. 2014;42:11349-62.

[183] Sebastian S, Faralli H, Yao Z, Rakopoulos P, Palii C, Cao Y, Singh K, Liu QC, Chu A, Aziz A, Brand M, Tapscott SJ, Dilworth FJ. Tissue-specific splicing of a ubiquitously expressed transcription factor is essential for muscle differentiation. Genes Dev. 2013;27:1247-59.

[184] Suehiro J, Kanki Y, Makihara C, Schadler K, Miura M, Manabe Y, Aburatani H, Kodama T, Minami T. Genome-wide approaches reveal functional vascular endothelial growth factor (VEGF)-inducible nuclear factor of activated T cells (NFAT) c1 binding to angiogenesis-related genes in the endothelium. J Biol Chem. 2014;289:29044-59.

[185] Chien Y, Scuoppo C, Wang X, Fang X, Balgley B, Bolden JE, Premsrirut P, Luo W, Chicas A, Lee CS, Kogan SC, Lowe SW. Control of the senescence-associated secretory phenotype by NF-kappaB promotes senescence and enhances chemosensitivity. Genes Dev. 2011;25:2125-36.

[186] Balza RO, Jr., Misra RP. Role of the serum response factor in regulating contractile apparatus gene expression and sarcomeric integrity in cardiomyocytes. J Biol Chem. 2006;281:6498-510.

[187] Dauer DJ, Ferraro B, Song L, Yu B, Mora L, Buettner R, Enkemann S, Jove R, Haura EB. Stat3 regulates genes common to both wound healing and cancer. Oncogene. 2005;24:3397-408.

[188] Wingender E, Chen X, Fricke E, Geffers R, Hehl R, Liebich I, Krull M, Matys V, Michael H, Ohnhauser R, Pruss M, Schacherer F, Thiele S, Urbach S. The TRANSFAC system on gene expression regulation. Nucleic Acids Res. 2001;29:281-3.

[189] Li GR, Lau CP, Leung TK, Nattel S. Ionic current abnormalities associated with prolonged action potentials in cardiomyocytes from diseased human right ventricles. Heart Rhythm. 2004;1:460-8.

[190] Nuss HB, Kaab S, Kass DA, Tomaselli GF, Marban E. Cellular basis of ventricular arrhythmias and abnormal automaticity in heart failure. Am J Physiol. 1999;277:H80-91.

[191] Sharova LV, Sharov AA, Nedorezov T, Piao Y, Shaik N, Ko MS. Database for mRNA half-life of 19 977 genes obtained by DNA microarray analysis of pluripotent and differentiating mouse embryonic stem cells. DNA Res. 2009;16:45-58.

[192] Assenov Y, Ramirez F, Schelhorn SE, Lengauer T, Albrecht M. Computing topological parameters of biological networks. Bioinformatics. 2008;24:282-4.

[193] Shannon P, Markiel A, Ozier O, Baliga NS, Wang JT, Ramage D, Amin N, Schwikowski B, Ideker T. Cytoscape: a software environment for integrated models of biomolecular interaction networks. Genome Res. 2003;13:2498-504.

[194] Baba HA, Stypmann J, Grabellus F, Kirchhof P, Sokoll A, Schafers M, Takeda A, Wilhelm MJ, Scheld HH, Takeda N, Breithardt G, Levkau B. Dynamic regulation of MEK/Erks and Akt/GSK-3beta in human end-stage heart failure after left ventricular mechanical support: myocardial mechanotransduction-sensitivity as a possible molecular mechanism. Cardiovasc Res. 2003;59:390-9.

[195] Katanosaka Y, Iwasaki K, Ujihara Y, Takatsu S, Nishitsuji K, Kanagawa M, Sudo A, Toda T, Katanosaka K, Mohri S, Naruse K. TRPV2 is critical for the maintenance of cardiac structure and function in mice. Nat Commun. 2014;5:3932.

[196] Zobel C, Rana OR, Saygili E, Bolck B, Diedrichs H, Reuter H, Frank K, Muller-Ehmsen J, Pfitzer G, Schwinger RH. Mechanisms of Ca2+-dependent calcineurin activation in mechanical stretch-induced hypertrophy. Cardiology. 2007;107:281-90.

[197] Sadoshima J, Jahn L, Takahashi T, Kulik TJ, Izumo S. Molecular characterization of the stretch-induced adaptation of cultured cardiac cells. An in vitro model of load-induced cardiac hypertrophy. J Biol Chem. 1992;267:10551-60.

[198] Shin SY, Choo SM, Kim D, Baek SJ, Wolkenhauer O, Cho KH. Switching feedback mechanisms realize the dual role of MCIP in the regulation of calcineurin activity. FEBS Lett. 2006;580:5965-73.

[199] Kudoh S, Komuro I, Hiroi Y, Zou Y, Harada K, Sugaya T, Takekoshi N, Murakami K, Kadowaki T, Yazaki Y. Mechanical stretch induces hypertrophic responses in cardiac myocytes of angiotensin II type 1a receptor knockout mice. J Biol Chem. 1998;273:24037-43.

[200] Yamazaki T, Komuro I, Kudoh S, Zou Y, Shiojima I, Mizuno T, Takano H, Hiroi Y, Ueki K, Tobe K, et al. Mechanical stress activates protein kinase cascade of phosphorylation in neonatal rat cardiac myocytes. J Clin Invest. 1995;96:438-46.

[201] Pikkarainen S, Tokola H, Majalahti-Palviainen T, Kerkela R, Hautala N, Bhalla SS, Charron F, Nemer M, Vuolteenaho O, Ruskoaho H. GATA-4 is a nuclear mediator of mechanical stretch-activated hypertrophic program. J Biol Chem. 2003;278:23807-16.

[202] Duquesnes N, Vincent F, Morel E, Lezoualc'h F, Crozatier B. The EGF receptor activates ERK but not JNK Ras-dependently in basal conditions but ERK and JNK activation pathways are predominantly Ras-independent during cardiomyocyte stretch. Int J Biochem Cell Biol. 2009;41:1173-81.

[203] Luosujarvi H, Aro J, Tokola H, Leskinen H, Tenhunen O, Skoumal R, Szokodi I, Ruskoaho H, Rysa J. A novel p38 MAPK target dyxin is rapidly induced by mechanical load in the heart. Blood Press. 2010;19:54-63.

[204] Boateng SY, Belin RJ, Geenen DL, Margulies KB, Martin JL, Hoshijima M, de Tombe PP, Russell B. Cardiac dysfunction and heart failure are associated with abnormalities in the subcellular distribution and amounts of oligomeric muscle LIM protein. Am J Physiol Heart Circ Physiol. 2007;292:H259-69.

[205] Rana OR, Zobel C, Saygili E, Brixius K, Gramley F, Schimpf T, Mischke K, Frechen D, Knackstedt C, Schwinger RH, Schauerte P. A simple device to apply equibiaxial strain to cells cultured on flexible membranes. Am J Physiol Heart Circ Physiol. 2008;294:H532-40.

[206] Del Re DP, Miyamoto S, Brown JH. Focal adhesion kinase as a RhoA-activable signaling scaffold mediating Akt activation and cardiomyocyte protection. J Biol Chem. 2008;283:35622-9.

[207] Yamane M, Matsuda T, Ito T, Fujio Y, Takahashi K, Azuma J. Rac1 activity is required for cardiac myocyte alignment in response to mechanical stress. Biochem Biophys Res Commun. 2007;353:1023-7.

[208] Aikawa R, Nagai T, Kudoh S, Zou Y, Tanaka M, Tamura M, Akazawa H, Takano H, Nagai R, Komuro I. Integrins play a critical role in mechanical stress-induced p38 MAPK activation. Hypertension. 2002;39:233-8.

[209] Gupta S, Das B, Sen S. Cardiac hypertrophy: mechanisms and therapeutic opportunities. Antioxid Redox Signal. 2007;9:623-52.

[210] Menges CW, McCance DJ. Constitutive activation of the Raf-MAPK pathway causes negative feedback inhibition of Ras-PI3K-AKT and cellular arrest through the EphA2 receptor. Oncogene. 2008;27:2934-40.

[211] Buday L, Warne PH, Downward J. Downregulation of the Ras activation pathway by MAP kinase phosphorylation of Sos. Oncogene. 1995;11:1327-31.

[212] Bi R, Liu P. Sample size calculation while controlling false discovery rate for differential expression analysis with RNA-sequencing experiments. BMC Bioinformatics. 2016;17:146.

[213] Fluss R, Faraggi D, Reiser B. Estimation of the Youden Index and its associated cutoff point. Biom J. 2005;47:458-72.

[214] Qi Y, Li Z, Kong CW, Tang NL, Huang Y, Li RA, Yao X. Uniaxial cyclic stretch stimulates TRPV4 to induce realignment of human embryonic stem cell-derived cardiomyocytes. J Mol Cell Cardiol. 2015;87:65-73.

[215] Patel A, Sharif-Naeini R, Folgering JR, Bichet D, Duprat F, Honore E. Canonical TRP channels and mechanotransduction: from physiology to disease states. Pflugers Arch. 2010;460:571-81.

[216] Fang X, Yu SX, Lu Y, Bast RC, Jr., Woodgett JR, Mills GB. Phosphorylation and inactivation of glycogen synthase kinase 3 by protein kinase A. Proc Natl Acad Sci U S A. 2000;97:11960-5.

[217] Koivisto E, Jurado Acosta A, Moilanen AM, Tokola H, Aro J, Pennanen H, Sakkinen H, Kaikkonen L, Ruskoaho H, Rysa J. Characterization of the regulatory mechanisms of activating transcription factor 3 by hypertrophic stimuli in rat cardiomyocytes. PLoS One. 2014;9:e105168.

[218] Heemers HV, Tindall DJ. Androgen receptor (AR) coregulators: a diversity of functions converging on and regulating the AR transcriptional complex. Endocr Rev. 2007;28:778-808.

[219] Tsai WC, Yang LY, Chen YC, Kao YH, Lin YK, Chen SA, Cheng CF, Chen YJ. Ablation of the androgen receptor gene modulates atrial electrophysiology and arrhythmogenesis with calcium protein dysregulation. Endocrinology. 2013;154:2833-42.

[220] Shan H, Zhang Y, Cai B, Chen X, Fan Y, Yang L, Liang H, Song X, Xu C, Lu Y, Yang B, Du Z. Upregulation of microRNA-1 and microRNA-133 contributes to arsenic-induced cardiac electrical remodeling. Int J Cardiol. 2013;167:2798-805.

[221] Kerckhoffs RC. Computational modeling of cardiac growth in the post-natal rat with a strain-based growth law. J Biomech. 2012;45:865-71.

[222] Young AA, Orr R, Smaill BH, Dell'Italia LJ. Three-dimensional changes in left and right ventricular geometry in chronic mitral regurgitation. Am J Physiol. 1996;271:H2689-700.

[223] Davis J, Davis LC, Correll RN, Makarewich CA, Schwanekamp JA, Moussavi-Harami F, Wang D, York AJ, Wu H, Houser SR, Seidman CE, Seidman JG, Regnier M, Metzger JM, Wu JC, Molkentin JD. A Tension-Based Model Distinguishes Hypertrophic versus Dilated Cardiomyopathy. Cell. 2016.

[224] Rommel C, Bodine SC, Clarke BA, Rossman R, Nunez L, Stitt TN, Yancopoulos GD, Glass DJ. Mediation of IGF-1-induced skeletal myotube hypertrophy by PI(3)K/Akt/mTOR and PI(3)K/Akt/GSK3 pathways. Nat Cell Biol. 2001;3:1009-13.

[225] Kuwahara K, Barrientos T, Pipes GC, Li S, Olson EN. Muscle-specific signaling mechanism that links actin dynamics to serum response factor. Mol Cell Biol. 2005;25:3173-81.

[226] Philippar U, Schratt G, Dieterich C, Muller JM, Galgoczy P, Engel FB, Keating MT, Gertler F, Schule R, Vingron M, Nordheim A. The SRF target gene Fhl2 antagonizes RhoA/MAL-dependent activation of SRF. Mol Cell. 2004;16:867-80.

[227] Lange S, Xiang F, Yakovenko A, Vihola A, Hackman P, Rostkova E, Kristensen J, Brandmeier B, Franzen G, Hedberg B, Gunnarsson LG, Hughes SM, Marchand S, Sejersen T, Richard I, Edstrom L, Ehler E, Udd B, Gautel M. The kinase domain of titin controls muscle gene expression and protein turnover. Science. 2005;308:1599-603.

[228] Willis MS, Ike C, Li L, Wang DZ, Glass DJ, Patterson C. Muscle ring finger 1, but not muscle ring finger 2, regulates cardiac hypertrophy in vivo. Circ Res. 2007;100:456-9.

[229] Hojayev B, Rothermel BA, Gillette TG, Hill JA. FHL2 binds calcineurin and represses pathological cardiac growth. Mol Cell Biol. 2012;32:4025-34.

[230] Fiedler B, Lohmann SM, Smolenski A, Linnemuller S, Pieske B, Schroder F, Molkentin JD, Drexler H, Wollert KC. Inhibition of calcineurin-NFAT hypertrophy signaling by cGMP-dependent protein kinase type I in cardiac myocytes. Proc Natl Acad Sci U S A. 2002;99:11363-8.

[231] Liu Q, Chen Y, Auger-Messier M, Molkentin JD. Interaction between NFkappaB and NFAT coordinates cardiac hypertrophy and pathological remodeling. Circ Res. 2012;110:1077-86.

[232] Frey N, Olson EN. Cardiac hypertrophy: the good, the bad, and the ugly. Annu Rev Physiol. 2003;65:45-79.

[233] Kerkela R, Kockeritz L, Macaulay K, Zhou J, Doble BW, Beahm C, Greytak S, Woulfe K, Trivedi CM, Woodgett JR, Epstein JA, Force T, Huggins GS. Deletion of GSK-3beta in mice leads to hypertrophic cardiomyopathy secondary to cardiomyoblast hyperproliferation. J Clin Invest. 2008;118:3609-18.

[234] El Jamali A, Freund C, Rechner C, Scheidereit C, Dietz R, Bergmann MW. Reoxygenation after severe hypoxia induces cardiomyocyte hypertrophy in vitro: activation of CREB downstream of GSK3beta. FASEB journal : official publication of the Federation of American Societies for Experimental Biology. 2004;18:1096-8.

[235] Mercurio F, Murray BW, Shevchenko A, Bennett BL, Young DB, Li JW, Pascual G, Motiwala A, Zhu H, Mann M, Manning AM. IkappaB kinase (IKK)-associated protein 1, a common component of the heterogeneous IKK complex. Mol Cell Biol. 1999;19:1526-38.

[236] Okamoto R, Li Y, Noma K, Hiroi Y, Liu PY, Taniguchi M, Ito M, Liao JK. FHL2 prevents cardiac hypertrophy in mice with cardiac-specific deletion of ROCK2. FASEB journal : official publication of the Federation of American Societies for Experimental Biology. 2013;27:1439-49.

[237] Lange S, Auerbach D, McLoughlin P, Perriard E, Schafer BW, Perriard JC, Ehler E. Subcellular targeting of metabolic enzymes to titin in heart muscle may be mediated by DRAL/FHL-2. J Cell Sci. 2002;115:4925-36.

[238] Bogomolovas J, Gasch A, Simkovic F, Rigden DJ, Labeit S, Mayans O. Titin kinase is an inactive pseudokinase scaffold that supports MuRF1 recruitment to the sarcomeric M-line. Open Biol. 2014;4:140041.

[239] Centner T, Yano J, Kimura E, McElhinny AS, Pelin K, Witt CC, Bang ML, Trombitas K, Granzier H, Gregorio CC, Sorimachi H, Labeit S. Identification of muscle specific ring finger proteins as potential regulators of the titin kinase domain. J Mol Biol. 2001;306:717-26.

[240] Waddell DS, Baehr LM, van den Brandt J, Johnsen SA, Reichardt HM, Furlow JD, Bodine SC. The glucocorticoid receptor and FOXO1 synergistically activate the skeletal muscle atrophy-associated MuRF1 gene. Am J Physiol Endocrinol Metab. 2008;295:E785-97.

[241] Shimizu N, Yoshikawa N, Ito N, Maruyama T, Suzuki Y, Takeda S, Nakae J, Tagata Y, Nishitani S, Takehana K, Sano M, Fukuda K, Suematsu M, Morimoto C, Tanaka H. Crosstalk between glucocorticoid receptor and nutritional sensor mTOR in skeletal muscle. Cell Metab. 2011;13:170-82.

[242] Gehmlich K, Geier C, Osterziel KJ, Van der Ven PF, Furst DO. Decreased interactions of mutant muscle LIM protein (MLP) with N-RAP and alpha-actinin and their implication for hypertrophic cardiomyopathy. Cell Tissue Res. 2004;317:129-36.

[243] Hoffman LM, Jensen CC, Chaturvedi A, Yoshigi M, Beckerle MC. Stretch-induced actin remodeling requires targeting of zyxin to stress fibers and recruitment of actin regulators. Mol Biol Cell. 2012;23:1846-59.

[244] Lange S, Ouyang K, Meyer G, Cui L, Cheng H, Lieber RL, Chen J. Obscurin determines the architecture of the longitudinal sarcoplasmic reticulum. J Cell Sci. 2009;122:2640-50.

[245] Ozes ON, Mayo LD, Gustin JA, Pfeffer SR, Pfeffer LM, Donner DB. NF-kappaB activation by tumour necrosis factor requires the Akt serine-threonine kinase. Nature. 1999;401:82-5.

[246] Dimmeler S, Fleming I, Fisslthaler B, Hermann C, Busse R, Zeiher AM. Activation of nitric oxide synthase in endothelial cells by Akt-dependent phosphorylation. Nature. 1999;399:601-5.

[247] Murphy TJ, Takeuchi K, Alexander RW. Molecular cloning of AT1 angiotensin receptors. Am J Hypertens. 1992;5:236S-42S.

[248] Zou Y, Akazawa H, Qin Y, Sano M, Takano H, Minamino T, Makita N, Iwanaga K, Zhu W, Kudoh S, Toko H, Tamura K, Kihara M, Nagai T, Fukamizu A,

Umemura S, Iiri T, Fujita T, Komuro I. Mechanical stress activates angiotensin II type 1 receptor without the involvement of angiotensin II. Nat Cell Biol. 2004;6:499-506.

[249] Oancea E, Meyer T. Protein kinase C as a molecular machine for decoding calcium and diacylglycerol signals. Cell. 1998;95:307-18.

[250] Chin D, Means AR. Calmodulin: a prototypical calcium sensor. Trends Cell Biol. 2000;10:322-8.

[251] Klee CB, Ren H, Wang X. Regulation of the calmodulin-stimulated protein phosphatase, calcineurin. J Biol Chem. 1998;273:13367-70.

[252] Sanna B, Bueno OF, Dai YS, Wilkins BJ, Molkentin JD. Direct and indirect interactions between calcineurin-NFAT and MEK1-extracellular signal-regulated kinase 1/2 signaling pathways regulate cardiac gene expression and cellular growth. Mol Cell Biol. 2005;25:865-78.

[253] Lemaire-Ewing S, Berthier A, Royer MC, Logette E, Corcos L, Bouchot A, Monier S, Prunet C, Raveneau M, Rebe C, Desrumaux C, Lizard G, Neel D. 7beta-Hydroxycholesterol and 25-hydroxycholesterol-induced interleukin-8 secretion involves a calcium-dependent activation of c-fos via the ERK1/2 signaling pathway in THP-1 cells: oxysterols-induced IL-8 secretion is calcium-dependent. Cell Biol Toxicol. 2009;25:127-39.

[254] Morton S, Davis RJ, McLaren A, Cohen P. A reinvestigation of the multisite phosphorylation of the transcription factor c-Jun. Embo J. 2003;22:3876-86.

[255] Nishimoto S, Nishida E. MAPK signalling: ERK5 versus ERK1/2. EMBO Rep. 2006;7:782-6.

[256] Akazawa H, Komuro I. Roles of cardiac transcription factors in cardiac hypertrophy. Circ Res. 2003;92:1079-88.

[257] Liang Q, Wiese RJ, Bueno OF, Dai YS, Markham BE, Molkentin JD. The transcription factor GATA4 is activated by extracellular signal-regulated kinase 1- and 2-mediated phosphorylation of serine 105 in cardiomyocytes. Mol Cell Biol. 2001;21:7460-9.

[258] Kasperk CH, Borcsok I, Schairer HU, Schneider U, Nawroth PP, Niethard FU, Ziegler R. Endothelin-1 is a potent regulator of human bone cell metabolism in vitro. Calcif Tissue Int. 1997;60:368-74.

[259] Dorn GW, 2nd, Brown JH. Gq signaling in cardiac adaptation and maladaptation. Trends Cardiovasc Med. 1999;9:26-34.

[260] Shah BH, Catt KJ. A central role of EGF receptor transactivation in angiotensin II -induced cardiac hypertrophy. Trends Pharmacol Sci. 2003;24:239-44.

[261] Brock C, Schaefer M, Reusch HP, Czupalla C, Michalke M, Spicher K, Schultz G, Nurnberg B. Roles of G beta gamma in membrane recruitment and activation of p110 gamma/p101 phosphoinositide 3-kinase gamma. J Cell Biol. 2003;160:89-99.

[262] Hilfiker-Kleiner D, Shukla P, Klein G, Schaefer A, Stapel B, Hoch M, Muller W, Scherr M, Theilmeier G, Ernst M, Hilfiker A, Drexler H. Continuous glycoprotein-130-mediated signal transducer and activator of transcription-3 activation promotes inflammation, left ventricular rupture, and adverse outcome in subacute myocardial infarction. Circulation. 2010;122:145-55.

[263] Digby GJ, Lober RM, Sethi PR, Lambert NA. Some G protein heterotrimers physically dissociate in living cells. Proc Natl Acad Sci U S A. 2006;103:17789-94.

[264] Zhu X, Birnbaumer L. G protein subunits and the stimulation of phospholipase C by Gs-and Gi-coupled receptors: Lack of receptor selectivity of Galpha(16) and evidence for a synergic interaction between Gbeta gamma and the alpha subunit of a receptor activated G protein. Proc Natl Acad Sci U S A. 1996;93:2827-31.

[265] Mignery GA, Sudhof TC. The ligand binding site and transduction mechanism in the inositol-1,4,5-triphosphate receptor. Embo J. 1990;9:3893-8.

[266] Henderson YC, Guo XY, Greenberger J, Deisseroth AB. Potential role of bcr-abl in the activation of JAK1 kinase. Clin Cancer Res. 1997;3:145-9.

[267] Sugden PH. Signaling in myocardial hypertrophy: life after calcineurin? Circ Res. 1999;84:633-46.

[268] Gupta S, Barrett T, Whitmarsh AJ, Cavanagh J, Sluss HK, Derijard B, Davis RJ. Selective interaction of JNK protein kinase isoforms with transcription factors. Embo J. 1996;15:2760-70.

[269] Bian ZY, Huang H, Jiang H, Shen DF, Yan L, Zhu LH, Wang L, Cao F, Liu C, Tang QZ, Li H. LIM and cysteine-rich domains 1 regulates cardiac hypertrophy by targeting calcineurin/nuclear factor of activated T cells signaling. Hypertension. 2010;55:257-63.

[270] Eble DM, Qi M, Waldschmidt S, Lucchesi PA, Byron KL, Samarel AM. Contractile activity is required for sarcomeric assembly in phenylephrine-induced cardiac myocyte hypertrophy. Am J Physiol. 1998;274:C1226-37.

[271] Whitehurst CE, Geppert TD. MEK1 and the extracellular signal-regulated kinases are required for the stimulation of IL-2 gene transcription in T cells. J Immunol. 1996;156:1020-9.

[272] Leenders JJ, Wijnen WJ, Hiller M, van der Made I, Lentink V, van Leeuwen RE, Herias V, Pokharel S, Heymans S, de Windt LJ, Hoydal MA, Pinto YM, Creemers EE. Regulation of cardiac gene expression by KLF15, a repressor of myocardin activity. J Biol Chem. 2010;285:27449-56.

[273] Fleming Y, Armstrong CG, Morrice N, Paterson A, Goedert M, Cohen P. Synergistic activation of stress-activated protein kinase 1/c-Jun N-terminal kinase (SAPK1/JNK) isoforms by mitogen-activated protein kinase kinase 4 (MKK4) and MKK7. Biochem J. 2000;352 Pt 1:145-54.

[274] Yan M, Dai T, Deak JC, Kyriakis JM, Zon LI, Woodgett JR, Templeton DJ. Activation of stress-activated protein kinase by MEKK1 phosphorylation of its activator SEK1. Nature. 1994;372:798-800.

[275] Derijard B, Raingeaud J, Barrett T, Wu IH, Han J, Ulevitch RJ, Davis RJ. Independent human MAP-kinase signal transduction pathways defined by MEK and MKK isoforms. Science. 1995;267:682-5.

[276] Tournier C, Whitmarsh AJ, Cavanagh J, Barrett T, Davis RJ. Mitogen-activated protein kinase kinase 7 is an activator of the c-Jun NH2-terminal kinase. Proc Natl Acad Sci U S A. 1997;94:7337-42.

[277] Nicol RL, Frey N, Pearson G, Cobb M, Richardson J, Olson EN. Activated MEK5 induces serial assembly of sarcomeres and eccentric cardiac hypertrophy. Embo J. 2001;20:2757-67.

[278] Sun W, Kesavan K, Schaefer BC, Garrington TP, Ware M, Johnson NL, Gelfand EW, Johnson GL. MEKK2 associates with the adapter protein Lad/RIBP and regulates the MEK5-BMK1/ERK5 pathway. J Biol Chem. 2001;276:5093-100.

[279] Takekawa M, Posas F, Saito H. A human homolog of the yeast Ssk2/Ssk22 MAP kinase kinase kinases, MTK1, mediates stress-induced activation of the p38 and JNK pathways. Embo J. 1997;16:4973-82.

[280] Nojima H, Tokunaga C, Eguchi S, Oshiro N, Hidayat S, Yoshino K, Hara K, Tanaka N, Avruch J, Yonezawa K. The mammalian target of rapamycin (mTOR) partner, raptor, binds the mTOR substrates p70 S6 kinase and 4E-BP1 through their TOR signaling (TOS) motif. J Biol Chem. 2003;278:15461-4.

[281] Yamazaki T, Komuro I, Kudoh S, Zou Y, Nagai R, Aikawa R, Uozumi H, Yazaki Y. Role of ion channels and exchangers in mechanical stretch-induced cardiomyocyte hypertrophy. Circ Res. 1998;82:430-7.

[282] Xu L, Chen J, Li XY, Ren S, Huang CX, Wu G, Jiang XJ. Analysis of Na(+)/Ca (2+) exchanger (NCX) function and current in murine cardiac myocytes during heart failure. Mol Biol Rep. 2012;39:3847-52.

[283] Barry SP, Davidson SM, Townsend PA. Molecular regulation of cardiac hypertrophy. Int J Biochem Cell Biol. 2008;40:2023-39.

[284] Knowles RG, Palacios M, Palmer RM, Moncada S. Formation of nitric oxide from L-arginine in the central nervous system: a transduction mechanism for stimulation of the soluble guanylate cyclase. Proc Natl Acad Sci U S A. 1989;86:5159-62.

[285] Tenhunen O, Rysa J, Ilves M, Soini Y, Ruskoaho H, Leskinen H. Identification of cell cycle regulatory and inflammatory genes as predominant targets of p38 mitogen-activated protein kinase in the heart. Circ Res. 2006;99:485-93.

[286] Kolodziejczyk SM, Wang L, Balazsi K, DeRepentigny Y, Kothary R, Megeney LA. MEF2 is upregulated during cardiac hypertrophy and is required for normal post-natal growth of the myocardium. Curr Biol. 1999;9:1203-6.

[287] Yang SH, Galanis A, Sharrocks AD. Targeting of p38 mitogen-activated protein kinases to MEF2 transcription factors. Mol Cell Biol. 1999;19:4028-38.

[288] Moon Z, Wang Y, Aryan N, Mousseau DD, Scheid MP. Serine 396 of PDK1 is required for maximal PKB activation. Cell Signal. 2008;20:2038-49.

[289] Scheid MP, Marignani PA, Woodgett JR. Multiple phosphoinositide 3-kinase-dependent steps in activation of protein kinase B. Mol Cell Biol. 2002;22:6247-60.

[290] Xuan YT, Guo Y, Zhu Y, Wang OL, Rokosh G, Messing RO, Bolli R. Role of the protein kinase C-epsilon-Raf-1-MEK-1/2-p44/42 MAPK signaling cascade in the activation of signal transducers and activators of transcription 1 and 3 and induction of cyclooxygenase-2 after ischemic preconditioning. Circulation. 2005;112:1971-8.

[291] Rebecchi MJ, Pentyala SN. Structure, function, and control of phosphoinositide-specific phospholipase C. Physiol Rev. 2000;80:1291-335.

[292] Goldschmidt-Clermont PJ, Kim JW, Machesky LM, Rhee SG, Pollard TD. Regulation of phospholipase C-gamma 1 by profilin and tyrosine phosphorylation. Science. 1991;251:1231-3.

[293] Gerwins P, Blank JL, Johnson GL. Cloning of a novel mitogen-activated protein kinase kinase kinase, MEKK4, that selectively regulates the c-Jun amino terminal kinase pathway. J Biol Chem. 1997;272:8288-95.

[294] Russell M, Lange-Carter CA, Johnson GL. Direct interaction between Ras and the kinase domain of mitogen-activated protein kinase kinase kinase (MEKK1). J Biol Chem. 1995;270:11757-60.

[295] Wang X, Tournier C. Regulation of cellular functions by the ERK5 signalling pathway. Cell Signal. 2006;18:753-60.

[296] Innocenti M, Tenca P, Frittoli E, Faretta M, Tocchetti A, Di Fiore PP, Scita G. Mechanisms through which Sos-1 coordinates the activation of Ras and Rac. J Cell Biol. 2002;156:125-36.

[297] Warne PH, Viciana PR, Downward J. Direct interaction of Ras and the amino-terminal region of Raf-1 in vitro. Nature. 1993;364:352-5.

[298] Nakaoka Y, Shioyama W, Kunimoto S, Arita Y, Higuchi K, Yamamoto K, Fujio Y, Nishida K, Kuroda T, Hirota H, Yamauchi-Takihara K, Hirano T, Komuro I, Mochizuki N. SHP2 mediates gp130-dependent cardiomyocyte hypertrophy via negative regulation of skeletal alpha-actin gene. J Mol Cell Cardiol. 2010;49:157-64.

[299] Lauriol J, Keith K, Jaffre F, Couvillon A, Saci A, Goonasekera SA, McCarthy JR, Kessinger CW, Wang J, Ke Q, Kang PM, Molkentin JD, Carpenter C, Kontaridis MI. RhoA signaling in cardiomyocytes protects against stress-induced heart failure but facilitates cardiac fibrosis. Sci Signal. 2014;7:ra100.

[300] Yanazume T, Hasegawa K, Wada H, Morimoto T, Abe M, Kawamura T, Sasayama S. Rho/ROCK pathway contributes to the activation of extracellular signal-regulated kinase/GATA-4 during myocardial cell hypertrophy. J Biol Chem. 2002;277:8618-25.

[301] Ikuta T, Ausenda S, Cappellini MD. Mechanism for fetal globin gene expression: role of the soluble guanylate cyclase-cGMP-dependent protein kinase pathway. Proc Natl Acad Sci U S A. 2001;98:1847-52.

[302] Schlaepfer DD, Jones KC, Hunter T. Multiple Grb2-mediated integrin-stimulated signaling pathways to ERK2/mitogen-activated protein kinase: summation of both

c-Src- and focal adhesion kinase-initiated tyrosine phosphorylation events. Mol Cell Biol. 1998;18:2571-85.

[303] Sadoshima J, Xu Y, Slayter HS, Izumo S. Autocrine release of angiotensin II mediates stretch-induced hypertrophy of cardiac myocytes in vitro. Cell. 1993;75:977-84.

[304] van Wamel AJ, Ruwhof C, van der Valk-Kokshoom LE, Schrier PI, van der Laarse A. The role of angiotensin II, endothelin-1 and transforming growth factor-beta as autocrine/paracrine mediators of stretch-induced cardiomyocyte hypertrophy. Mol Cell Biochem. 2001;218:113-24.

[305] Shyu KG, Chen CC, Wang BW, Kuan P. Angiotensin II receptor antagonist blocks the expression of connexin43 induced by cyclical mechanical stretch in cultured neonatal rat cardiac myocytes. J Mol Cell Cardiol. 2001;33:691-8.

[306] Yu T, Miyagawa S, Miki K, Saito A, Fukushima S, Higuchi T, Kawamura M, Kawamura T, Ito E, Kawaguchi N, Sawa Y, Matsuura N. In vivo differentiation of induced pluripotent stem cell-derived cardiomyocytes. Circ J. 2013;77:1297-306.

[307] Yamazaki T, Komuro I, Kudoh S, Zou Y, Shiojima I, Hiroi Y, Mizuno T, Maemura K, Kurihara H, Aikawa R, Takano H, Yazaki Y. Endothelin-1 is involved in mechanical stress-induced cardiomyocyte hypertrophy. J Biol Chem. 1996;271:3221-8.

[308] Nyui N, Tamura K, Mizuno K, Ishigami T, Kihara M, Ochiai H, Kimura K, Umemura S, Ohno S, Taga T, Ishii M. gp130 is involved in stretch-induced MAP kinase activation in cardiac myocytes. Biochem Biophys Res Commun. 1998;245:928-32.

[309] Sharp WW, Simpson DG, Borg TK, Samarel AM, Terracio L. Mechanical forces regulate focal adhesion and costamere assembly in cardiac myocytes. Am J Physiol. 1997;273:H546-56.

[310] Liao XD, Tang AH, Chen Q, Jin HJ, Wu CH, Chen LY, Wang SQ. Role of Ca2+ signaling in initiation of stretch-induced apoptosis in neonatal heart cells. Biochem Biophys Res Commun. 2003;310:405-11.

[311] Kato T, Muraski J, Chen Y, Tsujita Y, Wall J, Glembotski CC, Schaefer E, Beckerle M, Sussman MA. Atrial natriuretic peptide promotes cardiomyocyte survival by cGMP-dependent nuclear accumulation of zyxin and Akt. J Clin Invest. 2005;115:2716-30.